Enhancing Fiber Direction Estimation from Electrograms: A Comparative Study and Method Improvement for Clinical and Research Applications

M.Sc. Thesis Biomedical Engineering

Elena van Breukelen García

October 2023

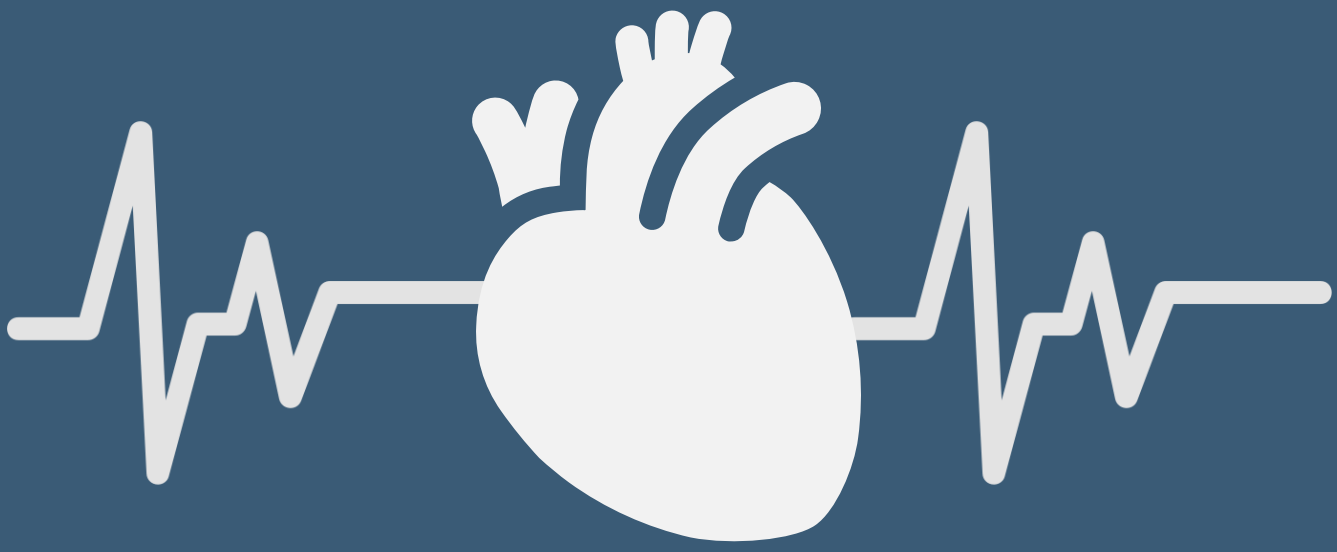

Erasmus MC

TU Delft Delft University of Technology

Enhancing Fiber Direction Estimation from Electrograms: A Comparative Study and Method Improvement for Clinical and Research Applications

Thesis

submitted in partial fulfillment of the
requirements for the degree of

Master of Science

in

Biomedical Engineering

by

Elena van Breukelen García
born in Vught, the Netherlands

This work was performed in:

Signal Processing Systems Group
Department of Microelectronics
Faculty of Electrical Engineering, Mathematics and
Computer Science
Delft University of Technology

Translational Electrophysiology Group
Department of Cardiology
Erasmus Medical Center

Delft University of Technology

Delft University of Technology
Department of
Microelectronics

The undersigned hereby certify that they have read and recommend to the Faculty of Mechanical, Maritime and Materials for acceptance a thesis entitled "*Enhancing Fiber Direction Estimation from Electrograms: A Comparative Study and Method Improvement for Clinical and Research Applications*" by Elena van Breukelen García in partial fulfillment of the requirements for the degree of Master of Science Biomedical Engineering.

Dated: October 26th, 2023

Chairman:

Dr.ir. R.C. Hendriks

Advisors:

Drs. M.S. van Schie

Ir. J.W. de Vries

Committee Members:

Prof.dr.ir. A.J. van der Veen

Dr. T. Costa

Abstract

For the heart to pump blood throughout the body, electrical impulses that trigger the cellular contraction must be generated and spread through the myocardial tissue. These signals propagate faster along the longitudinal cardiac fiber direction than the transverse direction, conferring the heart with anisotropic conduction properties. Therefore, the arrangement of the fibers within the tissue governs the impulse propagation. Given the variability of the fiber direction across the heart and between patients, incorporating it into electrophysiological models would enhance our understanding of the mechanisms and progression of different heart conditions, such as atrial fibrillation (AF). The study of this common cardiac arrhythmia relies on analyzing electrical recordings of the heart, known as electrograms (EGMs), which, if integrated together with the patient's fiber architecture into cardiac models, can enable effective personalized treatment. Over the years, researchers have proposed different approaches to estimate the fiber direction from EGMs. However, these methods have been evaluated in different, usually simplistic, cardiac tissue models, making their comparison, and therefore selection of the most accurate approach for clinical and research applications, challenging.

The current study aims to identify the best fiber direction estimation method under consistent and realistic conditions. To achieve this goal, synthetic EGMs and local activation time (LAT) maps were generated from 2D and 3D monodomain models that mimicked the muscle bundle, atrial bilayer, and ventricular transmural fiber rotation structures. A comparison analysis of existing fiber direction estimation methods, first as described by their authors and then standardized to have the same spatial resolution, showed the superior performance of the techniques based on fitting an ellipse to local conduction velocity or conduction slowness vectors from a whole LAT map. The estimation accuracy of these methods can be further improved by increasing the number of vectors to which the ellipse is fitted. Nonetheless, given the influence of underlying layers in the epicardial recordings, the estimation error increases in the tissue models where fibers in the epicardial and endocardial layers run perpendicularly. The effect on the estimate of such architecture, characteristic of the inferior side of the right atria and the ventricles, can be accounted for by combining epicardial electrical recordings obtained after pacing either in the endocardium or the epicardium. Although a preliminary assessment of the estimation methods was carried out with human EGMs, future studies should focus on validating the methods in a controlled experimental framework and refining them for more localized fiber direction estimation. All in all, the automation of the techniques and their integration into electrophysiological models brings us a step closer to creating valuable clinical tools for diagnosing and treating electropathologies.

Preface

The master thesis you are about to read, should you be up for turning the page, marks the culmination of my journey as a Biomedical Engineering master's student at TU Delft. Although this project has only been a fraction of a two-year program, it would not have been possible to complete it without all the knowledge gained and experiences lived throughout my academic path, particularly in the past two years in Delft. That is why, I would like to thank everyone who has accompanied me on this journey, for they, too, are co-authors of this master's thesis.

First and foremost, I would like to express my sincere gratitude to my supervisor, Richard Hendriks, who has been guiding me since day one of this nine-month project. He has continually shared his expertise, time, and, most importantly, enthusiasm during the research. Also, I am thankful to my daily supervisors, Mathijs van Schie and Jordi de Vries, who have provided invaluable assistance with all the medical and technical questions that I have encountered along the way. They have always been open to help and share their knowledge.

I am very grateful to have been given the opportunity to work with the Signal Processing Systems department at TU Delft, where I had the chance to learn from all the researchers and dive a bit deeper into the diversity of signal processing topics. I am also grateful to have been part of the Cardiology Translational Electrophysiological group at the Erasmus Medical Center during this project. It is every biomedical engineer's dream to conduct research that involves collaboration between the technical and medical world.

I would also like to extend my gratitude to the committee members, Alle-Jan van der Veen and Tiago Costa, for dedicating their time to reading and discussing the outcomes of this master's thesis.

Last but not least, it is my family and friends who I have to thank for making these past months so enjoyable. Even from far away, my family has provided unwavering support, both during the most euphoric moments and the most stressful ones. I am grateful to call them my family. Yet, I am also extremely thankful to the family I have met along the way, my friends. From near and far, they have always been there to listen to my thesis-related monologues, offer comfort in adversity, and always have a good time. I could not have felt more at home in the Netherlands if it were not for the parties at jumbo or having a night in for the 'bombs' drop.

All of them have made my time in Delft to be one of the most enriching and memorable chapters of my life.

A todos, muchísimas gracias

Elena
Delft, The Netherlands
October 26th, 2023

Contents

List of Figures

List of Tables

Acronyms

ACV	Average Conduction Velocity Vector
AF	Atrial Fibrillation
AR	Anisotropy Ratio
AVN	Atrioventricular Node
BB	Bachmann's Bundle
CCS	Cardiac Conduction System
CCW	Counterclockwise
CRT	Cardiac Resynchronization Therapy
CS	Conduction Slowness
CV	Conduction Velocity
ECS	Ellipse Fitting to Conduction Slowness Vectors
ECVGM	Ellipse Fitting to Local Conduction Velocity Vectors computed With a Wavefront Geometry Model
ECVPSF	Ellipse Fitting to Local Conduction Velocity Vectors computed through Polynomial Surface Fitting
EGM	Electrogram
EIC	Ellipse Fitting to Isochrone
EIP	Ellipse Fitting to Isopotential
LA	Left Atrium
LAT	Local Activation Time
LS	Least-Squares
LTEC	Linear Transformation from Elliptical to Circular Wavefront
LV	Left Ventricle
MAE	Mean Absolute Error
ODE	Ordinary Differential Equations
PDE	Partial Differential Equation
PIEMAP	Personalized Inverse Eikonal Model from Cardiac Electro-Anatomical Maps
PM	Potential Maxima
PSF	Polynomial Surface Fitting
RA	Right Atrium
RV	Right Ventricle
SAN	Sinoatrial Node
SR	Sinus Rhythm
SVM	Support Vector Machine

1 Introduction

The human heart is a muscular organ responsible for pumping blood through the body. This function is driven by the initiation and propagation of electrical impulses across the myocardial tissue. The signal propagation is anisotropic, meaning that the conduction is faster along the cardiac fibers than in the perpendicular direction. Consequently, the architectural arrangement of cardiac fibers does not only shape the mechanical properties of the heart, but also its electrical behavior. Therefore, its incorporation into electrophysiological models is critical for reliable predictions and accurate interpretation of electrical recordings of the heart. This thesis aims to compare the various methods developed to derive the fiber direction from electrograms (EGMs) obtained from a realistic tissue model. Furthermore, some suggestions on how to improve the accuracy of these methods will be given, with the ultimate goal of establishing a robust technique suitable for both clinical and research applications.

1.1 Anatomy and electrophysiology of the human heart

1.1.1 Anatomy of the human heart

The heart pumps blood throughout the body, supplying the required oxygen and nutrients to the tissues and organs, and removing waste products. It does this with the help of its four chambers, divided into two pumps, left and right, known as left atrium (LA), right atrium (RA), left ventricle (LV) and right ventricle (RV) [1]. The wall of these chambers consists of three layers; endocardium, myocardium, and epicardium (Figure 1.1 (a)). The middle layer, or myocardium, is composed of cardiomyocytes, which are the main responsible cells for heart's contractile function. These elongated cells are mechanically coupled through desmosomes and adherens junctions and electrically connected through gap junctions at their ends, forming muscle fibers (Figure 1.1 (b)). A group of fibers with the same alignment can be connected laterally and form muscle bundles or sheets.

The arrangement of the fibers within the walls varies across the cardiac tissue. The ventricular myocardium comprises multiple interconnected fiber sheets, forming a wall that is approximately 3 to 5 mm thick in the RV and 12 to 15 mm thick in the LV [2], [3]. The fiber orientation rotates counterclockwise (CCW) from the epicardium to the endocardium, with the fibers in the epicardium being perpendicular to the ones in the endocardium [4]. Contrarily, the atrial wall has a more irregular fiber structure and is thinner, 0.6 to 4.5 mm thick in the RA and 0.7 to 4.3 mm thick in the LA. In the atria, overlapping and intersecting muscle bundles are found, such as the pectinate muscles and the terminal crest in the RA and the Bachmann's and septopulomnary bundle in the LA [5]. Despite the intricate architecture of the atrial wall, the regions with a smooth laminar architecture are usually represented as a bilayer structure with fibers in the epicardial layer running perpendicular, in the posterior-inferior and anterior regions, or parallel, in the lateral wall and roof of the LA, to those in the endocardium [6].

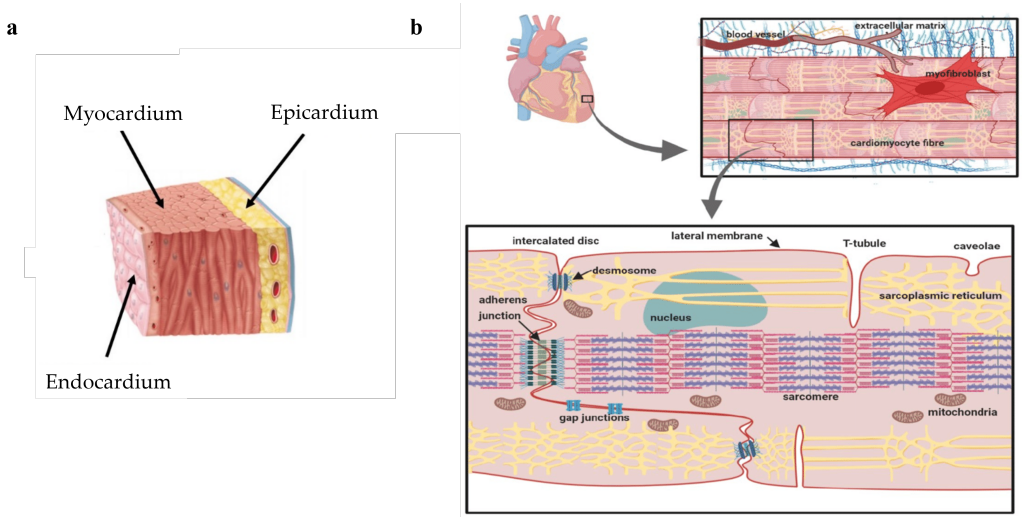

Figure 1.1: The structure and components of the heart wall. (a) Layers of the cardiac wall: epicardium, myocardium, and endocardium [7]. (b) Components of the cardiac muscle fibers found in the myocardium [8].

1.1.2 Electrophysiology of the human heart

The electrical impulses that stimulate the contraction of the cardiomyocytes propagate from cell to cell along the cardiac fibers reaching the entire muscle. This electrical signal, referred to as action potential, is a transient depolarizing current across the cell membrane that causes a rise in transmembrane potential V_{tm}. The potential increase activates voltage-sensitive calcium channels, allowing an influx of calcium ions (Ca^{2+}) into the cell, thereby enabling the myocyte's contraction [9]. A repolarization current follows the cell depolarization to return the V_{tm} back to its resting state value, around -90 mV. The typical action potential morphology of a cardiomyocyte is seen in Figure 1.2 (a).

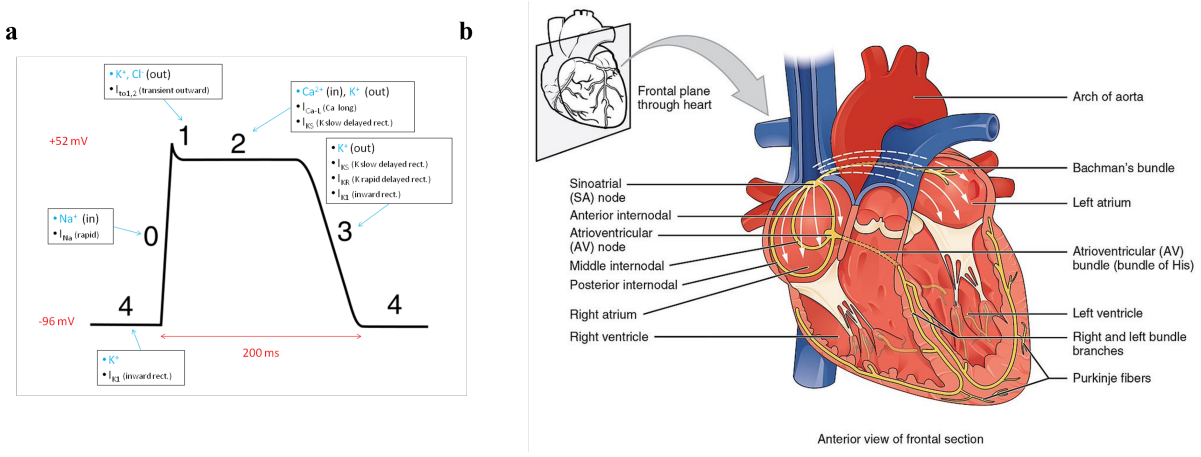

Figure 1.2: Action potential generated in the sinoatrial node (SAN) and distributed throughout the cardiac tissue with the help of the cardiac conduction system (CCS). (a) Cardiac action potential's morphology and phases [10]. (b) Anatomy and CCS of the heart [7].

The responsibility of generating and propagating this signal relies on a system of specialized cardiac cells, with varying electrophysiological properties, known as the cardiac conduction system (CCS) [9]. As seen in Figure 1.2 (b), the electrical impulse is initiated in the sinoatrial node (SAN), a group of pacemaker cells located subepicardially in the RA. Then, the signal propagates through the internodal pathways to

reach the atrioventricular node (AVN), and through the Bachmann's bundle (BB) to reach the LA. Afterward, from the AVN the depolarization wavefront goes into the bundle of His, the left and right bundle branches, and the Purkinje fibers triggering the contraction of the ventricles.

1.1.2.1 Anisotropic cardiac conduction

Transmission of the depolarizing current across the tissue is possible due to the intracellular coupling via gap junctions. These ionic channels facilitate the flow of charged particles between adjacent cells. Consequently, the gap junction density and distribution will determine the overall membrane resistance. Generally, more gap junctions are found at the ends of the cardiomyocytes' membrane surface than at the laterals, which, together with the elongated morphology of the cardiomyocytes, confers the cells with a lower resistivity along the longitudinal axis than the transverse axis [11]. This directional conduction difference is characterized by the anisotropy ratio (AR), defined as the ratio between longitudinal and transversal conductivity [12]. As cardiomyocytes form fibers, the electrical impulse also spreads faster along the direction of the fiber. Hence, the fiber organization within the cardiac tissue plays a crucial role in directing the impulse propagation throughout the heart.

In a three-dimensional scenario, the normal component of conduction should also be taken into account, which is comparable to the transverse conductivity. Thus, the bulk tissue in the heart is orthotopic, with the fastest signal propagation along the orientation of the muscle fibers. Furthermore, the heart has heterogeneous electrical properties due to the presence of conducting and nonconducting tissue and the nonuniform spatial arrangement of the fibers. To measure tissue conductivity, medical professionals use conduction velocity (CV) which indicates the speed at which action potentials are distributed throughout the heart [12]. As with conductivity, CV is higher in the longitudinal direction of the fibers than in the transverse direction.

1.1.3 Atrial Fibrillation

Heart rhythm abnormalities, known as arrhythmias, can appear due to defects in the CCS. One of the most common cardiac arrhythmia associated with a high risk of mortality and morbidity is atrial fibrillation (AF). AF is characterized by the desynchronized cardiomyocyte contraction in the atria and is initiated and maintained by a trigger and a substrate. An ectopic focus, or abnormal pacemaker cell site, can trigger the onset of AF, while structural or electrical changes in the tissue can become the substrate that maintains the abnormal conduction. These changes can be caused by atrial remodeling, induced by many processes, including aging, ischemia, infarction, or inflammation. For instance, the appearance of regions with sudden fiber direction or thickness changes may create conduction blocks or reentry pathways [13], [14].

Treatment for AF involves medication, ablation, or cardiac resynchronization therapy (CRT), aimed at restoring the heart rhythm and destroying the defective tissue. Ablation, a procedure that scars the defective tissue, relies on recordings of the heart's electrical activity, known as electrograms (EGMs), to guide the process. Research has shown that the orientation of cardiac fibers affects the treatment outcomes, which continues to have limited effectiveness in certain forms of AF [15], [16]. Specifically, ablation in patients with persistent AF has limited and variable clinical success, and the optimal ablation strategy is still not known. One of the ablation techniques con-

sists of the complete electrical isolation of the pulmonary vein, which can be very effective in only some patients. With the aim of identifying these patients, Roney *et al.* showed that areas with high pulmonary vein singularity phase density were suitable for ablation, as well as indicative of an effective AF termination with pulmonary vein isolation alone. This density depends on the pulmonary vein fiber direction, which greatly differs between patients. Hence, knowledge of the tissue architecture could help in providing a patient-specific successful treatment. Furthermore, fiber architecture is also important for determining the optimal positioning of pacing electrodes during CRT, focused on restoring the coordinated cell contractions [17].

1.2 Measuring the heart's electrical activity

A way of recording the heart's electrical activity is by placing an electrode directly on the cardiac tissue surface to record the product of the transmembrane currents and extracellular potential differences. Such recordings are known as electrograms (EGMs) and can be either epicardial or endocardial, depending on the wall layer where the electrodes are placed [18]. In both cases, unipolar or bipolar EGMs can be obtained. The former is derived from computing the difference between recordings from one electrode at the measurement site and a reference electrode far away, whereas the latter from the difference between recordings from adjacent electrodes located at the area of interest. Although the bipolar modality is less sensitive to remote electrical noise, unipolar recordings are independent of the direction of the wavefront and allow for a straightforward interpretation [19]. The morphology and dependency on the wavefront direction of unipolar and bipolar EGMs can be seen in Figure 1.3 (a). The unipolar EGM usually has an RS morphology, a positive deflection (R-wave) followed by a negative deflection (S-wave). The generation of this signal is seen in Figure 1.3 (b).

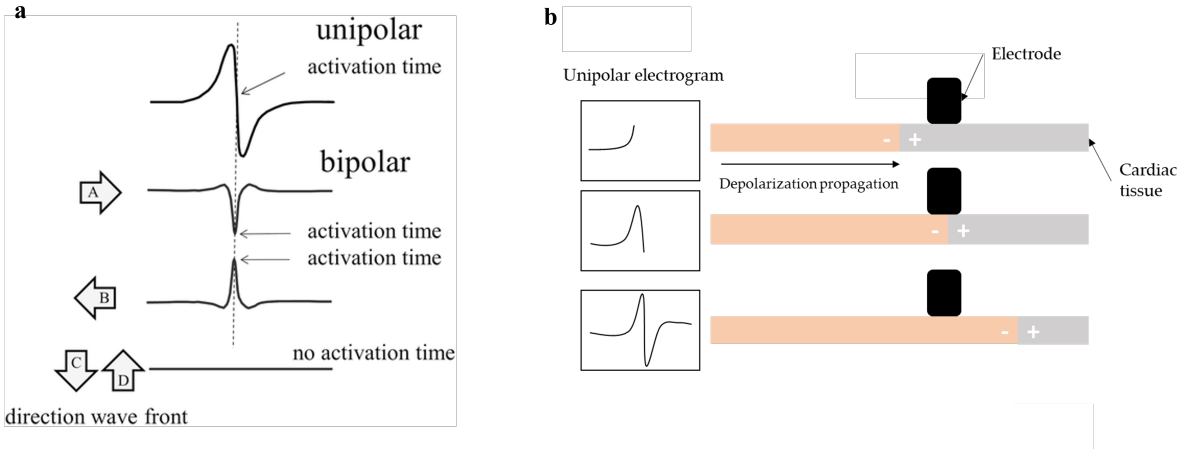

Figure 1.3: Electrograms (EGMs). (a) Unipolar and bipolar EGMs morphology, and their dependency on the wavefront direction [19]. (b) Unipolar EGM recorded by an electrode placed on the cardiac tissue as a depolarizing wave propagates.

For improved interpretability, EGMs can be translated to local activation time (LAT) or voltage maps. These maps display the temporal and spatial distribution of the action potential. The LAT is the time at which the maximum negative time derivative is found in a unipolar EGM, indicating the time at which the cells underneath the electrode activate and depolarize. On the other hand, the voltage is the peak-to-peak

amplitude of the EGM, reflecting tissue conductivity. Lower values are associated with slow conduction which may indicate arrhythmogenic tissue. From this data, the longitudinal and transverse CV vectors and AR can also be derived, when fiber direction information is known [20]. The process of recording epicardial or endocardial EGMs and obtaining the abovementioned maps is commonly referred to as cardiac mapping.

The electrical recordings can be used for research, therapeutic and diagnostic purposes. In research, the analysis of high-resolution epicardial LATs serves to better comprehend the heart's behaviors under diverse clinical conditions. For instance, these recordings are facilitating a deeper exploration of the underlying mechanisms of AF, which continue to be not fully understood. On the therapeutic and diagnostic front, endocardial mapping can help detect arrhythmia onset when integrated into pacemakers and guide clinicians during ablative therapy, ensuring precise and effective treatment approaches [19], [21]. Consequently, the multifaceted utility of electrical recordings in cardiology underscores their significance in improving healthcare.

1.3 Electrophysiological cardiac models

Over the years, mathematical descriptions of the electrical and chemical processes that take place at the molecular, cellular and tissue level have been developed in order to model the spatiotemporal dynamics of healthy and diseased cardiac tissue.

First, ordinary differential equations (ODE) can describe the opening and closing of an ionic channel and the generated ionic flow. Second, several ODEs can be coupled by means of the cell's V_{tm} and the total membrane ionic current flow I_{ion} to replicate cellular behavior. Third, the cardiac tissue can be either modeled as a group of individual cells, resulting in discrete models (e.g. Cellular Automaton model or Coupled Map Lattices), or as a functional syncytium, resulting in continuum models (e.g. Monodomain, Bidomain and Eikonal model). Continuum models, and specifically the reaction-diffusion system approach, are usually the preferred choice to model the action potential propagation [22], [23], [24], [25]. One of these models is the monodomain model which assumes that the intracellular and extracellular domains, separated by a membrane, have equal AR. It uses partial differential equations (PDEs) to model the excitability of the cell (reaction term) and the spatial spreading of the action potential (diffusion term). In such a model, the direction-dependent conductivity properties are represented in the Σ conductivity tensor,

$$\Sigma = \begin{bmatrix} \sigma_{xx} & \sigma_{xy} \\ \sigma_{yx} & \sigma_{yy} \end{bmatrix}, \tag{1.1}$$

where its components are the electrical conductivities σ in different directions. When performing eigenvalue decomposition,

$$\Sigma = \begin{bmatrix} \cos(\theta) & -\sin(\theta) \\ \sin(\theta) & \cos(\theta) \end{bmatrix} \begin{bmatrix} \sigma_l & 0 \\ 0 & \sigma_t \end{bmatrix} \begin{bmatrix} \cos(\theta) & \sin(\theta) \\ -\sin(\theta) & \cos(\theta) \end{bmatrix}, \tag{1.2}$$

the tensor can be decomposed into the eigenvalues, which describe the conductivities in the longitudinal σ_l and transverse σ_t direction, and the eigenvectors, which express the longitudinal and transverse direction with respect to a coordinate system, i.e., the angle between the fiber and the x-axis of the coordinate system θ.

These models can be used to solve the inverse problems, i.e., estimation of the conductivity parameters from EGMs. Differently from CV values, conductivity values directly portray the intrinsic conduction properties of the tissue, holding the potential to improve the diagnosis and treatment of arrhythmias. Some methods have already been developed, such as simultaneous confirmatory factor analysis, [26], compact matrix model [27], one step ahead predictions [28] or personalized inverse eikonal model from cardiac electro-anatomical maps (PIEMAP) [29]. Yet, for accurate estimation, such methods require not only the EGMs but also information on the underlying tissue fiber orientation. Once the conductivity parameters have been estimated, together with the fiber architecture, patient-specific electrophysiological and anatomical models can be created to analyze the tissue electro-pathology, or guide ablation or pacemaker implantation procedures.

1.4 Existing methods for determining the fiber direction

Several imaging techniques to accurately derive the fiber direction in cardiac tissue have been reported over the years, including difussion tensor magnetic resonance imaging, micro-computed tomography, or microscopy imaging [30]. However, these techniques require the use of either bulky and expensive equipment or ionizing radiation, or can only be performed ex vivo. Furthermore, given the significance of fiber direction for estimating conductivity parameters and interpreting EGMs obtained during a cardiac mapping procedure, employing these imaging techniques would require an additional image acquisition procedure prior to cardiac mapping.

Therefore, researchers have focused on developing methods to determine the fiber architecture from EGMs, an overview of the existing approaches can be seen in Table 1.1 [20], [22], [29], [31], [32], [33], [34]. The methods vary according to the type of parameter used as a surrogate for the fiber direction, such as isopotentials, isochrones, or CV vectors, the number of data points required for estimation, and the spatial resolution. For a more comprehensive understanding of the existing methods we refer to the literature review carried out prior to this thesis (Appendix A).

Table 1.1: Summary table of the methods proposed to derive the fiber direction from EGMs: author, description of the methods, evaluation setup and results of evaluation experiments [20], [22], [29], [31], [32], [33], [34]. The methods are chronologically ordered from top to bottom according to the publication date.

Author	Method	Validation setup	Absolute mean error of fiber direction estimation
Taccardi *et al.*	Potential maxima [31]	Monodomain model and 3D tissue block with rotating fiber orientation	4.6 ± 0.8°
Muzikant *et al.*	Ellipse fitting to stimulus isopotential [22]	Monodomain model and 3D tissue block with rotating fiber orientation	4.7 ± 1.5°
	Ellipse fitting to 1.5 ms isochrone [22]	Monodomain model and 3D tissue block with rotating fiber orientation	3.7 ± 0.8°
Houben *et al.*	Ellipse fitting to local CV vectors (PSF) [32]	EGM from pectinate muscles	<2°
Linnenbank *et al.*	Average CV vector method [33]	N.A.	N.A.
Roney *et al.*	Linear transformation from elliptical to circular wavefront [20]	Monodomain model with atrial MRI scan and fiber atlas (endocardium)	24.78 ± 2.37°
	Ellipse fitting to local CV vectors (Geometrical Model) [20]	Monodomain model with atrial MRI scan and fiber atlas (endocardium)	11.53 ± 0.73°
Grandits *et al.* and Lubrecht *et al.*	Personalized Inverse Eional Model from cardiac Electro-Anatomical maps [29]	Eikonal model with atrial MRI scan and fiber atlas (endocardium)	38.88 ± 0.84°
De Vries *et al.*	Ellipse fitting to conduction slowness vectors [34]	Monodomain model and 2D surface	<3°

As observed in Table 1.1, each method has been evaluated under very different conditions, which differ depending on the model used to generate the data (monodomain model, eikonal model, or human heart), the complexity of the model (2D or 3D), the type of recording (endocardial or epicardial), the anatomical location in

which the electrodes are placed (fiber homogeneity or heterogeneity), and the electrode array used (number of electrodes and spacing between the electrodes). Hence, in order to identify the best approach and further improve it, it is necessary to compare the methods under the same conditions. This will be the primary goal of this project.

1.5 Problem statement

Patient-specific models have emerged as important tools in the study of cardiac electrophysiology. Given the influence of fiber direction in the conduction of electrical impulses, the incorporation of the wall fiber architecture into these models will not only enable accurate electrical behavior simulations and predictions but also facilitate the estimation of conductivity parameters. This would help in increasing our understanding of arrhythmia mechanisms, including AF, and enhancing the diagnosis and treatment of electropathologies. Numerous approaches for deriving the tissue fiber direction from EGMs have been developed over the years. Nevertheless, these methods have been validated under diverse yet overly simplified conditions, hampering the selection of the most suitable method for clinical and research applications. The ultimate aim is to identify and improve the most robust and effective approach, evaluating them with synthetic and clinical epicardial recordings, in order to be used for research, diagnosis, and treatment of cardiac electropathologies.

1.6 Thesis outline

To find the best approach for estimating the fiber direction from EGMs, several tests with synthetic and clinical data have been performed and will be described in this report following the structure explained hereafter.

First, the methods employed to carry out the experiments will be described in Chapter 2. This includes a description of the implementation of the existing fiber direction estimation methods (Section 2.1) followed by an explanation of the applied modifications for standardization and accuracy enhancement (Section 2.1.2 and 2.1.3). The chapter ends with a description of the models used to generate the data for the comparison analysis. Both synthetic data, generated with a monodomain 3D cardiac model (Section 2.2), and clinical data, recorded from patients undergoing open heart surgery (Section 2.3), are used . In Chapter 3, the influence of the 3D structure of the cardiac model on the epicardial EGMs will be shown (Section 3.1), as well as the results of the comparison analysis in synthetic (Section 3.2) and clinical (Section 3.3) data. These outcomes will be further discussed in Chapter 4, ending with a proposal on the most accurate fiber direction estimation method for clinical and research applications (Section 4.4). The report is finalized with some concluding remarks and steps to be taken in the future (Chapter 5).

2 Methods

This chapter will describe the implementation of the fiber direction estimation methods as they were described by their authors and after being modified for comparison analysis and optimization. The chapter ends with an explanation of the different cardiac models used to generate the EGMs and LAT maps for evaluating the estimation methods.

2.1 Methods for estimating the fiber direction from EGMs

Several techniques to derive the fiber direction from EGMs have been reported over the years, which vary according to the parameters considered surrogates of the fiber direction and the spatial resolution. While the methods in question also vary in their utilization of endocardial or epicardial recordings, the primary emphasis of this study is on deriving the epicardial fiber direction using epicardial EGMs. The results can then be extended to endocardial recordings.

All the fiber estimation methods require either one or multiple LAT or voltage maps to derive the fiber direction. The former is generated by taking the steepest downslope in the unipolar EGMs, and indicates the time at which the depolarization wavefront reaches the cells underneath the electrode. The latter is generated by taking the voltage measurements recorded by the electrodes at a particular time instance, i.e. the amplitude of the EGMs at a specific point in time. Subsequently, the values recorded by the entire electrode array are organized into an M_x x M_y matrix.

Moreover, the parameter of interest, estimated by all methods, is the angle between the longitudinal axis of the epicardial fiber or group of fibers and the x-axis. As a result, these methods can be classified based on whether they yield a single angle estimate for the entire M_x x M_y map, denoted as the global fiber direction, or one angle estimate for each individual electrode, generating M_x x M_y = M angle estimates, referred to as the local fiber direction.

Table 2.1 presents the authors and approaches of the fiber direction estimation techniques, along with the designated terminology to be used henceforth for each respective method. The first five methods derive the global fiber direction, whereas the last four methods determine the local fiber direction.

This project started with an evaluation of the different methodologies according to the specifications outlined by their original authors. Following this, the best-performing approaches were standardized to have the same spatial resolution and use an identical quantity of data points for a consistent performance analysis. Hence, the methods were adjusted to estimate a global fiber direction and to make use of a larger dataset or incorporate endocardial information. Finally, some methods were altered to provide the local fiber direction.

2.1.1 Existing methods for estimating the fiber direction

Nine distinct approaches have been described previously in the literature, whose algorithmic and implementation details will be described hereunder. First, the methods

Table 2.1: Authors, approaches, and names of the existing methods to derive the fiber direction from epicardial EGMs [20], [22], [29], [31], [32], [33], [34].

Author	Method approach	Resolution	Abbreviation
Taccardi *et al.*	Potential maxima	Global	PM
Muzikant *et al.*	Ellipse fitting to stimulus isopotential	Global	EIP
	Ellipse fitting to 1.5 ms isochrone	Global	EIC
Linnenbank *et al.*	Average CV vector method	Global	ACV
de Vries *et al.*	Ellipse fitting to conduction slowness vectors	Global	ECS
Houben *et al.*	Ellipse fitting to local CV vectors (PSF)	Local	ECVPSF
Roney *et al.*	Linear transformation from elliptical to circular wavefront	Local	LTEC
	Ellipse fitting to local CV vectors (Geometric Model)	Local	ECVGM
Grandits *et al.* and Lubrecht *et al.*	Personalized Inverse Eikonal Model from cardiac Electro-Anatomical maps	Local	PIEMAP

that derive the global fiber direction will be described (PM, EIP, EIC, ACV and ECS) followed by the methods that give a local fiber direction (ECVPSF, LTEC, ECVGM and PIEMAP).

2.1.1.1 Potential Maxima (PM)

The PM method employs the potential distribution recorded 10 ms after epicardial pacing for the estimation of the fiber direction [31]. The fiber direction is obtained from the orientation of the line joining the two positive voltage maxima present at either side of the pacing side. Consequently, a global fiber direction is found. Since not all the recordings show a positive voltage at the same instant, the time elapsed between stimulus and measurement is either increased or decreased by a few milliseconds for each map.

2.1.1.2 Ellipse fitting to stimulus isopotential (EIP)

The second method assessed was described by Muzikant *et al.*, in which isopotentials are fitted to an ellipse using a least-squares (LS) error approach [22]. First, the 5 mV isopotential is found from the potential pattern at the earliest activation time using the contour function in MATLAB, after which an ellipse is fitted. Since Muzikant *et al.* did not specify a particular LS ellipse fitting approach, the equations provided by Hart *et al.* and de Vries *et al.* were used [35] [34]. Hence, the ellipse is parameterized using the following equation,

$$p_1 x^2 + p_2 xy + p_3 y^2 = 1, \tag{2.1}$$

where p_1, p_2 and p_3 are unknown coefficients defining the ellipse geometry and x and y are the cartesian coordinates of the ispotential. The ellipse coefficients are grouped into a row vector $\boldsymbol{p}$ and the N cartesian coordinates of the isopotential into a matrix $\boldsymbol{A}$, such that

$$\boldsymbol{A} = \begin{bmatrix} x_1^2 & x_1 y_1 & y_1^2 \\ \vdots & \vdots & \vdots \\ x_N^2 & x_N y_N & y_N^2 \end{bmatrix}. \tag{2.2}$$

Hence, the fitting problem can be formulated as

$$\min_{\boldsymbol{p}} \|\boldsymbol{A}\boldsymbol{p} - \mathbf{1}\|_2^2, \tag{2.3}$$

which can be solved using the LS technique, as follows,

$$\boldsymbol{p} = \boldsymbol{A}^{\dagger}\mathbf{1}. \tag{2.4}$$

The Moore-Penrose pseudoinverse $\boldsymbol{A}^{\dagger}$ is used as $\boldsymbol{A}$ is generally non-invertible. From the coefficients, the rotation angle of the ellipse θ is obtained using,

$$\theta = \arctan\left(\frac{p_3 - p_1 - \sqrt{(p_2 - p_1)^2 + p_2^2}}{p_2}\right). \tag{2.5}$$

This angle, indicative of the longitudinal conduction direction, is considered to be the orientation of the fibers within the epicardial region from which the voltage map is obtained.

2.1.1.3 Ellipse fitting to 1.5 ms isochrone (EIC)

Similarly to the isopotential approach, in this method, MATLAB's contour function is used to find the isochrones from the recorded LAT maps [36]. The 1.5 ms isochrone displays an elliptical shape centered around the stimulation location. To define this form, the orientation and dimensions of the ellipse's major axis are determined. The major axis is identified as the line connecting the two farthest points on opposite sides of the pacing site within the isochrone. The orientation of this line corresponds to the direction of the underlying fibers.

2.1.1.4 Average CV vector method (ACV)

Deriving the fiber direction using the Average CV Vector method involves computing the CV vectors at each electrode location by applying the polynomial surface fitting (PSF) technique to a 3-by-3 electrode subgrid [33]. To accomplish this, a quadratic surface is fitted to nine neighboring LATs using the LS technique, defined as,

$$T(x, y) = ax^2 + by^2 + cxy + dx + ey + f, \tag{2.6}$$

where x and y are the coordinates indicating the electrode position and $T(x, y)$ the LAT value of that same electrode. Following the estimation of the surface coefficients using LS (Equations (2.3) and (2.4)), the LATs within the subgrid are recalculated using the surface equation presented earlier (Equation (2.6)). Subsequently, the CV vector at the mth electrode in the subgrid's center, denoted as $\boldsymbol{v_m}$, is determined from the gradient of the fitted surface as follows,

$$\boldsymbol{v_m} = \begin{bmatrix} \frac{dx}{dT} \\ \frac{dy}{dT} \end{bmatrix} = \begin{bmatrix} \frac{T_x}{T_x^2 + T_y^2} \\ \frac{T_y}{T_x^2 + T_y^2} \end{bmatrix}, \tag{2.7}$$

where $T_x = \partial T/\partial x$ and $T_y = \partial T/\partial y$. For more information on the PSF technique and the derivation of Equation (2.7), we refer to [37].

Once all the $\boldsymbol{v_m}$ are computed they are grouped into ten bins according to their direction. The direction of the bin with the greatest average CV magnitude is considered as the tissue's global fiber direction underneath the electrode array.

2.1.1.5 Ellipse fitting to conduction slowness vectors (ECS)

The method proposed by de Vries *et al.* consists of fitting an ellipse to the reciprocal of the CV vector, known as the conduction slowness (CS) vector [34]. The CS vectors are calculated at each electrode computing the gradient of the LAT map, and the set of values from a single LAT map are projected into the CS space. The coordinates of the CS vectors in the slowness space are fitted to the ellipse equation as in previous methods, using Equations (2.1) and (2.4). The major axis of the ellipse corresponds to the direction of the slowest conduction, hence, the resulting angle should be rotated by $\pi/2$ rad to find the direction of the fastest conduction, indicative of the fiber direction.

2.1.1.6 Ellipse fitting to local CV vectors computed through Polynomial Surface Fitting (ECVPSF)

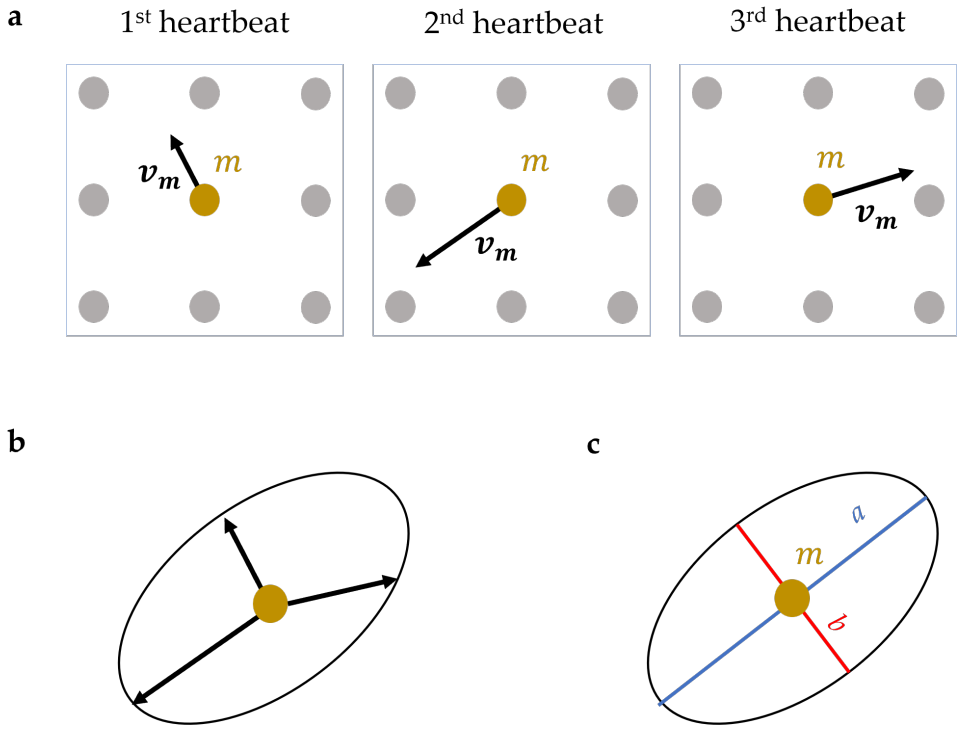

Figure 2.1: Steps in the ECVPSF method proposed by Houben *et al.* [32]. (a) The local CV vectors are computed for each electrode in different LAT maps using the polynomial surface fitting (PSF) approach. (b) An ellipse is fitted to the local CV vectors of different LAT maps but the same electrode location. (c) The long axis, a, and short axis, b, of the fitted ellipse indicate the longitudinal and transverse direction of the fibers, respectively.

In the technique proposed by Houben *et al.*, the local CV vectors v_m are derived by means of the PSF technique, as in the ACV method (Equations (2.6) and (2.7)) [32]. CV vector maps are generated for three LAT maps, all recorded at the same location but corresponding to consecutive heartbeats (Figure 2.1 (a)). Afterward, an ellipse is fitted into the set of local CV vectors (Figure 2.1 (b)), associated with the same electrode but different heartbeats, using the previously outlined LS method (Equations (2.1) and (2.4)). The orientation of the ellipse's major axis a is taken as the fiber direction, yielding an angle estimate for each electrode, i.e., local fiber direction (Figure 2.1 (c)). Figure 2.1 illustrates a schematic representation of the various stages involved in the described methodology.

2.1.1.7 Linear transformation from elliptical to circular wavefront (LTEC)

In this approach, the fiber orientation is obtained by mapping an elliptical wavefront into a circular wavefront, from which the local CV vectors can be computed. The anisotropy of the tissue will result in a faster propagation in one direction than the other, hence, the wavefront adopts an elliptical shape instead of a circular shape.

All the equations employed to accomplish this linear transformation can be referenced in the work by Roney *et al.* [20].

First, the spatial coordinates of the mth measuring location are subjected to a linear transformation from an elliptical wave, denoted as x_m and y_m, to a circular wave, represented as $\hat{x}_m$ and $\hat{y}_m$,

$$\hat{x}_m - \hat{x}_0 = (x_m - x_0)\cos\theta + (y_m - y_0)\sin\theta, \tag{2.8}$$

$$\hat{y}_m - \hat{y}_0 = \frac{CV_L}{CV_T}((y_m - y_0)\cos\theta + (x_m - x_0)\sin\theta), \tag{2.9}$$

where x_0 and y_0, and $\hat{x}_0$ and $\hat{y}_0$ are the original and transformed coordinates of the wavefront source, respectively. The orientation of the ellipse is denoted by θ, and CV_L and CV_T are the longitudinal and transversal CV magnitudes, respectively. Considering $\hat{X}_m = \hat{x}_m - \hat{x}_0$ and $\hat{Y}_m = \hat{y}_m - \hat{y}_0$, the circular wavefront can be modeled as,

$$t_m = T + \frac{1}{v}\sqrt{\hat{d}_0^2 + 2\hat{d}_0(\cos\phi_0\hat{X}_m + \hat{d}_0\sin\phi_0\hat{Y}_m) + \hat{X}_m^2 + \hat{Y}_m^2}. \tag{2.10}$$

Hence, the activation time at the measuring location t_m depends on the activation time of the source T, the angle between the x-axis and the line joining the source and the first measuring point ϕ_0, the velocity of the wavefront v, and the radius of curvature of the wavefront $\hat{d}_0$. Replacing the transformed coordinates with the known coordinates, the following equation is obtained,

$$t_m = \gamma_0 + \gamma_1 \begin{bmatrix} (\gamma_2^2 + \gamma_3^2) + 2\gamma_2(\sqrt{1-\gamma_5^2}X_m + \gamma_5 Y_m) \\ +2\gamma_3(\gamma_4\sqrt{1-\gamma_5^2}Y_m - \gamma_y\gamma_5 X_m) \\ (\sqrt{1-\gamma_5^2}X_m + \gamma_5 Y_m)^2 + (\gamma_4\sqrt{1-\gamma_5^2}X_m + \gamma_4\gamma_5 Y_m)^2, \end{bmatrix}^{1/2} \tag{2.11}$$

where $\boldsymbol{\gamma} = [T, \frac{1}{CV_L}, \hat{d}_0\cos\theta, \hat{d}_0\sin\theta, \frac{CV_L}{CV_T}, sin\theta]^T$. The model is solved for $\boldsymbol{\gamma}$ through a nonlinear LS approach, using the inbuilt lsqnonlin function in MATLAB. This function demands an initial guess of $\boldsymbol{\gamma}$, which was derived from an initial fit with the planar wavefront model,

$$t_m = T + v^{-1}\cos\phi_0 X_m + v^{-1}\sin\phi_0 Y_m. \tag{2.12}$$

By isolating the variable θ from $\boldsymbol{\gamma}$, the orientation of the fiber direction underneath the electrode under study is obtained.

2.1.1.8 Ellipse fitting to local CV vectors computed with a wavefront geometry model (ECVGM)

In this method, the planar wavefront model (Equation (2.12)) is used to compute the local CV vectors across three distinct LAT maps with varying wavefront source locations, obtained after pacing or from different heartbeats. Subsequently, similar to the ECVPSF technique, an ellipse is geometrically fitted to three local CV vectors at the same locations obtained from different LAT maps through LS (Equations (2.1) and (2.4)). The orientation of the ellipse's major axis (Equation (2.5)) is taken as the tissue's fiber direction under the analyzed electrode.

2.1.1.9 Personalized Inverse Eikonal Model from cardiac Electro-Anatomical Maps (PIEMAP)

The PIEMAP method, consists in solving the inverse problem to obtain the conductivity tensor. First, the anisotropic Eikonal Model equations of the form

$$\begin{cases} \sqrt{\nabla_S u \ \mathbf{\Sigma} \ \nabla_S u} = 1, \quad in \ \boldsymbol{x} \in \Omega \\ u(\boldsymbol{x}_0) = 0 \end{cases} \tag{2.13}$$

were implemented in MATLAB. In this equation, Ω denotes the myocardium surface, ∇_S the surface gradient, u the spread of activation, $\boldsymbol{x}_0$ the source site, and $\mathbf{\Sigma}$ the conductivity tensor at a specific location. The latter is acquired by minimizing the error between the measured data and the output from the eikonal model in the LS sense, using a Primal-Dual optimization algorithm as explained by Chambolle *et al.* [38]. Thus, the following problem is solved,

$$\min_{\mathbf{\Sigma}} \frac{1}{2} \sum_{i=1}^{N} (FIM_{\mathbf{\Sigma}}(\boldsymbol{x}_i) - t_i)^2 + \lambda R(\mathbf{\Sigma}), \tag{2.14}$$

where $FIM_{\mathbf{\Sigma}}(\boldsymbol{x}_i)$ is the numerical solution to the eikonal equation (Equation (2.13)) at a specific location $\boldsymbol{x}_i$ and $R(\mathbf{\Sigma})$ is a regularization term. Once the conductivity tensor $\mathbf{\Sigma}$ is found for each electrode, it undergoes an eigenvalue decomposition, shown in Equation (1.2). The direction of the eigenvector with the largest eigenvalue is taken as the fiber direction of the tissue under the electrode.

2.1.2 Methods for estimating the global fiber direction

Following the assessment of the methods in their original forms (see Section 3.2.1), the best-performing methods were adjusted to be able to compare them under equal circumstances, this is, to estimate a global fiber direction from a cluster of M electrodes. The subsequent step entailed evaluating the impact of enlarging the input dataset, both spatially, utilizing additional electrodes and temporally, employing more than one LAT map, obtained from different heartbeats. Afterward, the most effective techniques were further improved by incorporating prior knowledge concerning the wall structure of the tissue region under study.

2.1.2.1 Adaption to output a global fiber direction from a single LAT map

The EIC, ECS, ECVPSF, ECVGM methods in their original implementation showed the lowest mean fiber direction estimation error when evaluated with synthetic data. The former two mentioned techniques already yielded a global fiber direction estimate, whereas the latter two approaches needed to be modified in order to do so. To

differentiate them from their original version, we will add the letter G, from *'Global'*, as a subscript to the abbreviation of each modified method.

The ECVPSF approach, which involved fitting an ellipse to local CS vectors, was adapted to be aligned with the ECS method. After computing the local CV vectors using PSF, they were projected into the CV space, and their coordinates were fitted to an ellipse through LS (Equations (2.1) and (2.4)). The resultant orientation of the ellipse's long axis indicated the fiber direction. The same approach was used for the ECVGM, although in this case, the local CV vectors were generated by solving the planar wavefront model (Equation (2.12)).

Despite not being among the top-performing methods, the PIEMAP approach was also further assessed due to its high resolution. This method was adapted using two distinct approaches termed PIEMAP_G (*Average Angle*) and PIEMAP_G (*Average Conductivity tensor*). In the first approach, the local fiber orientation was computed with the original PIEMAP implementation, and the angular mean of these values was taken as the global fiber direction. In the second approach, the average tensor of all the local conductivity tensors was subjected to eigenvalue decomposition. The direction of the eigenvector with the largest eigenvalue was considered the global fiber direction.

2.1.2.2 Adaption to use a larger input dataset

Based on the outcomes obtained when comparing the global fiber direction estimation methods (see Section 3.2.2), the ECVPSF_G, ECVGM_G and ECS methods were further assessed when they use, on the one hand, one single LAT map with a larger number of M electrodes and on the other hand, multiple LAT maps from consecutive heartbeats.

To evaluate the impact of varying the number of M electrodes, the methods did not undergo any additional modification. To make use of additional LAT maps, the local CS or CV vectors of all the maps used are projected into the CS and CV space. After which, one ellipse is fitted to all the data points and the long axis' orientation of this single ellipse indicates the fiber direction. We will refer to this approach as *All Vectors* approach. Other ways of employing several LAT maps were also evaluated, but, as they did not significantly and consistently reduce the estimation error, they will not be further discussed (see Figure B.1).

2.1.2.3 Adaption to incorporate prior knowledge

As evidenced by the LAT maps recorded from regions of the heart where the fibers in the epicardium run perpendicular to the ones in the endocardium, the epicardial measurements contain information on the propagation of the electrical signal in the underlying layers as well [31], [22]. Hence, the epicardial fiber direction estimation could be improved if the methods would account for the transmural signal propagation. To evaluate this, it was considered that when the epicardium is stimulated, the epicardial EGMs will predominantly reflect the signal propagation in the epicardium. Hence, the estimated fiber direction $\hat{\theta}_{epi}$ would align closely to the true epicardial fiber direction θ_{epi},

$$\hat{\theta}_{epi} = \theta_{epi} - \varepsilon, \tag{2.15}$$

where ε is the estimation error associated with the effect of endocardial signal propagation on epicardial maps. Conversely, when the endocardium is stimulated the

endocardial EGMs will predominantly reflect the signal propagation in the endocardium, but the estimated endocardial fiber direction $\hat{\theta}_{endo}$ from these EGMs will also be affected by the epicardial signal propagation. If it is assumed that the absolute error associated with estimating $\hat{\theta}_{epi}$ and $\hat{\theta}_{endo}$ is equal, and that the the endocardium and epicardium have a perpendicular fiber orientation, with a CCW rotation from the epicardium to the endocardium, the following correction can be applied to the epicardial fiber direction estimate $\hat{\theta}_{epi}$,

$$\hat{\theta}_{epi,corrected} = \hat{\theta}_{epi} - \frac{\hat{\theta}_{epi} - \hat{\theta}_{endo} + \frac{\pi}{2}}{2}, \tag{2.16}$$

which can be rewritten as,

$$\hat{\theta}_{epi,corrected} = \frac{\hat{\theta}_{epi} + (\hat{\theta}_{endo} - \frac{\pi}{2})}{2}. \tag{2.17}$$

Alternatively, given that simultaneous endocardial and epicardial measurements are challenging in a clinical setting, the $\hat{\theta}_{endo}$ could be estimated from epicardial recordings obtained after endocardial stimulation. Only the global fiber direction estimation methods with the lowest mean estimation error, ECS, ECVPSF_G and ECVGM_G, were adapted to incorporate this information.

2.1.3 Methods for estimating the local fiber direction

Four different methods that yield a high-resolution fiber direction map were compared. The ECVPSF, ECVGM and PIEMAP already output one single angle value for each electrode location. Yet, a fourth method, ECS, was adapted to estimate the local fiber direction. Such modification, analogous to the ECVPSF but with CS vectors instead of CV, consisted of fitting an ellipse to the three CS vectors from three distinct LAT maps, but the same electrode. The modified version of the ECS method will be referred to as ECS_L.

2.2 Experiments on synthetic data

2.2.1 Electrophysiological cardiac model

To generate the synthetic epicardial EGMs and LAT maps an electrophysiological model of the heart was used. The action potential of one individual cell n was modeled using the Courtemanche ionic current model [39], and the propagation of this action potential between neighboring cells was emulated using the monodomain model, based on a reaction-diffusion equation,

$$\beta^{-1}\nabla \cdot \mathbf{\Sigma}_n \nabla V_{tm,n} = C\frac{dV_{tm,n}}{dt} - I_{ion,n} + I_{st,n}. \tag{2.18}$$

In this model, the transmembrane current density $I_{tm,n}$, defined by $\beta^{-1}\nabla \cdot \Sigma_n \nabla V_{tm,n}$ depends on the surface-to-volume ratio β, the conductivity tensor Σ_n and the change in the transmembrane voltage $V_{tm,n}$, and is equal to the capacitive current $C\frac{dV_{tm,n}}{dt}$, the ionic current $I_{ion,n}$ and the stimulus current $I_{st,n}$. Considering the electrical signal propagation in the x, y and z direction a 3D cardiac model with axially symmetric anisotropy, i.e., equal conductivity in both orthogonal directions to the fiber direction,

was generated. Hence, the eigenvalue decomposition of the conductivity tensor for one cell, which was previously described in Equation (1.2), expands to,

$$\mathbf{\Sigma}_n = \begin{bmatrix} \cos(\theta_n) & -\sin(\theta_n) & 0 \\ \sin(\theta_n) & \cos(\theta_n) & 0 \\ 0 & 0 & 1 \end{bmatrix} \begin{bmatrix} \sigma_{l,n} & 0 & 0 \\ 0 & \sigma_{t,n} & 0 \\ 0 & 0 & \sigma_{t,n} \end{bmatrix} \begin{bmatrix} \cos(\theta_n) & \sin(\theta_n) & 0 \\ -\sin(\theta_n) & \cos(\theta_n) & 0 \\ 0 & 0 & 1 \end{bmatrix}. \quad (2.19)$$

The model could be adapted to represent different conduction properties and variable transmural fiber orientation distribution, as found in the different regions of the human heart [6].

The potential recorded by electrodes was derived using a unipolar EGM model, based on the current source approximation for a large-volume conductor [40]. This model assumes that the potential ϕ_m recorded by the mth electrode will depend on a weighted sum of the transmembrane voltages generated by its surrounding N cells, such that,

$$\phi_m = \frac{\Delta x \Delta y}{4\pi\sigma_e} \sum_{n=1}^{N} \frac{I_{tm,n}}{r_{m,n}}, \quad (2.20)$$

where Δx and Δy is the distance between the cells in the x and y-axis, respectively, σ_e is the extracellular conductivity, $I_{tm,n}$ is the transmembrane current density in the nth cell, and $r_{m,n}$ is the distance from the nth cell to the mth electrode.

2.2.2 Datasets and evaluation of the method's performance

The performance of each existing fiber orientation estimation method has previously been assessed in simple and distinct cardiac tissue models. Hence, the aim of this project was to evaluate and compare performance within a consistent and highly realistic atrial and ventricular wall model, taking into account the three-dimensional nature of the tissue and incorporating the structural heterogeneity observed across various regions of the heart.

Therefore, four datasets were generated corresponding to four different tissue types with axially symmetric anisotropy and homogeneous conductivity in one layer. All the models had the same longitudinal conductivity (σ_l = 1.2 nS/μm/pF), anisotropy ratio ($\alpha = \sigma_l/\sigma_t$ = 5), extracellular conductivity (σ_e = 1.1 nS/μm/pF), capacitance (C = 1 μ/cm^2), distance between cells in the x, y, and z direction (Δx, Δy, Δz = 100 μm), number of cells in one layer (N_x x N_y = 140 x 140), surface-to-volume ratio (β = 0.24 μm^{-1}), stimulation current (I_{st} = 40 pA/pF), stimulation time (Δt_{st} = 2 ms) and heart beat duration (Δt_{beat} = 1 s). In the case of a 3D tissue slab, the heart was simulated with ten cell layers ($N_z = 10$), resulting in a 1 mm thick tissue model. The values were chosen based on described monodomain cardiac tissue models [27], [26], [36].

Moreover, to replicate the clinical set-up at Erasmus Medical Center (EMC), the recording electrodes were placed 1 mm above the tissue surface with an interelectrode distance of 2 mm, resulting in the electrical activity of a 14 x 14 mm^2 tissue area being recorded from an 8 x 8 electrode array. Given the wide range of morphological variations present in the epicardial EGMs, automatically generating LAT maps from EGMs affected the quality and reliability of the LAT maps subsequently influencing the accuracy of the estimation methods. To mitigate this issue, the actual activation

time of the cell located at the electrode location was taken as the activation time of the electrode, generating an 8 x 8 LAT map.

The assessment of the methods was conducted on datasets generated from four distinct models:

- *2D configuration*: a simplified 2D heart model consisting of a single layer comprising 140 x 140 cells, with a homogeneous fiber direction.
- *Unimodal configuration*: a 3D tissue slab model characterized by uniform fiber direction spanning ten layers. This configuration mimicked the arrangement of parallel fibers seen in structures like Bachmann's bundle [6].
- *Bilayer configuration*: a 3D tissue slab model emulating the bilayer structure found in specific regions of the atria [6]. Here, all the fibers in the lower five layers had the same orientation but were perpendicular to the fibers in the upper five layers, creating a bilayered configuration.
- *Transmural fiber rotation configuration*: a 3D tissue slab model with each of the ten layers having a different fiber orientation. The epicardial layer had fibers perpendicular to those in the endocardial layer, and the fibers underwent a CCW rotation from the epicardium to the endocardium. This setup replicated the structural characteristics of ventricular walls [31].

Fiber direction was homogeneous within each layer, however, a total of 36 maps were generated with diverse fiber directions and stimulation sites for each wall configuration. The evaluation of the methods' ability to estimate the epicardial fiber angle relative to the x-axis was conducted using metrics such as mean absolute error (MAE), maximum non-outlier absolute error, and minimum non-outlier absolute error. The MAE gives the absolute difference between the estimated $\hat{\theta}_i$ and true θ angle across k number of estimations, and take values between 0^o and 90^o,

$$MAE = \frac{1}{k}\sum_{i=1}^{k}|\hat{\theta}_i - \theta|. \tag{2.21}$$

The maximum and minimum non-outlier absolute errors give an indication of the range of uncertainty of the estimation, which as with the MAE, should be low for well-performing methods. An outlier is defined as an error value that is more than three scaled median absolute deviations from the median error.

2.3 Experiments on clinical data

The performance of the methods was also evaluated on clinical data, provided by the Cardiology Translational Electrophysiology group at EMC. The epicardial EGMs were recorded from the atria and ventricles of adult patients with aortic valve or coronary artery disease who underwent open heart surgery. All the measurements were taken under different study protocols approved by the Medical Ethics Committee in the EMC and after obtaining informed consent from the patient. An 8 x 24 unipolar custom-made electrode array, with an inter-electrode distance of 2 mm was used, as seen in Figure 2.2. The obtained EGM signals underwent amplification, filtering (bandwidth 0.5 to 400 Hz), sampling (1 kHz), and analog-to-digital conversion (16 bits) processes. Afterward, the EGMs were manually annotated using the steepest

descent approach, by researchers from the EMC Cardiology Translational Electrophysiology research group. Finally, the LAT maps were processed by removing and replacing outliers through shape-preserving piecewise cubic spline interpolation.

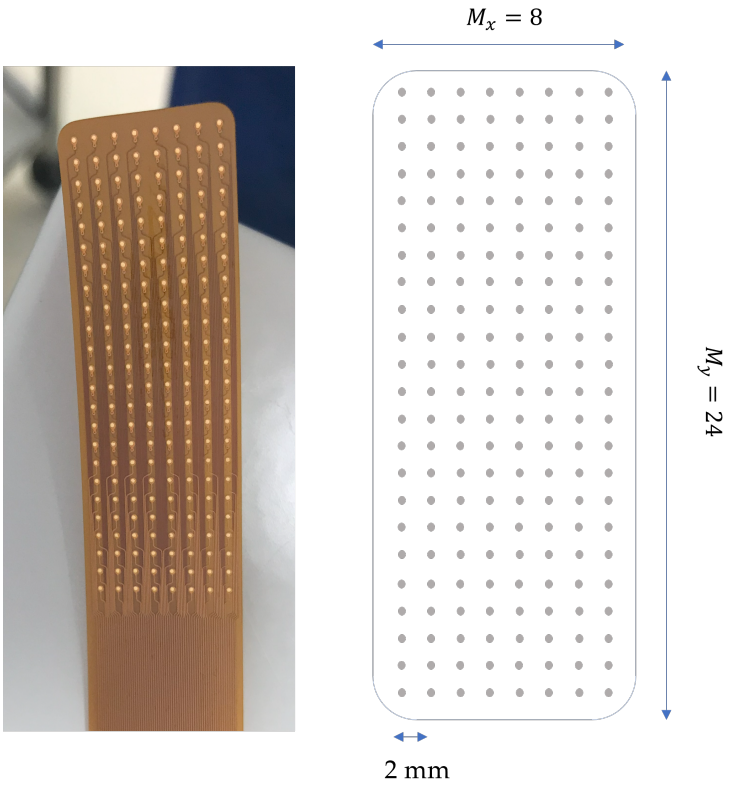

Figure 2.2: Unipolar electrode array used for mapping, composed of 8 x 24 electrodes with a 2 mm separation.

2.3.1 Datasets and evaluation of the method's performance

The data used to evaluate the method's performance correspond to recordings obtained during sinus rhythm from three different locations with varying fiber architecture: BB, the inferior side of the RA and the RV. In such a way, the BB location matches the unimodal configuration, the RA of the bilayer configuration, and the RV of the transmural fiber rotation configuration. Furthermore, the methods were also evaluated in scenarios with more complex activation patterns by employing recordings from BB acquired during AF and from pacing from three distinct sites: the LA appendage (LAA), the RA appendage (RAA), and the inferior RA (RAinf). The mapping scheme is shown in Figure 2.3.

Since no reference fiber orientation was obtained, the methods' variability was assessed by the extent of change in estimates obtained from LAT maps acquired during different heartbeats but at identical mapping locations. Moreover, based on a fiber atlas and the exact position and orientation of the mapping array, some assumptions could be made regarding the underlying fiber orientation. This facilitated an assessment of the methods' accuracy. The fiber direction within the BB, RA and RV were assumed to be 90º, 90º, and 0º, respectively.

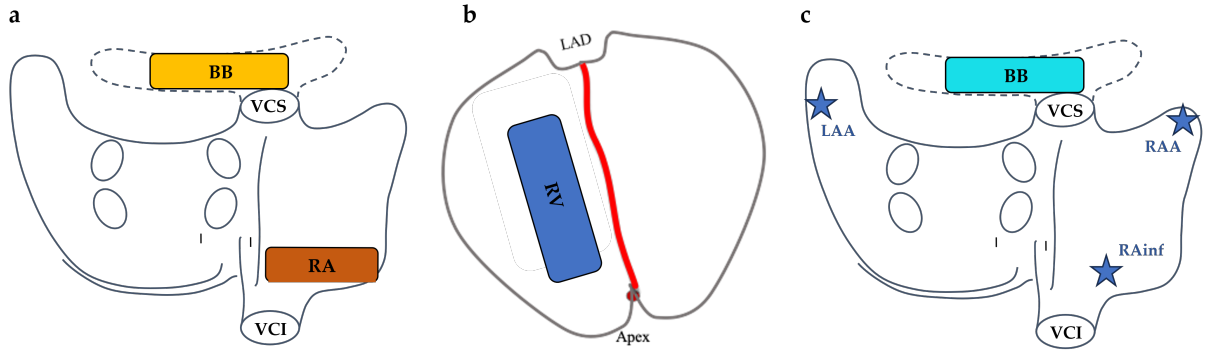

Figure 2.3: Mapping locations in the human heart. (a) The Buchmann's bundle (BB) and the right atria (RA). (b) The right ventricle (RV). (c) The Bachmann's bundle (BB) after stimulation in three distinct locations indicated with a star: the LA appendage (LAA), the RA appendage (RAA), and the inferior RA (RAinf).

3 Results

3.1 Electrophysiological cardiac model

First, to verify that the 3D monodomain model portrayed the reality, assess the influence of underlying layers in the epicardial measurements, and better interpret the outcome of the estimation methods, the EGMs and LAT maps generated by four different cardiac models, 2D, unimodal, bilayer and transmural fiber rotation configuration, were analyzed. In all cases, the signals were generated with the epicardial fibers of the cardiac tissue model oriented at a 0^o angle relative to the x-axis.

3.1.1 3D models of the cardiac wall

The epicardial EGMs recorded by three electrodes positioned at varying distances from the stimulation point, located at the top left corner of the epicardial layer or position (1, 1), are shown in Figure 3.1. From this figure, it can be seen that the EGMs recorded at the point of stimulation consists of solely an S-wave (negative deflection), whereas when the electrode is further away, it only records an R-wave (positive deflection). The electrode in the middle of the tissue records the cleanest signal, with an R-S morphology.

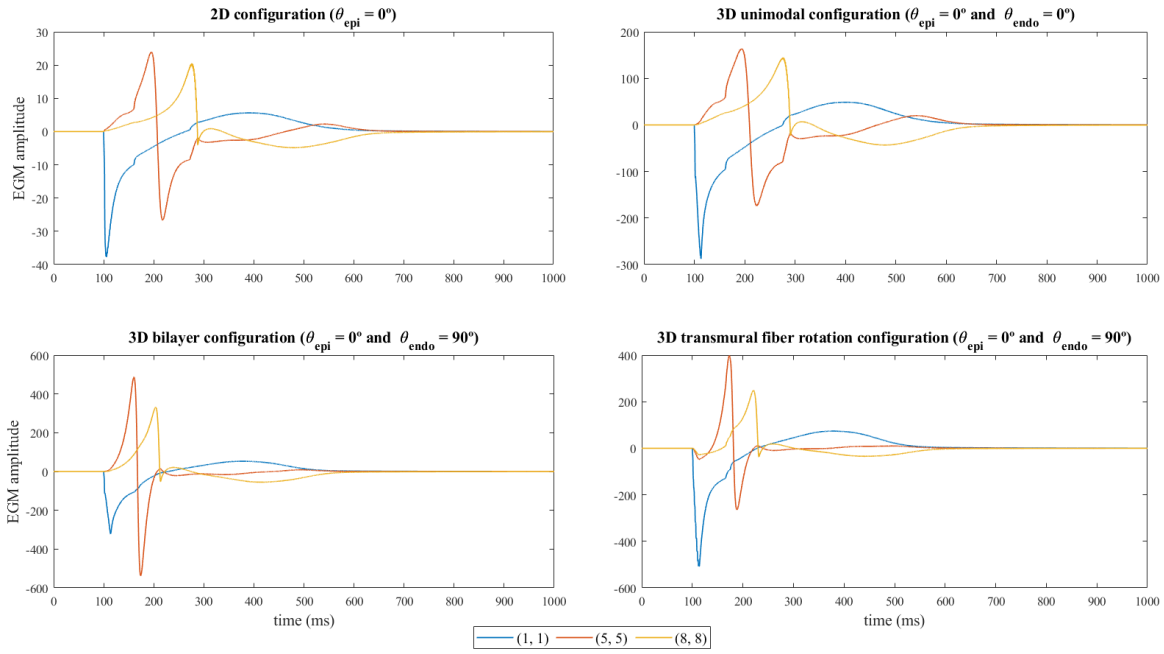

Figure 3.1: Comparison of the epicardial EGMs recorded by the electrodes at positions (1, 1), (5, 5) and (8, 8), in four different cardiac tissue model configurations: 2D, unimodal, bilayer and transmural fiber rotation.

A lower amplitude of the EGM and a more distorted morphology are observed in the data obtained from the 2D and unimodal configurations, compared to the bilayer and transmural fiber rotation models. Furthermore, the different EGMs present the

steepest negative slope at different time points. In the case of the EGMs recorded by the electrode at position, the bilayer configuration has the earliest maximum downward slope, followed by the transmural fiber rotation, the unimodal, and the 2D configurations. However, the influence of the underlying layers' architecture on epicardial recordings can be better observed in the LAT maps. Figure 3.2 displays the activation map corresponding to the 140 x 140 cell epicardial grid.

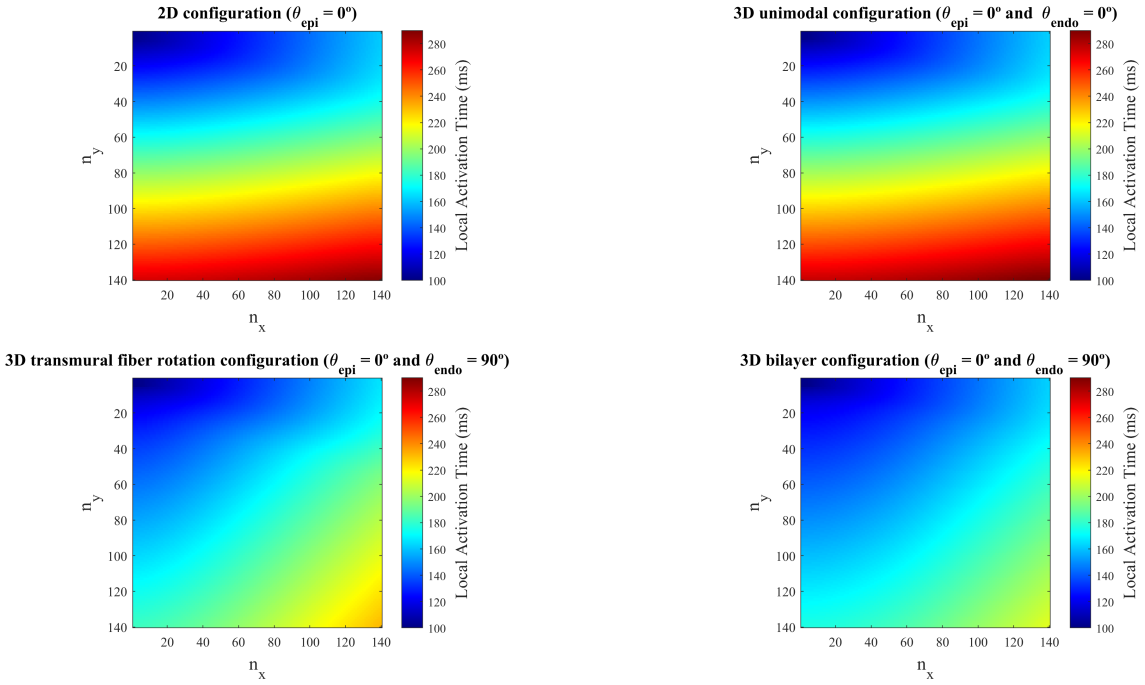

Figure 3.2: Comparison of the epicardial LAT maps generated by four different cardiac tissue model configurations: 2D, unimodal, bilayer and transmural fiber rotation.

In all four models, the epicardial wavefront adopts an elliptical shape. When the fiber orientation is uniform across all the tissue slabs, as it happens to be in the unimodal configuration, the orientation of the elliptical wavefront reflects the fiber orientation in the epicardium. However, in cases where the fiber orientation varies across distinct layers, such as in the bilayer and transmural fiber rotation configuration, the wavefront undergoes a CCW rotation leading to an accelerated activation of all the epicardial cells. Moreover, the isochrones from the transmural fiber rotation configuration do not show a purely elliptical shape, instead, they display two dimples next to the pacing site.

3.1.2 Impact of intramural stimulation

After analyzing the data generated by the models when stimulating the epicardial layer, the effect of stimulating at different depths was also evaluated. The epicardial EGMs recorded by the electrode positioned at (5, 5) and LAT maps when pacing at the 1st, 3rd, 6th and 9th layer of the 3D cardiac models are seen in Figures 3.3 and 3.4. The 1st layer corresponds to the epicardium.

As depicted in Figure 3.3, the four electrical signals recorded from the unimodal configuration model are nearly the same. However, an attenuation and shift to the left on the time axis of the signal with increased pacing depth is observed in the recorded

EGMs from the bilayer configuration model. This effect is even more pronounced in the EGMs generated from the transmural fiber rotation configuration model.

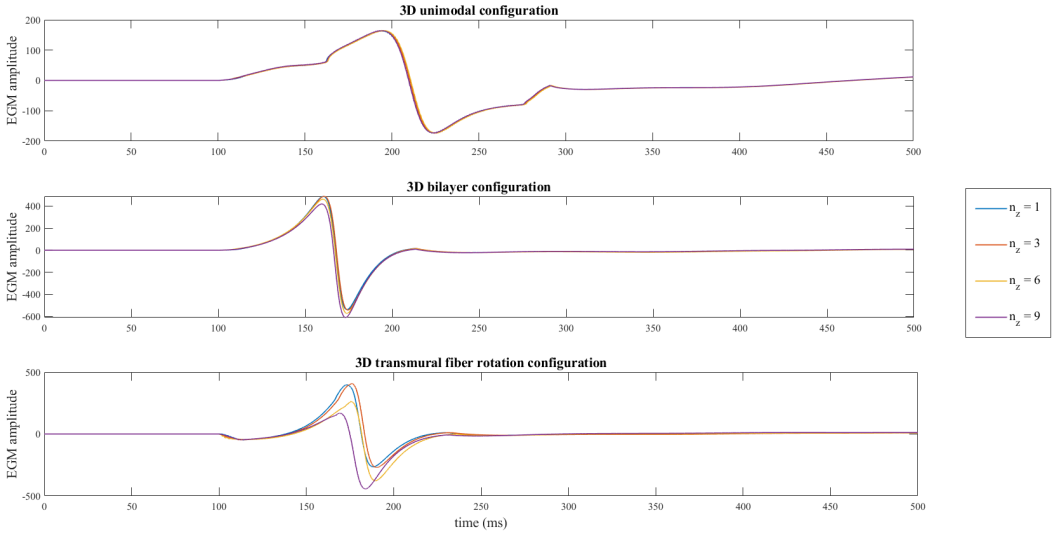

Figure 3.3: Comparison of the epicardial EGMs recorded by the electrode located at (5, 5) when stimulating at different depths, specifically at the 1st, 3rd, 6th and 9th layer (n_z), in the three 3D cardiac model configurations: unimodal, bilayer and transmural fiber rotation.

Comparable results are observed in the LAT maps, shown in Figure 3.4. As with the EGMs, the wavefront distribution remains unchanged in the case of the unimodal configuration. Yet, the isochrones of the maps originating from the bilayer and transmural fiber rotation configurations experience a CCW rotation, mirroring the fiber orientation of the underlying layers.

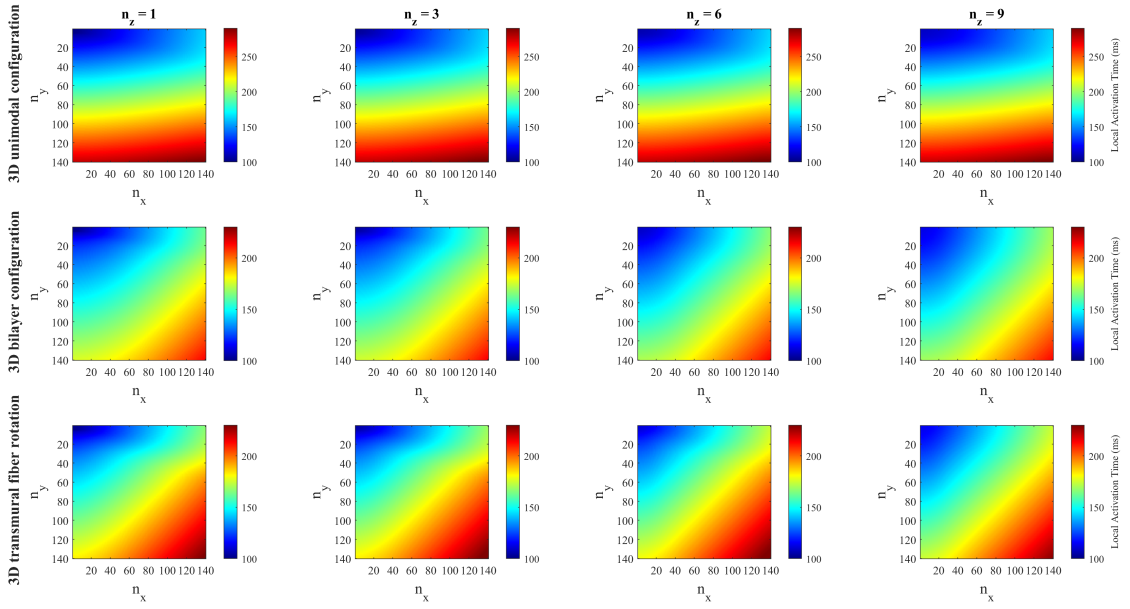

Figure 3.4: Comparison of the epicardial LAT maps obtained when stimulating at different depths, specifically at the 1st, 3rd, 6th and 9th layer (n_z), in the three 3D cardiac model configurations: unimodal, bilayer, and transmural fiber rotation.

3.2 Experiments on synthetic data

The performance of the methods was evaluated when applied to synthetic LAT or voltage maps. In this section, the fiber direction estimation methods were first compared when implemented as described by their respective authors, after which they were modified such that they use the same number of data points and find a global fiber direction value. The influence of increasing the size of the input dataset, incorporating endocardial information and the stimulation location, was assessed for the best-performing techniques. Finally, approaches to derive the local fiber direction were also compared under the same realistic conditions.

3.2.1 Existing methods for estimating the fiber direction

The first step involved evaluating the methods implemented as outlined by their respective authors. MAE, alongside maximum and minimum non-outlier errors, in estimating the fiber direction from 8 x 8 LAT maps generated with the four distinct models are illustrated in Figure 3.5. Each method is referred to by its acronym, as specified in Table 2.1.

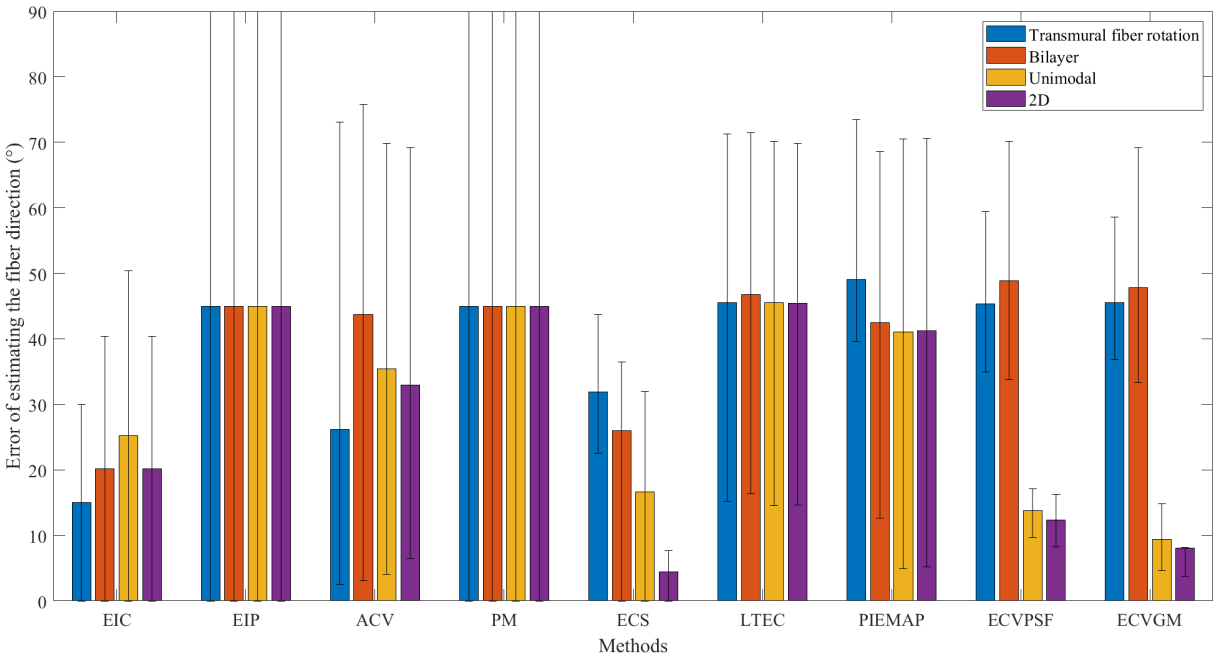

Figure 3.5: Comparison of mean absolute error, along with the maximum and minimum non-outlier errors, for fiber direction estimation methods previously reported in the literature: EIC, EIP, ACV, PM, ECS, LTEC, PIEMAP, ECVPSF and ECVGM.

When employing the epicardial maps obtained from a 2D model, EIC, ECS, ECVPSF, and ECVGM exhibit notably low MAE and standard deviation of the estimation error (MAE $\pm$ SD): EIC (20.17º $\pm$ 28º), ECS (4.48º $\pm$ 9.44º), ECVPSF (12.39º $\pm$ 3.33º), and ECVGM (8.1º $\pm$ 35.2º). The latter two, however, show diminished accuracy when dealing with data derived from the bilayer and transmural fiber rotation configuration. In contrast, the potential-based methods, EIP (45º $\pm$ 37.81º) and PM (45º $\pm$ 37.81º), are the least accurate and have the highest variability with data from the 2D model. Although the variability is lower, the LTEC method (45.45º $\pm$ 18.13º) also shows large MAE values, followed by the PIEMAP (40.97º $\pm$ 10.72º) and ACV (32.93º $\pm$ 23.65º) methods.

3.2.2 Methods for estimating the global fiber direction

Considering the differences in resolution and data point requirement among the methods, the approaches that showed the lowest errors in the 2D configuration (EIC, ECS, ECVPSF and ECVGM) were standardized to compute a single and global fiber direction from one 8 x 8 LAT map (EIC, ECS, $ECVPSF_G$ and $ECVGM_G$). Although the PIEMAP method showed large errors in its original format, given its high resolution, it was also modified to meet the same conditions by averaging either the local angle values (*Average Angle*) or the local conductivity tensors (*Average Conductivity tensor*).

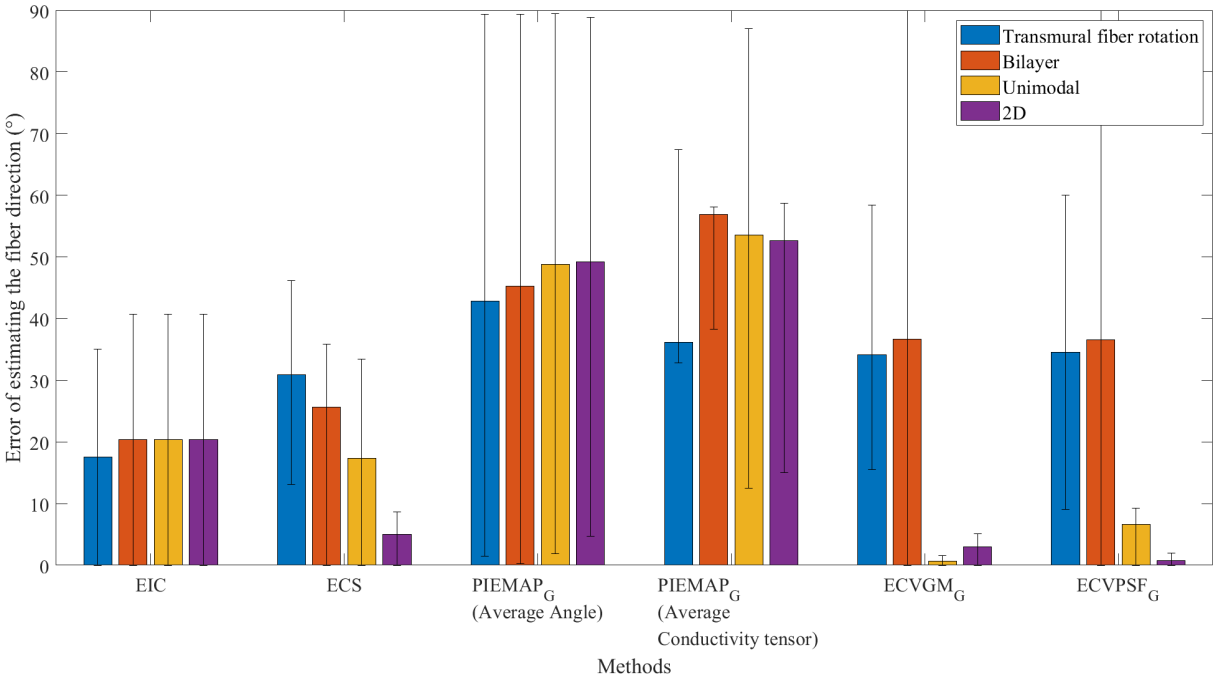

Figure 3.6: Comparison of mean absolute error, along with the maximum and minimum non-outlier errors, in global fiber direction estimation methods using one single epicardial LAT map. The methods included are: EIC, ECS, $PIEMAP_G$ (*Average Angle*), $PIEMAP_G$ (*Average Conductivity tensor*), $ECVGM_G$, $ECVPSF_G$.

The estimation error of the global fiber direction estimation methods is shown in Figure 3.6. The ellipse fitting to local CV vectors approach, used in $ECVPSF_G$ and $ECVGM_G$, perform the best when all the fibers in the sample tissue had the same direction (2D and unimodal configurations). As expected, the estimation accuracy diminishes when the endocardium and epicardium have perpendicular fiber directions (bilayer and transmural fiber rotation configurations). Despite the apparent effectiveness of the EIC, the estimation results show significant variability accompanied by a high MAE value in the 2D scenario. Moreover, the two modified $PIEMAP_G$ methods are not more accurate than its original version PIEMAP.

3.2.2.1 Impact of expanding the input dataset size in the estimation performance

a. *LAT map's size*

Considering the results displayed in Figure 3.6, the ECS, $ECVPSF_G$ and $ECVGM_G$ methods were further modified to use a larger number of data points.

On the one hand, the size of the LAT maps can be increased so that there are more activation values available from the same tissue area, 14 x 14 mm. The influence of varying the map size from 3 x 3 (M = 9) to 140 x 140 (M = 19600) points in the estimation performance is displayed in Figure 3.7, with the x-axis in a logarithmic scale. In the 2D and unimodal model configurations, the MAE values decrease with the size of the input array in all three methods. This enhanced performance is not as evident in the more complex wall structures, represented by the bilayer and transmural fiber direction configurations, in which accuracy fluctuations are observed. Only the ECS method benefits from an increased map size in all four different tissue models.

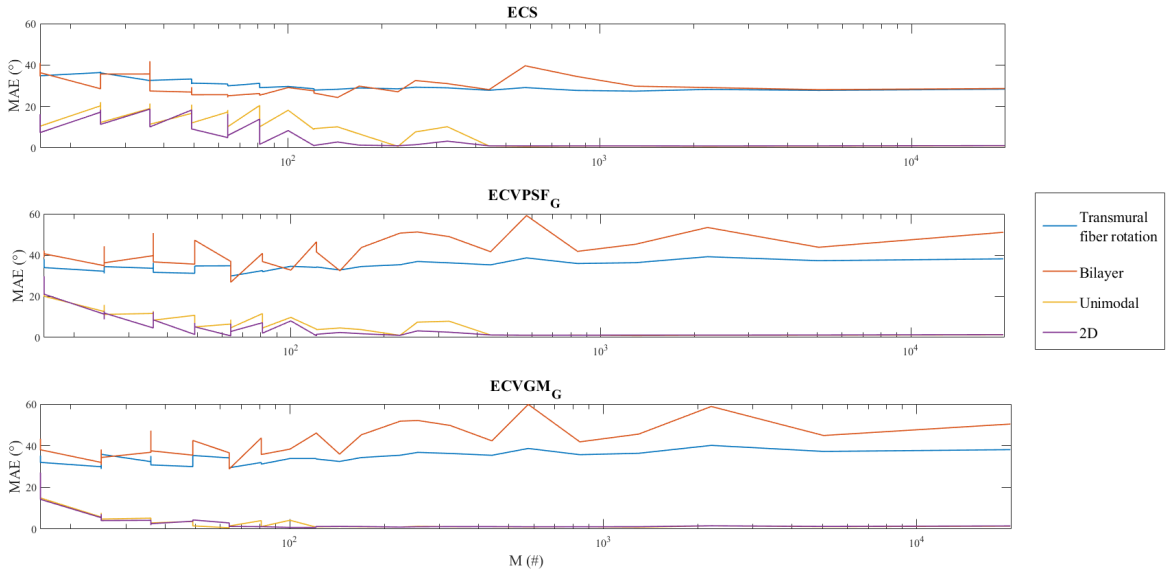

Figure 3.7: Mean absolute error (MAE) in estimating the fiber direction when using ECS, $ECVPSF_G$ and $ECVGM_G$ as a function of the size of the LAT maps (M).

b. *Number of LAT maps*

On the other hand, the input data can be increased by employing several LAT maps recorded in the same tissue configuration but with the wavefront originating from distinct sites, i.e., different pacing sites. The methods can be adapted to use the LAT maps in the *All Vector* approach.

The effect of increasing the number of maps by fitting an ellipse to all the CV and CS vectors can be seen in 3.8. When using the data obtained from the 2D and unimodal configuration models, increasing the number of maps reduces the MAE. A great reduction in the estimation error is already achieved when using two maps instead of one. However, this correlation is not observed when the maps are generated from the models with perpendicular endocardial and epicardial fibers.

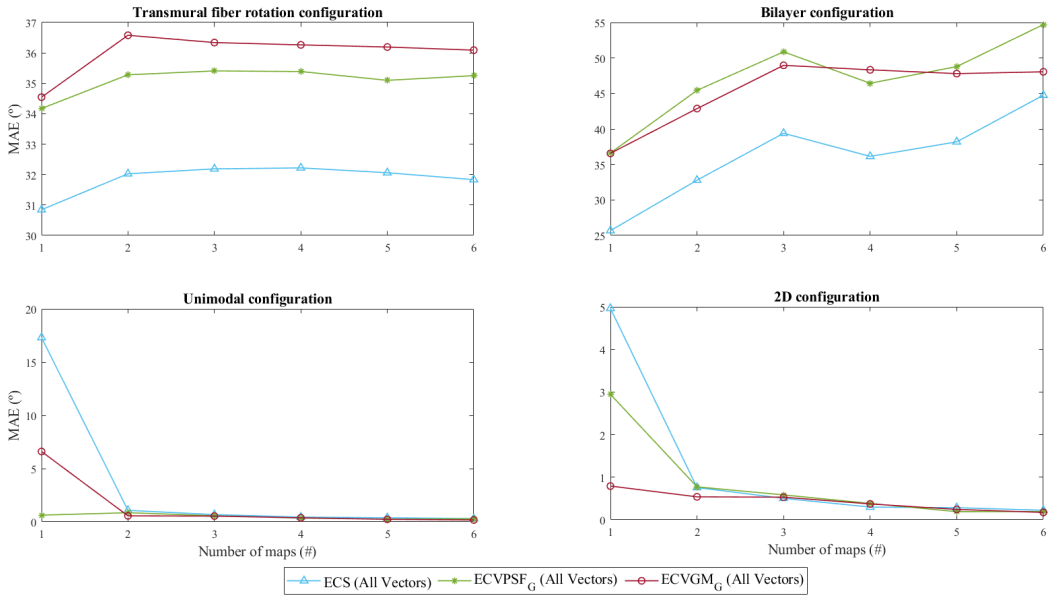

Figure 3.8: Mean absolute error (MAE) in estimating the global fiber direction of ECS, $ECVPSF_G$ and $ECVGM_G$ modified to use several LAT maps using the *All vectors* approach. The LAT maps used are generated by stimulating at six different locations the epicardial layer of four different tissue model configurations: 2D, unimodal, bilayer and transmural fiber rotation.

3.2.2.2 Impact of adding prior knowledge in the estimation performance

When estimating the epicardial orientation from the maps generated with a tissue slab where endocardial fibers run perpendicular to the epicardial fibers, transmural fiber rotation and bilayer configuration, the epicardial fiber orientation estimates were corrected removing the error associated with the epicardial wavefront rotation observed in Figure 3.2.

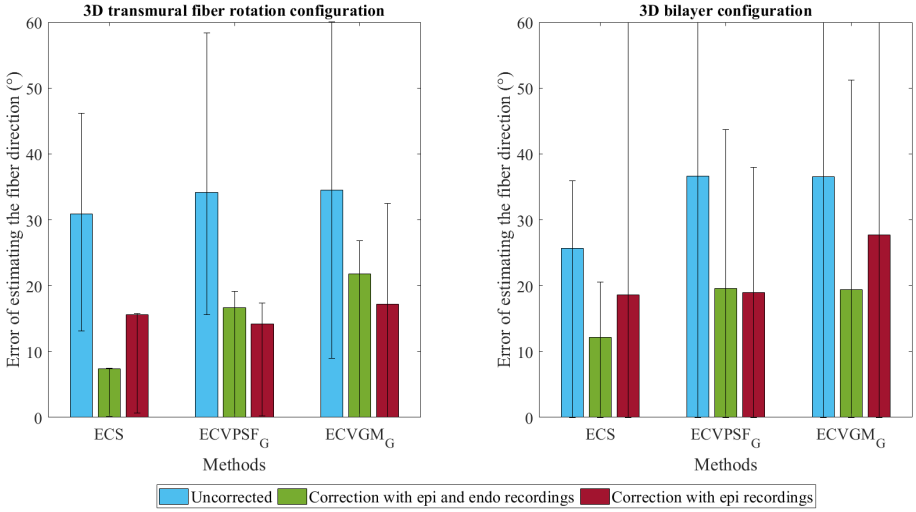

Figure 3.9: Mean absolute error, along with maximum and minimum non-outlier error, in estimating the fiber direction when using the ECS, $ECVPSF_G$ and $ECVGM_G$ methods directly on epicardial recordings (blue) and when modifying the methods to use endocardial information obtained by stimulating the endocardium and recording at the endocardium (green) or stimulating the endocardium and recording at the epicardium (red). The correction is applied to data obtained from the transmural fiber rotation configuration (left) and bilayer configuration (right).

The error can be either estimated with epicardial LAT maps recorded during endo-

cardial and epicardial stimulation or with epicardial and endocardial maps recorded during endocardial and epicardial pacing, respectively. Figure 3.9 depicts the estimation before applying the correction. Improvement of the estimation accuracy for all methods is possible by adding endocardial information obtained from the epicardial activation maps when stimulating the endocardium. When endocardial EGMs are also available, the ECS would yield even more accurate fiber direction estimated, whereas the $ECVPSF_G$ and $ECVGM_G$ methods do not consistently exhibit the same behavior.

3.2.2.3 Impact of wavefront source location

The pacing location also determined the accuracy of the estimation methods. As seen in Figure 3.10, when using maps obtained by pacing at the center of the 14 x 14 mm area under study, the estimation error is lower. This decrease is the most pronounce in the unimodal configuration.

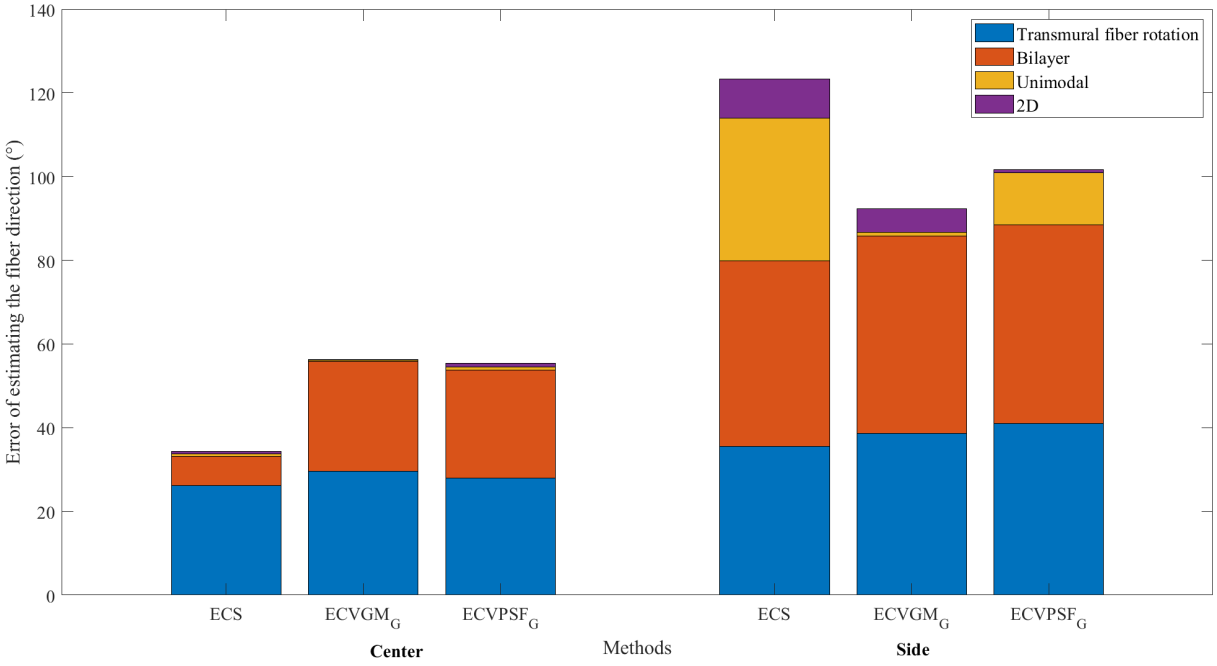

Figure 3.10: Mean absolute error in estimating the fiber direction when using the ECS, $ECVPSF_G$ and $ECVGM_G$ methods on LAT maps obtained after epicardial pacing either at the center (left) or at the side (right) of the tissue area under study.

3.2.3 Methods for estimating the local fiber direction

Finally, the methods that output the local fiber direction, including ECS_L, ECVPSF, ECVGM and PIEMAP, were compared. These approaches are able to derive a fiber direction at each electrode location, increasing the resolution of estimation.

Figure 3.11 shows the estimated local fiber directions in LAT maps obtained from a tissue model with the epicardial fibers at a 0^o angle relative to the x-axis. The fiber direction estimates diverges more from its true value when the fiber direction varies across the different layers of the cardiac tissue models, specifically, in the bilayer and transmural fiber rotation configuration models. Moreover, even though the PIEMAP method gives the most consistent local fiber direction across a map, it was concurrently associated with the highest error in all four tissue wall architectures.

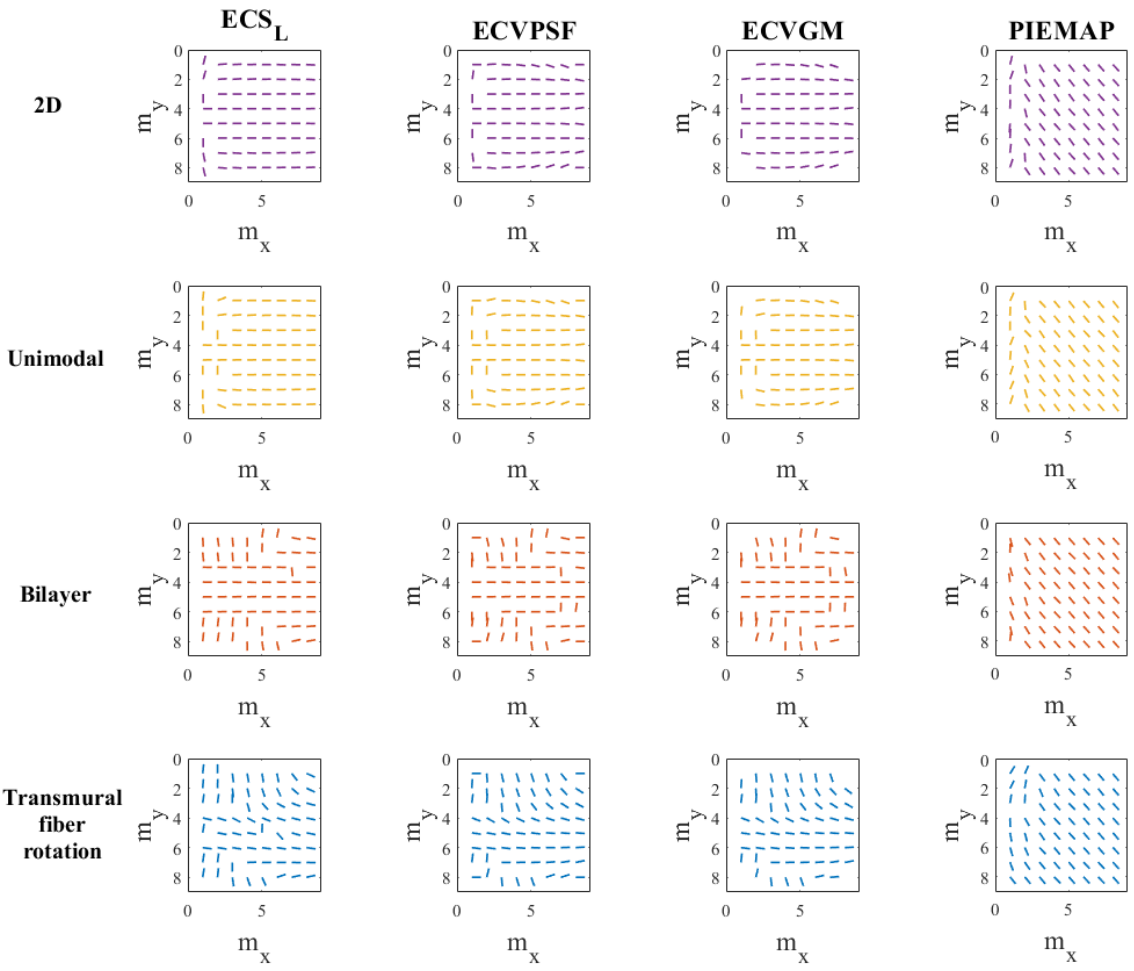

Figure 3.11: Local fiber direction estimates computed with four methods, ECS_L, ECVPSF, ECVGM and PIEMAP. The LAT maps used are obtained when stimulating the side of the epicardium in the 2D, unimodal, bilayer and transmural fiber rotation tissue model configurations. The true local fiber direction is 0º for all maps and all electrodes.

A comparison of the MAE values is seen in Figure 3.12, which also demonstrates the superior performance of ECS_L, ECVPSF and ECVGM above PIEMAP. The MAE values versus the number of maps used were also analyzed for the ECS_L, ECVPSF and ECVGM methods. From Figure 3.13 it can be seen that the MAE value does decrease with the number of maps used when employing ECS_L. However, it has the opposite behavior when using the ECVPSF and ECVGM methods.

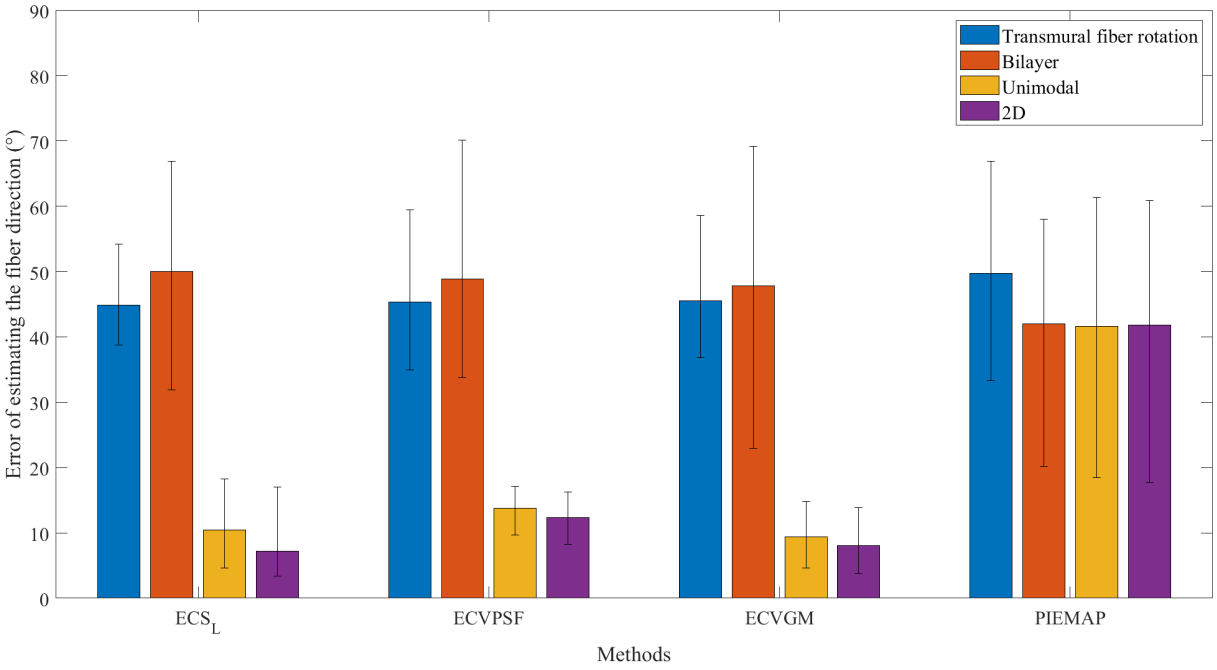

Figure 3.12: Mean absolute error, along with maximum and minimum non-outlier error, in estimating the local fiber direction when using the ECS_L, ECVPSF, ECVGM and PIEMAP methods on epicardial LAT maps obtained from four different cardiac model configurations: 2D, unimodal, bilayer and transmural fiber rotation.

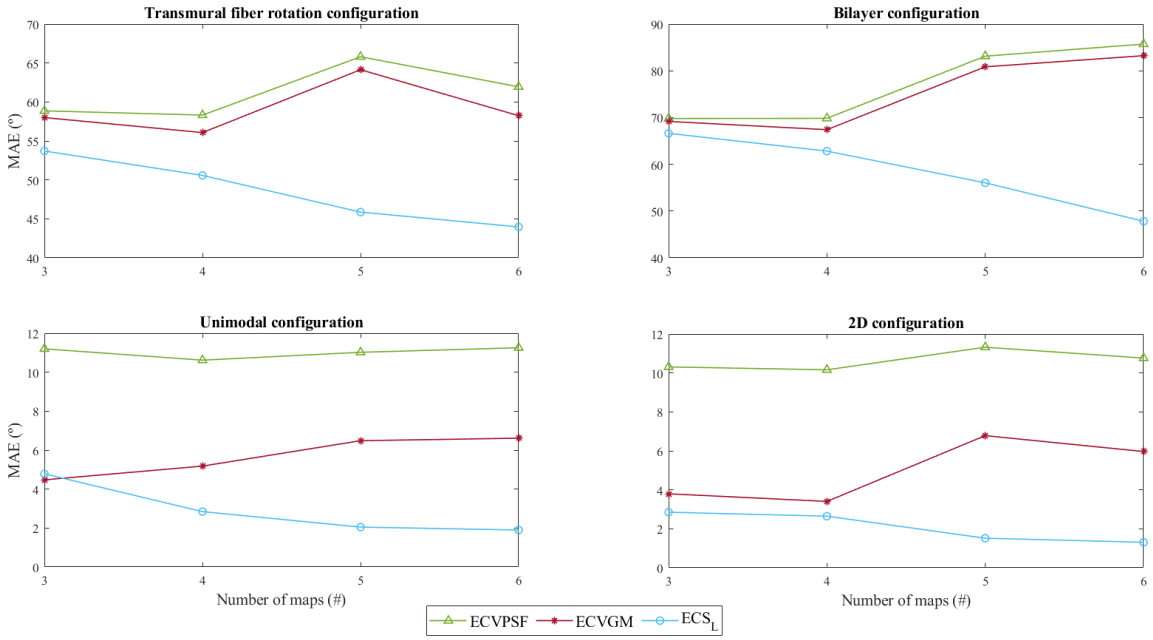

Figure 3.13: Mean absolute error (MAE) in estimating the local fiber direction when using the ECS_L, ECVPSF and ECVGM methods modified to use from three to size epicardial LAT maps. The LAT maps are obtained from the epicardial layer of four different cardiac model configurations: 2D, unimodal, bilayer and transmural fiber rotation.

3.3 Experiments on clinical data

Given the results with simulated data, the most accurate global fiber direction estimation methods were tested with human EGMs. Specifically, the methods compared were the ECS, $ECVPSF_G$ and $ECVGM_G$ modified to utilize three maps using the *All Vectors* approach. While lacking clinical data accompanied by a reference fiber direction, EGMs recorded during sinus rhythm (SR) in three different locations, the BB, the inferior side of the RA, and the RV, were employed to evaluate the methods in a clinical setting.

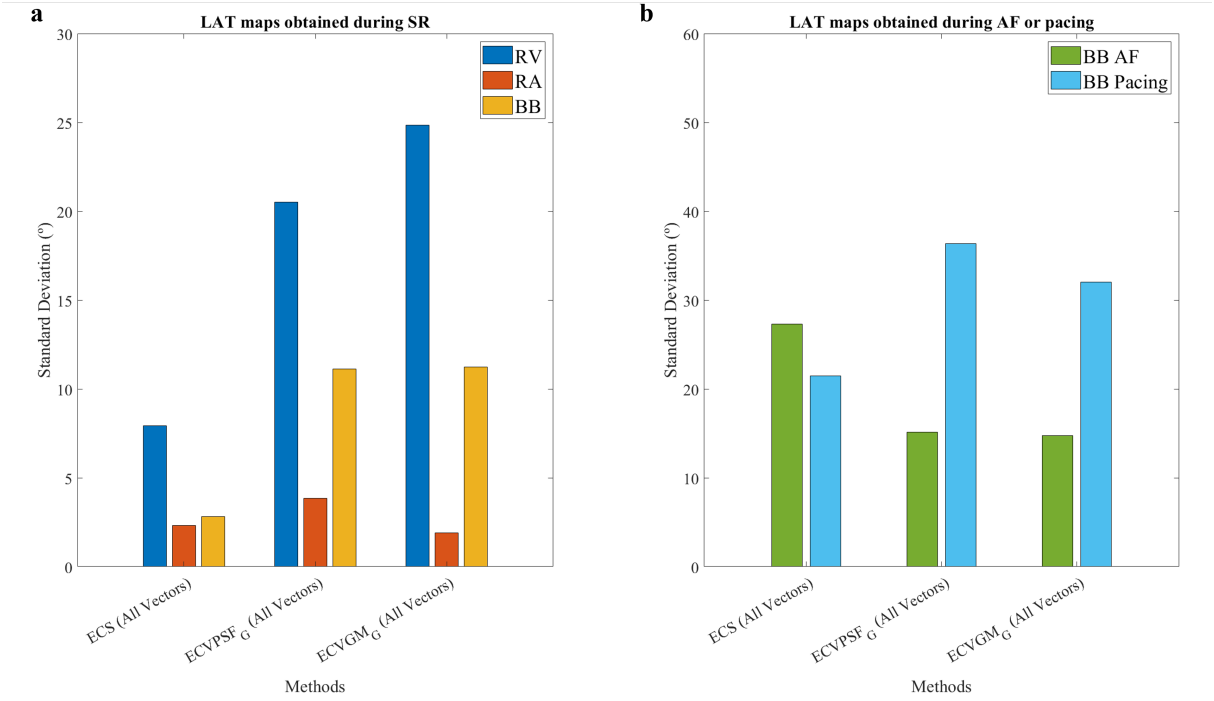

Figure 3.14: Comparison of the standard deviation in estimating the global fiber direction when using the ECS, $ECVPSF_G$, $ECVGM_G$ methods adapted to utilize three maps recorded with a 24 x 8 electrode array using the *All Vectors* approach. (a) Variability of the methods when the LAT maps are obtained from the BB, RA and RV during SR. (b) Variability of the methods when the LAT maps are obtained from the BB during AF and pacing.

To begin, the variability in estimating the global fiber direction from maps recorded by a 24 x 8 electrode array at the same location but during different heartbeats was assessed (Figure 3.14). As seen in Figure 3.14 (a) the standard deviation values for the various methods when the LAT maps are obtained during SR are notably low, with the lowest values observed in the RA location. Yet, the variability increases when utilizing LAT maps obtained during AF and after pacing, as observed in Figure 3.14 (b).

Moreover, based on a fiber atlas and the exact position and orientation of the mapping array, some assumptions were made on the underlying fiber orientation in order to compute the MAE values, which are depicted in Figure 3.15. Even though the true fiber direction remains uncertain, all the methods performed well in SR. The ECS method clearly represents the highest level of accuracy with recordings obtained during SR, pacing, and AF, albeit with a somewhat greater degree of variability in the latter scenario in comparison with the other approaches.

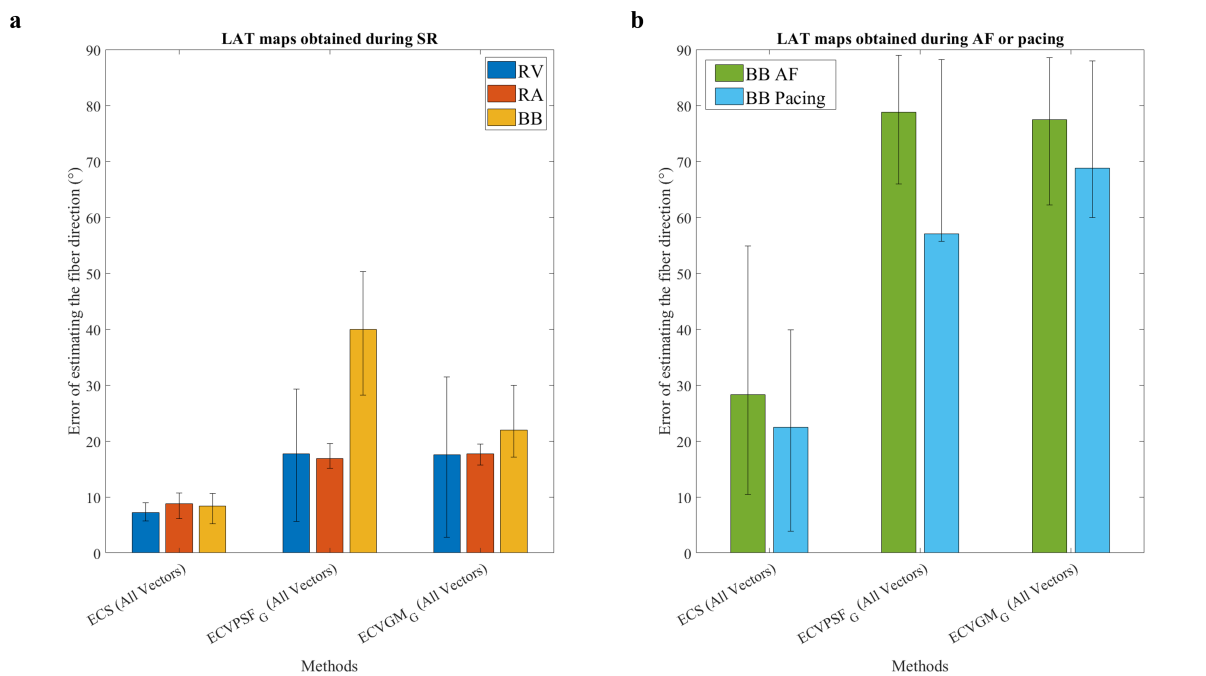

Figure 3.15: Mean absolute error, along with the maximum and minimum non-outlier error, in estimating the local fiber direction when using the ECS, $ECVPSF_G$, $ECVGM_G$ methods adapted to utilize three maps recorded by a 24 x 8 electrode array using the *All Vectors* approach, on human epicardial LAT maps. (a) Estimation error of the methods when the LAT maps are obtained from the BB, RA and RV during SR. (b) Estimation error of the methods when the LAT maps are obtained from the BB during AF and pacing.

The local fiber direction estimation methods, ECS_L, ECVPSF and ECVGM, were also applied to clinical data. However, given the variability of estimated fiber directions and time constrains, they were not further assessed (see Appendix B). Figures B.4 and B.6, show the local fiber estimates derived from LAT maps obtained from BB during SR and pacing, respectively. Figures B.5 and B.7 the corresponding LAT maps used for the local fiber direction estimation.

4 Discussion

Following the same order as in Chapter 3, in this section of the report the results will be discussed. First, to ensure the performance assessment was carried out with data closely mimicking the living cardiac tissue behavior, the data generated with 3D monodomain models were compared with reported observations on human and animal electrical recordings. After confirming its similarity with clinical data, the accuracy of the fiber direction estimation methods was assessed. The best-performing methods were also standardized to compute the global or local fiber direction, and evaluated. Since the global methods performed better than the local ones, a preliminary study on the ECS, $ECVPSF_G$ and $ECVGM_G$ techniques' performance when using clinical data was carried out. This chapter ends with a proposal on the method that should be used for clinical and research applications.

4.1 Electrophysiological cardiac model

Since most validation efforts for fiber direction estimation methods have primarily focused on simplified cardiac models, this project aimed to assess and compare their performance in a more realistic tissue model simulating a muscle bundle, atrial bilayer, and ventricular transmural fiber rotation structure. The experimental setup comprised a 2D tissue model, which served as a control, and three 3D tissue slab models with axially symmetric anisotropy closely mimicking the intricate architecture of the heart wall. These models were constructed using the Courtemanche and Monodomain equations (Equation (2.18)).

4.1.1 3D models of the cardiac wall

As already observed in human EGMs recorded near the SAN and further away, in all four models the recorded EGMs at the pacing site showed a negative S-wave, which became positive R-waves at the termination of the wavefront (Figure 3.1) [19]. Yet, differences in amplitude and time shifts were visible among the EGMs derived from the various configurations.

The amplitude variance can be attributed to the dissimilarities in the number of cells (N) contributing to the EGM generation, much lower in the 2D configuration. Furthermore, the amount of I_{tm} present in the cells underneath the electrode, distributed across distinct layers, also impacts the EGMs amplitude (Equation (2.20)). The signals displayed in Figure 3.1 are obtained from a model with the epicardial fibers forming a 0^o angle with the x-axis, and after stimulating in the (1, 1) location. In the unimodal configuration, since all the fibers from all the layers have a larger conductivity in the direction parallel to the x-axis, the current propagates primarily in that direction. Hence, cells underneath the electrodes positioned in a diagonal direction with respect to the stimulation site, (5, 5) and (8, 8), will have less I_{tm} going through them than those positioned at (1, 5) or (1, 8). Conversely in the bilayer and transmural fiber rotation configuration, the perpendicular direction of the endocardial fibers enables more current to reach the (5, 5) location.

Differences in time shift were manifested by the early appearance of the negative slope of the EGM at the (5, 5) electrode in the models where the endocardial fibers were oriented perpendicular to the epicardial fibers. As mentioned above, in these scenarios, due to the conductivity in the endocardial layers being larger in the perpendicular direction with respect to the epicardial layers, the electrical signal propagates faster along the diagonal direction reaching the (5, 5) electrode sooner. Such effects are also observed in the LAT maps (Figure 3.2). Conduction anisotropy, this is, a larger longitudinal conductivity σ_l, in the horizontal direction, than transverse one σ_t, in the vertical direction, causes the wavefront to adopt an elliptical shape. This ellipse experiences a rotation in the bilayer and transmural fiber rotation configurations which is aligned with the transmural CCW fiber rotation present in the two models and indicates faster propagation along the diagonal direction. Additionally, the LAT maps from the transmural fiber rotation configuration showed a dimple-like inflection (Figure 3.2), caused by an initial local wavefront acceleration as previously observed in canine ventricles by Taccardi *et al.* [41], [42].

The orientation of the isochronal lines or the wavefront direction in the epicardium of the bilayer and transmural fiber direction models could be altered through intramural pacing (Figure 3.4). The depth of stimulation was found to intensify the influence of endocardial fibers on epicardial measurements, causing a CCW rotation of the ellipse with increased stimulation depth [41]. This led to an earlier activation of the (5, 5) electrode as the pacing depth increased. Extensive research has been carried out by Taccardi *et al.*, demonstrating in canine ventricles that increasing pacing depth not only causes the CCW rotation of the elliptical isochrones but also an enhancement in transmural propagation from the pacing site to the epicardial surface and an increase of the epicardial wavefront propagation velocity [42].

Thus, the epicardial EGMs and LAT maps not only reflect the epicardial signal propagation but also the spread across the entire wall thickness. This should be taken into account when estimating the epicardial fiber direction from epicardial recordings. The simplicity of the 2D model, which exclusively portrays the signal propagation across the epicardium, makes it an appropriate control dataset for the comparative analysis of the estimation methods. While it is anticipated that the methods using the data from the unimodal configuration will yield similar results as with 2D data, the transmural fiber rotation and bilayer configurations, replicating the heterogeneous fiber direction across the wall, may potentially diminish the efficacy of the methods.

4.1.2 Limitations of the cardiac models

It is worth mentioning some limitations of the models and the data used for the subsequent performance analysis. First, the tissue model was thinner (1 mm) compared to the real ventricular wall thickness (over 3 mm). This choice was motivated by the substantial reduction in computational time while having a small effect on signal propagation and isochronal rotation. Second, to limit the complexity of the model, it was assumed that all the fibers run parallel to the epicardial surface. Fibers within the cardiac wall can present an inclination with respect to the epicardial plane, which is characterized by the imbrication angle [42]. This angle varies across different regions of the heart and the depth of the cardiac wall. Finally, the LAT maps presented in Figure 3.2 and 3.4 are generated by taking the time at which the transmembrane potentials of the individual cells in the epicardial layer reach -40 mV, and not from the recorded EGMs. The latter, used in the clinical setting to derive the activation

maps, does not only capture the local epicardial cell activation but also the far-field epicardial and endocardial activation. Consequently, the activation pattern derived from the EGMs may slightly differ from those used in this study. However, automatic derivation of the LAT values from EGMs can introduce errors, potentially impacting the accuracy of the fiber direction estimation methods. Therefore, it was opted to generate the maps from the local epicardial cell activation.

Despite these limitations, the tissue models and recordings employed in this study offer a more realistic representation of the activation spread within the cardiac tissue compared to the commonly used 2D models. The observed dependence of the 3D cardiac wall structure on the epicardial recordings reinforces the need to evaluate fiber direction estimation in conditions that closely mimic reality. Moreover, intramural pacing offers additional insights that can be employed to enhance the fiber direction estimation methods.

4.2 Experiments on synthetic data

The existing fiber direction estimation methods vary not only according to the surrogate they use to derive the fiber direction but also the resolution in which they can derive the fiber direction, global and local. These resolution differences complicate the direct comparison of the methods. Despite this, an initial evaluation focused on assessing the performance of the methods, as outlined by their authors, in terms of estimation error was carried out. This analysis aimed to identify the methods suitable for subsequent resolution standardization.

As seen in Figure 3.5, with data from the 2D and unimodal configuration, the EIC, ECS, ECVPSF and ECVGM show the lowest MAE. However, the methods' accuracies decrease when the endocardial fiber direction deviates from the epicardial fiber direction, caused by the alteration of the underlying parameters these methods rely on, such as CV direction and isochronal lines. In certain scenarios, the estimation errors exceeded 45º, which might indicate that the degree of rotation experienced by the isochrones observed in the LAT maps was estimated instead.

The potential-based methods (EIP and PM) showed large MAE values (45º) in all the configurations with always a maximum error of 90º and a minimum of 0º, indicating the randomness of the estimation. This stems from their dependence on features that appear in the voltage maps at only specific time points. Automatic selection of these critical time points is prone to errors, requiring manual visual inspection of the maps. Consequently, EIP and PM may not be appropriate methods for processing large quantities of clinical data and doing this in real time.

The ACV and LTEC methods also demonstrated suboptimal performance in all the model configurations. ACV performs well with high resolution LAT maps, yet the estimation error increases with smaller map sizes (see Figure B.2). This method is based on grouping the local CV vectors into bins according to their direction. When a limited number of CV vectors are available, the likelihood of the bin containing the fiber direction angle being empty increases. This issue, as previously reported by its authors, becomes more pronounced with higher anisotropic ratios. Their study also demonstrated that a minimum 14 x 14 map size was required to reduce to 5% the probability of having an empty bin, which was not the case for the current analysis [33]. LTEC employs the lsqnonlin function in MATLAB to solve the nonlinear LS errors problem proposed by Roney *et al.*. However, the solution substantially depends

on the constraints and initial starting parameter estimates from Equation (2.11), which were not clearly defined by the author, resulting in significant estimation errors [20]. Furthermore, this method fits the data to an elliptical wavefront model, restricting the applicability to the scenarios where a purely elliptical-shaped wavefront is found.

Finally, the PIEMAP method, with slightly lower error values than the LTEC, had the most complex implementation, as the inverse problem needs to be solved. The usage of a cardiac model makes it the only approach to account for the physics of electrical propagation, as pointed out by Coveney *et al.*, which should ensure more realistic outcomes [43]. Moreover, it also stands as one of the few methods, alongside LTEC, ECVPSF and ECVGM, capable of estimating the local fiber direction, making it relevant for clinical applications. Despite its poor performance, given the aforementioned advantages, its accuracy in estimating a local and global fiber direction was further analyzed.

Hence, given the strong performance of the EIC, ECS, ECVPSF and ECVGM approaches, as well as the high-resolution capability of PIEMAP, they were standardized to ensure a direct comparison. The first objective was to compare their performance when estimating the global fiber direction.

4.2.1 Methods for estimating the global fiber direction

While higher resolution is typically favored for clinical and research purposes due to the small dimensions of the cardiac fibers, generally, the fiber direction in healthy atrial and ventricular walls varies smoothly [6]. Consequently, obtaining an accurate estimate from a 14 x 14 mm^2 surface, corresponding to the electrode array area, would already be valuable for the creation of patient-specific cardiac fiber models.

In the comparative analysis of the methods for global direction estimation (Figure 3.6), several observations came to light. Notably, the EIC method exhibited a large variability and high mean errors in both the 2D and unimodal scenarios, even after adjusting the ellipse fitting approach to solving an LS error problem. It was observed that not all maps featured an elliptical isochrone 1.5 ms after stimulation. Instead, the optimal isochrone for ellipse fitting varied significantly across maps ranging from 2 to 20 ms. As with the potential-based methods, selecting the optimal isochrone requires manual inspection of isochrone shapes in each map. However, this process is time-consuming and impractical for the integration of the fiber direction on electrophysiological models or to improve the interpretability of the EGMs.

Furthermore, the $PIEMAP_G$ method, in its two variations (*Average Angle* and *Average Conductivity tensor*) continued to be inaccurate. Since most of the local conductivity tensor and angle estimates deviated from their true local values, the average estimates also displayed notable discrepancies. The results suggest potential issues with the method's implementation. However, a further assessment of the method's limitations will be presented in the following section, where its performance in estimating the local fiber direction will be evaluated.

Conversely, methods employing an ellipse fitting to local CS or CV vectors approach, used in ECS, $ECVPSF_G$ and $ECVGM_G$, demonstrated their superior performance when all the fibers within the tissue model shared the same direction. These methods have the advantage of not depending directly on the elliptical shape of the wavefront but on the magnitudes of the CS or CV vectors' components. Moreover, in these scenarios, the estimation error decreased with increasing map size (Figure 3.7) due to the larger range of vector directions. Increasing the size of the activation maps,

derived from EGMs, is possible through either LAT or potential interpolation. Reiger *et al.* suggested that potential interpolation, using the Kriging, gives better results than directly interpolating the LAT map. However, such interpolation would require the annotation of a larger EGMs dataset, and with it, an accurate automated method for LAT map generation should be created [44]. An alternative approach is the use of support vector machine (SVM) interpolation, which has already been combined with electroanatomical mapping, or an improved Kriging Interpolation Technique based on SVM, developed by Huang *et al.* [45], [46].

Continuing in the 2D and unimodal tissue model, a significant improvement was observed when using the information from distinct activation maps through the *All Vectors* approach (Figure 3.8). Given the dependence of the CV and CS vectors' direction on the wavefront source, adding LAT maps, obtained after pacing at slightly different locations, can reduce the influence of the wavefront direction on the estimation results which has been previously reported [34].

However, estimation of the fiber direction from LAT maps obtained from complex wall structures represented by the bilayer and transmural fiber direction configurations continued to yield poor results despite increasing the volume of input data. Such diminished performance was primarily attributed to the wavefront rotation caused by the perpendicularity of the epicardial and endocardial fibers. Hence, the methods rely on information that reflects not only the epicardial wavefront propagation but also the interplay between the different wall layers of the cardiac wall.

To account for the epicardial-endocardial interaction, prior knowledge of the heart structure together with information on endocardial activation was incorporated in the estimation process using Equation (2.17). The LAT maps obtained after stimulating the endocardium, whether by placing the electrode array in the endocardium or on the epicardium, give information on the transmural signal propagation and the attributed epicardial fiber direction estimation error. This error is subtracted from the epicardial estimates to obtain more accurate results, as seen in Figure 3.9. However, the correction can only be used with EGMs where the assumptions of perpendicular epicardial and endocardial fibers apply. Such knowledge can be extracted from available non-patient specific fiber atlases or fiber imaging studies [6] [47].

Although having epicardial and endocardial activation maps significantly reduced the error in the ECS method, it requires the placement of two electrode arrays on opposite sides of the cardiac wall for simultaneous mapping. Such a procedure is challenging in the clinical setting and limits the mapping to only some anatomical locations. An alternative approach is the use of epicardial measurements taken after intramural pacing. Taccardi *et al.* demonstrated the feasibility of this approach, by fabricating an electrode array on top of a flexible surface which allowed for the insertion of intramural needles, with multiple electrodes for stimulating at various depths, through the supportive surface [31]. These needles should have a diameter under 1.1 mm to avoid myocardial tissue damage, such as perforation [48], [49]. Alternatively, to circumvent the need for endocardial stimulation or mapping entirely, new methods could focus on estimating both the epicardial and endocardial fiber directions from the projection of the epicardial CS vectors in the CS space. Since epicardial recordings reflect the transmural propagation, the CS vectors projection deviates from a purely elliptical shape. This deviation can offer information on the influence of endocardial signal propagation on the epicardial measurements, and aid in deriving a more accurate epicardial fiber direction estimate.

Furthermore, an electrode array with a pacing electrode at the center would also

increase the accuracy of the ECS, $ECVPSF_G$ and $ECVGM_G$ methods. As it is observed in Figure 3.10, pacing in the center provides better fiber direction estimates than when the wavefront comes from the sides.

4.2.2 Methods for estimating the local fiber direction

Fibers in specific anatomical regions of the heart, for instance, those surrounding the pulmonary veins, have a more heterogeneous arrangement [6]. Moreover, diseased hearts suffer from remodeling resulting in alterations in heart wall thickness, shape and fiber orientation [50]. This remodeling can even lead to myocardial disarray, characterized by a random organization of the myocytes. Considering the typical diameter of cardiac fibers falls within the range of 5 to 10 μm, higher resolution fiber direction estimation becomes essential to capture these local heterogeneities. With more detailed patient-specific models researchers can gain a deeper understanding and improved identification of cardiac arrhythmia substrates [51].

Therefore, the ECS_L, ECVPSF, ECVGM and PIEMAP methods were employed to derive a fiber direction for each electrode location, generating an 8 x 8 fiber map (Figure 3.11). As seen in Figure 3.12, the estimation errors obtained with the PIEMAP method were significant across the different models. This suggests potential issues with its implementation as previous algorithm evaluation with human EGMs reported much higher accuracy [29]. This approach is based on solving the inverse problem to derive the tissue's conductivity parameters. Hence, the method aims to find the optimal conductivity tensor without knowledge of the fiber direction, as the latter is estimated through the eigenvalue decomposition of the conductivity tensor. An attempt to jointly estimate both parameters would result in worse estimates given the additional unknowns. Furthermore, if the fiber direction is initially required for solving the inverse problem, using this method to derive the fiber direction to later be combined with other inverse techniques seems redundant. Efforts would be better directed towards enhancing the ability of the PIEMAP to directly estimate the conductivity tensor. Moreover, less computationally expensive methods are preferred if the end goal is to solely estimate the fiber direction.

Conversely, the ECS_L, ECVPSF, and ECVGM methods demonstrated strong performance when applied to activation maps derived from the 2D and unimodal tissue configuration, but exhibited diminished accuracy in the bilayer and transmural fiber direction configuration, which could not be corrected with endocardial information (see Figure B.3). In the latter two models, the local angle estimates from the electrodes located around the pacing location and where the wavefront propagation followed the fiber direction did coincide with the true fiber orientation. Whereas further away from the pacing location, and where the wavefront propagates perpendicularly, the estimates were very inaccurate. In these locations, the wavefront is planar and completely perpendicular to the fiber direction and so will be the CS and CV vectors. Such an effect could be somewhat mitigated when using wavefronts that come from different directions. However, increasing the number of maps used to more than three only had a positive influence on the estimation accuracy of the ECS_L method (Figure 3.13). In the regions with a relatively smooth local fiber direction variation, by combining the global fiber direction estimate and controlled pacing one could obtain an accurate local estimate at specific regions. Alternatively, a localized fiber direction could be obtained by applying the global approaches to subgrids in the electrode array.

Furthermore, the used techniques for computing the CV vectors, PSF and solving

the planar wavefront model, have been shown to smoothen the CV maps. Hence, the use of an alternative technique able to detect the local conduction heterogeneity, such as the discrete velocity vector approach proposed by van Schie *et al.*, could be beneficial [52]. Nonetheless, all these techniques compute a 2D CV vector and do not take into account the intramural conduction. With intramural needle electrodes, Padilla *et al.* demonstrated that the CV vectors are generally not parallel to the mapping surface, and consequently, 2D CV computation overestimates the CV values [53]. If conduction in the normal direction is accounted for, the wavefront will adopt an ellipsoidal shape to which the 3D CV vectors could be fitted. Although the orientation of the ellipsoid might be a better fiber direction estimate, intramural EGMs recorded with a needle array are needed which can cause damage to the tissue.

4.3 Experiments on clinical data

Given the results with synthetic data, the most accurate global fiber direction estimation methods, ECS, ECVPSF_G and ECVGM_G, were tested with EGMs recorded during SR from the BB, RA and RV, and during AF and pacing from the BB. The methods were modified to utilize three maps, obtained in three distinct heartbeats, using the *All Vectors* approach.

The Bachmann's bundle (BB) is a muscle bundle that connects the RA to the LA, providing an interatrial conduction pathway. The fibers run parallel to each other, resulting in a highly preferential conduction along the bundle direction. Hence, fiber direction estimation in this structure was expected to have minimal variability, as with the LAT maps from the unimodal configuration. That was the case for all the methods with maps obtained during SR, but not during AF (Figure 3.14). In the former, the electrical signal follows a more consistent path, whereas in the latter, the chaotic behavior of the wavefront results in a large estimation variability. It has been previously observed that EGM recorded during AF capture abnormal conduction patterns, including conduction blocks or collision of different activation waves, resulting in complex LAT maps [54].

Remarkably, similar results as with AF were observed during pacing. Pacing is performed in the RA appendage, the LA appendage, and inferior RA, which are far away from the BB, allowing the electrical signal to take unpredictable and abnormal paths towards the BB. Pacing in the RA appendage has comparable activation patterns as during SR, whereas when pacing in the other two locations the wave reaches the BB from the center or the opposite side (LA) and it experiences a conduction delay [55]. This diversity of the wavefront source and delays are reflected in the LAT maps, and might be the cause of large variability.

The standard deviation values were comparable when employing the methods with data from the inferior side of the RA and RV. Unexpectedly, the RA location with a more intricate wall structure gave less variable estimates compared to the BB during SR, both recorded from the same patient. In both cases, since the data is annotated manually, the temporal resolution is low. This will be reflected in the limited number of values taken by the CS and CV vectors which will not conform an elliptical shape when projected in the CS and CV space. Nonetheless, in general, the ECS showed the lowest standard deviation, as well as the highest accuracy in the estimation error analysis in the different scenarios (Figure 3.15). However, it should be stated that the underlying fiber direction from the mapped location was not known, hence, some

assumptions were made to gain initial insights into the accuracy of the methods.

4.3.1 Limitations of the experiments on clinical data

There are two main limiting factors that impeded a direct and accurate comparative assessment of the methods with real EGMs. First, the recordings in SR come from patients who underwent open heart surgery due to aortic valve disease. While these patients were chosen due to the absence of inherent heart conduction disorders, it is important to note, that aortic valve disease can cause mechanical stress on the cardiac tissue which can alter the electrical conduction properties of the atria, thereby having a detrimental effect on both the quality of the EGMs and the performance of the fiber direction estimation methods.

Second, as aforementioned, there was a lack of information on the true underlying fiber direction at the mapped locations. Thus, future research should focus on evaluating the performance of the global and local fiber direction estimation methods, specifically the ECS, ECVPSF and ECVGM, using EGMs from living myocardial tissue with known true fiber directions. Such a study could be conducted with data from patients undergoing open heart surgery or an isolated animal heart. In the case of human data, patients would undergo an electrical mapping procedure followed by the acquisition of ultrasound images from the mapping location to obtain the tissue fiber direction. Ultrasound-based imaging techniques that allow for the non-invasive and in vivo reconstruction of myocardial fiber direction have been developed, such as 3D Ultrasound Backscatter Tensor Imaging (3D-BTI) [56]. If mapping a human heart is not feasible, EGMs can be recorded from a Langendorff-perfused porcine heart. Subsequently, the true fiber orientation can be determined by a histological study of the mapped tissue, which would involve tissue sectioning and fixation. Some studies have already employed this approach, either directly measuring the fiber direction or staining the tissue for microscopy imaging [57], [58]. In both scenarios, the initial priority should be the evaluation of healthy conducting tissue before assessing the methods in the context of a more disordered activation pattern.

4.4 Selection of the most suitable fiber direction estimation method for clinical applications

The best-performing methods for estimating both the local and global fiber direction are the original and modified versions of ECS, ECVPSF, and ECVGM. Generally, the methods are able to accurately estimate the global and local fiber direction in simple scenarios, whereas their accuracy diminishes when endocardial and epicardial fibers do not run parallel due to the wavefront rotation. Even more, global fiber direction is more accurately estimated due to the larger amount of data points from which the direction can be inferred.

Overall, the ECS method and its adaptation for local fiber direction estimation, ECS_L, stand out as the most promising approaches. These results are also supported by de Vries *et al.*, which showed that ellipse fitting to CS vectors outperformed ellipse fitting to CV when deriving the global fiber direction, also when the tissue presents conduction blocks [34]. To enhance the accuracy of the ECS method, several strategies can be employed, including; increasing the size of the activation maps, relying on three maps applying the *All Vectors* approach, employing activation maps recorded

after point stimulation at the central electrode and incorporating endocardial information. The local approach, ECS_L, could also benefit from using more LAT maps, and in areas where not very disorganized fiber arrangement is expected from the combination of an accurate global estimate with controlled pacing. However, future work should focus on improving the accuracy of this method to obtain accurate local angle estimates that can reflect the tissue heterogeneity.

5 Conclusion

The observed dependence of the 3D cardiac wall structure on the epicardial recordings reinforces the need to evaluate fiber direction estimation methods in equal and realistic conditions. Through a combination of the Courtemanche and 3D monodomain models, the propagation of the electrical signal through a tissue section of the atria, ventricles and muscle bundles could be closely mimicked. Therefore, the resulting LAT maps were used to compare the accuracy and variability of the fiber direction estimation methods.

The performance analysis shows that the most accurate approaches for estimating the local and global fiber direction are based on ellipse fitting of local CV or CS vectors, as proposed by Roney *et al.*, Houben *et al.* and de Vries *et al.* [20], [32], [34]. Specifically, the ECS method is the most promising approach for global fiber direction estimation, and its accuracy can be enhanced by increasing the number of data points used, either through interpolation or by using activation maps recorded during consecutive heartbeats. Furthermore, removing the influence of endocardial propagation through the combination of epicardial mapping with intramural pacing, and pacing at the center of the electrode array also has a positive impact on the estimation. However, the equivalent local approach, ECS_L, needs further improvement to accurately capture the architectural heterogeneity of the tissue.

Given the lack of reference epicardial fiber direction data, the clinical study was limited to a preliminary evaluation of the methods based on their robustness. Hence, future studies should focus on validating the ECS and ECS_L methods with EGM recorded from living tissue. A high-resolution accurate fiber direction map can be used to create detailed patient-specific cardiac computational models that can deepen our understanding of electropathologies and the influence of structural features on electrical signal conduction. Moreover, the automation of the fiber direction estimation methods in combination with inverse problem-solving approaches such as confirmatory factor analysis, [26] or compact matrix model [27], can enable real-time conductivity mapping. Conductivity values can be directly related to abnormal conduction, and this has the potential to replace voltage or LAT measures for more effective personalized diagnosis and treatment of arrhythmias.

Appendix A

Determining the local fiber direction from epicardial electrograms. A literature review.

Elena van Breukelen. March 2023.

Main supervisor: Dr. ir. R.C. Hendriks, Associate Professor Signal Processing Systems, Department of Microelectronics, TU Delft
Daily supervisor: Drs. M.S. van Schie, Cardiology Electrophysiology group, Erasmus MC and Ir. J.W. de Vries, PhD candidate Signal Processing Systems Department of Microelectronics, TU Delft

Abstract

The pumping function of the heart is driven by the initiation and propagation of electrical impulses throughout the myocardial tissue. The signal propagation is anisotropic, meaning that conduction is faster along the fibers of the myocardial tissue than across them. Hence, the cardiac wall architecture is a major determinant of the organ's electrical behavior and its incorporation into electrophysiological models is critical for reliable predictions and accurate interpretation of electrical recordings of the heart, such as electrograms (EGMs). This is especially relevant in patients with atrial fibrillation (AF), one of the most common cardiac arrhythmias, as the pathophysiological mechanisms are still not fully understood and intrinsic fiber orientation has been demonstrated to be the cause of reentries and conduction blocks.

Therefore, the aim of this review is to present an overview of the methods that have been developed to derive the local fiber direction from EGMs and the factors that will influence their outcomes. The proposed techniques either use the activation or voltage maps directly or compute the local conduction velocity vectors, which are considered surrogates of fiber orientation. However, generally, these methods do not take into account important cardiac characteristics such as intramural fiber rotation, breakthroughs, or source and sink mismatch, all of which can significantly influence the acquired data and estimation outcomes. Furthermore, the methods are often tested with very different cardiac models, making performance comparisons difficult. Thus, after an evaluation study with clinical data, the most optimal approaches should be selected. Combining methods, averaging maps, or using priors could possibly address some of the techniques' limitations. An accurate fiber architecture estimation method would enable the creation of patient-specific electrophysiological models and, ultimately, improve atrial fibrillation knowledge.

1 Introduction

The heart is a muscular organ responsible for pumping blood throughout the body. This function is achieved trhough the synchronous contraction of cardiomyocytes, which is triggered by a rapid depolarization of the cell membrane known as the action potential [1]. Given the elongated morphology of the cardiomyocytes and their large membrane resistivity, the generated depolarizing current propagates through the cytoplasm arriving at the ends, where the cardiac cells are electrically and mechanically coupled to adjacent cells forming fiber strands. As a result, the action potential propagates faster along the fiber than across it, conferring the cardiac tissue with anisotropic conduction properties [2]. Consequently, the fiber arrangement plays a major role in dictating the spread of the electrical signal throughout the heart. Even more, research has shown that an irregular fiber architecture is responsible for the initiation and maintenance of cardiac arrhythmias such as Atrial Fibrillation (AF) [3].

AF is suffered by around 47 million people worldwide and is characterized by abnormal electrical activity in the atria [4]. This common cardiac arrhythmia is initiated by a trigger, usually abnormal pacemaker sites, and perpetuated by a substrate, such as atrial tissue with heterogeneous conduction properties. However, the interactions between the trigger and substrate are complex, and the mechanisms underlying AF are yet not fully understood. To study the electrical impulse propagation throughout the heart, researchers record the electrical activity of the cardiac tissue using high-resolution microelectrode arrays [5]. The measured signals, known as electrograms (EGMs), reflect the cellular transmembrane potentials and can be acquired by placing the electrode array in the outer layer of the cardiac wall (epicardium) during open-heart surgery.

Interpretation of the EGMs is required for the identification of abnormal tissue and potential mechanisms for arrhythmogenesis. Currently, conduction velocity measurements made from the EGMs are used, but their values are heavily affected by the calculation method employed or are unable to detect local conduction heterogeneities [6]. Thus, the derivation of the tissue conductivity from EGMs instead, might provide better insight into the tissue properties and electrical signal behavior. Many approaches have been proposed over the years to solve the inverse problem and extract conductivity values from EGMs using mathematical cardiac models [7], [8], [9]. However, these methods have limited accuracy since it is assumed that the fiber direction is known. Incorporation of the fiber architecture in the models is possible through the use of atrial fiber atlases, constructed through Diffusion Tensor Magnetic Resonance Imaging (DT-MRI) images or histological studies of healthy tissue, or mathematical algorithms, such as the rule-based approach which generates a smooth varying fiber orientation [10], [11]. These approaches do not account for the structural changes present in AF patients and the intersubject variability and are incapable of reproducing the complex architecture of the atrial wall. Therefore, in order to obtain better estimates, the fiber direction could be derived from the EGMs and used as input for solving the inverse problem. Additionally, knowledge of the fiber architecture of AF patients will help in better understanding the importance of structural heterogeneity in abnormal wave propagation and to create patient-specific cardiac models for further electrophysiological analysis.

Several techniques have been developed to determine the fiber orientation from EGMs [12], [13], [14]. Nevertheless, the accuracy and applicability of these approaches are restricted by the complex behavior of the electrical wave propagation in the cardiac tissue, especially under pathological conditions. Therefore, this review aims to present an overview of the methods developed for deriving the fiber direction from EGMs and the factors that will influence the output of the described methods. First, fundamental concepts of heart electrophysiology and anatomy are explained to provide the reader with the necessary background knowledge. Afterward, the search method is presented, followed by a detailed description of the search results. Finally, the results are discussed and suggestions for future improvements are given. The outcomes of this review will provide more insight into the available techniques for atrial fiber reconstruction, to improve the interpretation of EGMs, our understanding of AF and the clinical outcomes of cardiac arrhythmias treatment.

2 Methods

This review is twofold and investigates, on the one hand, the methods that have been proposed in the literature to derive the fiber architecture of the cardiac wall, specifically the atria, from EGMs, and on the other hand, the factors that will affect the observed electrical activity, and therefore, impact the fiber direction estimation. Thus, the academic work evaluated in this review should

address one of these matters in order to be included in the review. Furthermore, non-English articles were excluded as they would provide insufficient information.

2.1 Search Strategy

Three databases were employed; Scopus, Web of Science, and PubMed. The search terms, or analogs of it, that needed to be present in the articles' title, abstract, or keywords were: *anisotropy, conduction, heart, electrophysiology, electrogram, model* and *fiber*. Derived words from these terms were included in the search by adding an asterisk to the right or left side of the term, and analog word, seen in Table 1, were added using the OR operator. *Mechanic**, *stress* and *strain* terms were excluded from the search using the NOT operator, to avoid retrieving records that were addressed to evaluate the mechanical function of the heart. The final search query was: (heart OR cardi* OR myocardi* OR atri*) AND (electrophysiolog* OR "electrical activity") AND (anisotropy) AND (conduct*) AND (electrogram OR "electrical recording" OR voltage OR map* OR "activation time" OR "electric potential") AND (model OR simulation OR human OR computat* OR "mathematical description") AND (*fiber OR *fiber OR architecture OR structure) AND NOT (mechanic*) AND NOT (stress) AND NOT (strain).

To further narrow the number of references the subject areas were limited to Medicine, Mathematics, Engineering, and Computer Science, or similar, in those databases with this functionality available.

Table 1: Terms and analogous terms used in the search query.

1	2	3	4	5
heart	electrical activity	electrogram	model	*fiber
cardi*	electrophysiolog*	electrical recording	simulation	*fibre
myocardi*		map*	human	architecture
atri*		activation time	computat*	structure
		electric potential	mathematical description	
		voltage		

Additionally, a MeSH search was carried out in the PubMed database with the following search query: "Heart Conduction System" AND "Anisotropy" AND ("Electrophysiologic techniques, Cardiac" OR "Electric Stimulation Therapy" OR "Atrial Fibrillation") AND ("Computer Simulation" OR "Models, Cardiovascular" OR "Humans" OR "Animals"). No exclusion terms were added, as this search already outputs a limited number of references.

2.2 Selection Process

After gathering all the references into an Excel Sheet, duplicates were removed. An abstract screening followed a title screening to remove all articles that were either focused on the efficacy of a treatment, the behavior of the cardiomyocytes at a molecular level, cellular cultures, cardiac mechanical behavior, imaging techniques, anatomy of the heart, electrical recordings other than EGMs, or non-cardiac related topics. The remaining literature was subject to a full-text evaluation. After selection, the articles were divided into two groups according to the contents: methods to determine the local fiber direction or phenomenons that will influence the observed conduction properties of the tissue. Although the main interest lies in estimating the fiber direction from the epicardial atrial tissue to be able to create models that can help in the understanding of AF, research focused on the ventricles or recordings of the endocardial tissue were also considered, as the outcomes of these studies could potentially be adapted for epicardial and atrial applications. Articles from which not the full text was available were removed. Additional relevant references, found when reviewing the selected writings, were retrieved using Google Scholar or the TU Delft library and included in the final selection.

3 Results

In Figure 1 the flow diagram for record selection can be seen. Using the search query described previously, Scopus, Web of Science, and PubMed selected 87, 45, and 31 papers, respectively. Additionally, a MeSH search in PubMed resulted in the inclusion of 54 records. Following the removal

of duplicates, 163 references underwent screening. The title and abstract screening process led to the exclusion of 80 and 35 records, respectively. Forty-eight articles were then subject to a full assessment for eligibility, two of which were excluded due to the unavailability of the full text. Out of the remaining 46 articles, 26 were deemed relevant and included in this review. Supplemental relevant references were obtained from sources such as Google Scholar or the TU Delft library, which led to the inclusion of eight additional papers. In this section, the literature's methods for determining fiber direction will be presented, followed by an analysis of the factors influencing their effectiveness.

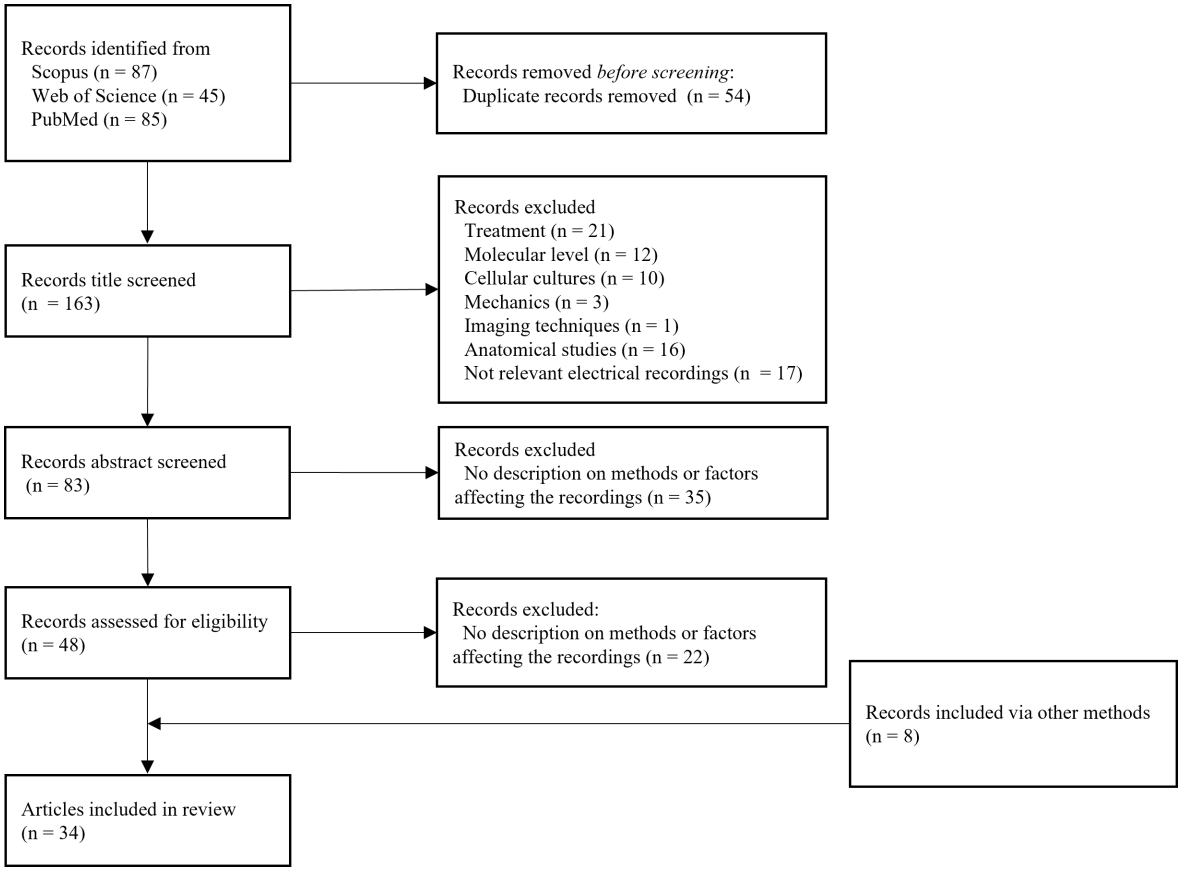

Figure 1: Flow diagram for selection of articles included in the literature review.

3.1 Methods to derive the local fiber direction from electrical recordings

Several techniques to derive the fiber direction from EGMs have been reported across the years (Table 2). The methods can be divided according to the type of parameters that are considered surrogates of the fiber direction. Thus, this section will be divided into; methods that use voltage or activation time maps, methods that use CV vectors, and other methods that use other parameters, such as conduction slowness vectors or the conductivity tensor.

Table 2: Summary table of the methods proposed to derive the fiber direction from EGM: author, description of the methods, evaluation setup and results of evaluation experiments [15], [12], [16], [17], [13], [18], [14].

Author	Method	Validation setup	Absolute mean error of fiber direction estimation
Taccardi *et al.*	Potential maxima	Monodomain model and 3D tissue block with rotating fiber orientation	4.6 ± 0.8º
Muzikant *et al.*	Ellipse fitting to stimulus equipotential	Monodomain model and 3D tissue block with rotating fiber orientation	4.7 ± 1.5º
	Ellipse fitting to isochrone	Monodomain model and 3D tissue block with rotating fiber orientation	3.7 ± 0.8º
Houben *et al.*	Geometric ellipse fitting to local CV vectors (PSF)	EGM from pectinate muscles	<2º
Linnenbank *et al.*	Average CV Method	N.A.	N.A.
Roney *et al.*	Linear transformation from elliptical to circular wavefront	Monodomain model with atrial MRI scan and fiber atlas (endocardium)	24.78 ± 2.37º
	Ellipse fitting to local CV vectors (geometrical approach) from three maps	Monodomain model with atrial MRI scan and fiber atlas (endocardium)	11.53 ± 0.73º
Grandits *et al.* and Lubrecht *et al.*	PIEMAP	Eikonal model with atrial MRI scan and fiber atlas (endocardium)	38.88 ± 0.84º
De Vries *et al.*	Conduction slowness vectors	Monodomain model and 2D surface	<3º

3.1.1 Voltage and activation time maps

In 1994, Taccardi *et al.* published one of the earliest papers on the use of electrical recordings of the heart to determine the local fiber direction [15]. Their study involved recording unipolar epicardial EGMs using electrode arrays comprising 182 to 744 electrodes, during and after 2ms point stimulation in the ventricles of canine hearts. The acquired data were presented as excitation time and potential maps. These maps, in the first few milliseconds (5 to 10ms) after epicardial pacing, revealed a negative potential at the pacing site with two positive potential maxima on either side and a densely packed array of negative equipotential lines representing the wavefront. The LAT maps from these experiments displayed elliptical-shaped isochrones. By comparing the orientation of these maps with histological samples of the epicardium, the researchers concluded that the orientation of the line joining the two maxima, the major axis of the elliptical negative equipotentials and the major axis of the elliptical isochrones were indicative of the fiber orientation in the vicinity of the pacing site. Macchi *et al.* observed similar patterns, suggesting that EGM recordings could be utilized to derive local fiber architecture in the stimulation location [19].

Simultaneously, Muzikant *et al.* proposed a technique to reconstruct the local fiber direction using 1.5 ms isochrones and validated its efficacy through a simulation [20]. Their model considered the epicardial surface as a 2D sheet with nonuniform fiber orientations, and a measuring array comprising 484 electrodes with 0.75 mm spacing was employed. The monodomain model was utilized to generate EGM recordings, which were then transformed into LAT maps by determining the time point at which V_m was greater than 50 mV. From the discrete activation maps, interpolation was carried out to obtain isochrone contour maps. The fiber direction is indicated by the line joining the stimulation point and the furthest location at the 1.5 ms isochrone. Knowing the fiber direction, the anisotropy ratio can be calculated from the CV along (CV_l) and across (CV_t) the fibers. The absolute mean error in estimating the fiber orientation and anisotropy ratio using this approach was 3.22º±1.08º and 0.8º±0.44º, respectively.

Nevertheless, Muzikant *et al.* continued the work of Taccardi *et al.* by converting the observations into methods that could derive the fiber direction from epicardial EGMs obtained after pacing [12]. They also established a procedure to determine fiber orientation from EGMs recorded during point stimulation. This approach involved fitting an ellipse into the stimulus equipotential and activation isochrones using a least-squares (LS) technique, with the major axis of the ellipse considered the fiber orientation at the pacing location. The methods were compared through simulation with the bidomain electrophysiological model and a 21 x 21 electrode array with 1 mm spacing. Interestingly, the fiber orientation derived from activation maps constructed by considering the LAT the time at which the V_m is higher than 70 mV, compared to the standard of the maximum time derivative, showed minor differences (lower than 0.2º) between each other. Techniques using EGMs acquired during stimulation and after stimulation showed similar performance. However, when evaluating intramural pacing, the two positive maxima approach (only applicable with after-stimulation EGM) was better. Furthermore, in the RV, where high transmural fiber rotation is present, using isochrone ellipse fitting during stimulation showed higher accuracy than the other methods (3.5º more accurate).

3.1.2 Conduction velocity vectors

As an alternative to activation maps, Houben *et al.* proposed using local CV vectors as surrogates of the fiber direction [16]. They divided an electrode array of 244 electrodes, with 2.25 mm spacing, into sub-squares of 3 x 3 electrodes and fitted a quadratic surface to the nine LATs. The maximum gradient of the quadratic surface at the center was taken as the local CV vector of the central electrode. This technique for finding the local CV vectors is known as Polynomial Surface Fitting (PSF). The CV vector map was obtained for a number of consecutive measurements at each electrode location. Subsequently, an ellipse was geometrically fitted into the set of CV vectors corresponding to the same location but different time points. The ellipse was parameterized using Equation 1, where CV_x and CV_y denote the CV vector components, a and b denote the length of the long and short axes, ϕ denotes the polar angles, and θ denotes the rotation angle.

$$\begin{bmatrix} CV_x \\ CV_y \end{bmatrix} = \begin{bmatrix} a\cos(\theta) & b\sin(\theta) \\ -a\sin(\theta) & b\cos(\theta) \end{bmatrix} \begin{bmatrix} \cos(\phi) \\ \sin(\phi) \end{bmatrix} \tag{1}$$

When θ, a and b of the best-fitting ellipse are obtained, the local fiber direction can be derived from θ and the local anisotropy from the ratio a/b. Figure 2 shows a scheme of the different steps of the described method. The high performance of this method, mean error lower than 2º, was proved with EGMs from AF patients undergoing open heart surgery and a macrophotography image of the heart as a reference.

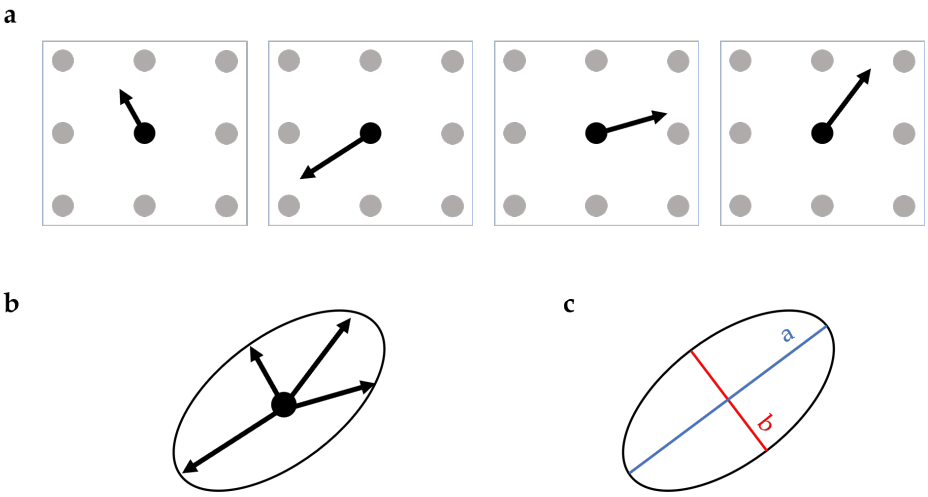

Figure 2: Steps in the method proposed by Houben *et al.*. The local CV vectors are calculated for each electrode in different LAT maps (a). Ellipse fitting to local CV vectors (b). The long axis, a, and short axis, b, of the ellipse indicate the longitudinal and transverse direction of the fibers, respectively (c).

Yet, besides PSF, other ways of calculating the local CV vectors have been described, such as the Finite Differences (FiD) and the Discrete Velocity Vectors (DVV) methods (Figure 3) [6]. In FiD, the horizontal and vertical gradients of activation are computed to determine the two components of the CV vector at the center of the grid. Differently, the DVV method derives the velocity vector from the average of the CVs in the horizontal, vertical, and diagonal directions. Although FiD and PSF are widely used, they are either sensitive to noise or not able to identify local conduction heterogeneity. DVV requires an electrode array with a minimum of 3 x 3 electrodes, but it can detect local variations of CV in a region with a non-uniform fiber direction.

These approaches are all employed to determine the local CV vector (in a 3 x 3 grid), but various local CV vectors can be combined to compute a global CV vector indicative of the fiber orientation in a larger area. This approach, proposed by Linnenbank *et al.* and termed the 'Average Vector method', consists of determining the local CV vectors through PSF, grouping the CV vectors with the same direction into bins, and computing the average CV magnitude in each bin [17]. The two bins with the largest and smallest magnitude, are selected as the longitudinal and transverse direction, respectively. The suggested method is very sensitive to the global grid size (spacing and the number of electrodes averaged out) and bin size (orientations included within the same bin), leading to under or overestimation of the CV. They conclude that a 5 x 5 subgrid and 30º bins give

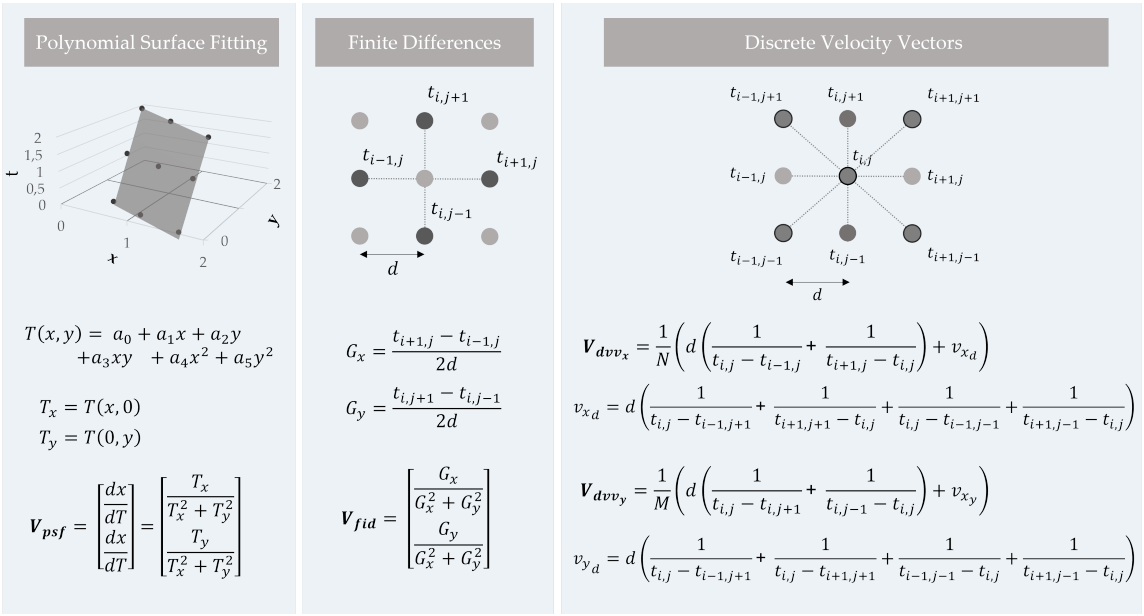

Figure 3: Methods to calculate the local CV vectors, 3 x 3 electrode grid in which calculations are done, and equations needed to derive the CV vector components. Polynomial Surface Fitting consists in fitting the equation $T(x,y)$ to the LAT in the grid, and using the gradient of the fitted polynomial to derive the CV. Finite Differences are based on computing the gradient of activation in the horizontal and vertical direction, considering the activation times at each electrode (t) and the distance between electrodes (d). Discrete Velocity Vectors consist of deriving the CV components from the average of the velocities along all the directions (horizontal, vertical and diagonal) [6].

overall the best global CV estimate results, independent of the global grid size. Nevertheless, this study does not evaluate its performance in deriving the fiber orientation.

Another interesting technique to determine the CV vector and the fiber orientation has been developed by Roney *et al.* [13]. In a previous study, they generate a geometric model of the planar (Equation 2) and circular (Equation 3) depolarization wavefront which depends on; the first measuring point (x_0, y_0), activation time of the source (T), the angle between the x-axis and the line joining the source and the first measuring point (ϕ_0), the velocity of the wavefront (v), and, in the case of a circular wavefront, the radius of curvature of the wavefront (d_0).

$$t_i = T + v^{-1}\cos\phi_0(x_i - x_0) + v^{-1}\sin\phi_0(y_i - y_0) \tag{2}$$

$$t_i = T + \frac{1}{n}\sqrt{d_0^2 + 2(d_0 \quad \cos\phi_0(x_i - x_0) \quad d_0\sin\phi_0(y_i - y_0)) + (x_i - x_0)^2 + (y_i - y_0)^2} \tag{3}$$

With linear or non-linear LS, they derive the source and velocity of the planar or circular wavefront, respectively, that minimizes the difference between modeled and clinical LATs [21]. Since only the planar and circular wavefront geometries are modeled, the method is limited to the cases where the conduction is entirely along the fibers or equal across and along the fibers. Therefore, in a second study, they propose mapping the elliptical wavefront to a circular wavefront through a linear transformation (Equation 4 and 5). The transformed coordinates ($\hat{x}_i, \hat{x}_0, \hat{y}_i$ and $\hat{y}_0$) will be obtained by rotating the ellipse by an angle θ to be aligned with the x-axis. This angle of rotation is the indicator of fiber orientation.

$$\hat{x}_i - \hat{x}_0 = (x_i - x_0)\cos\theta + (y_i - y_0)\sin\theta, \tag{4}$$

$$\hat{y}_i - \hat{y}_0 = \frac{CV_L}{CV_T}((y_i - y_0)\cos\theta + (x_i - x_0)\sin\theta) \tag{5}$$

Through non-linear LS errors of the fitted circular wavefront, the source, CV in the longitudinal and transverse direction (CV_l and CV_t, respectively) and rotation angle (θ) are derived. Furthermore, they incorporate additional steps to the technique to account for the tissue curvature when electro-anatomical measurements (EAM) are available. An area (1 cm x 1 cm) on the 3D tissue is selected,

the geodesic distances are calculated, and a multi-dimensional scaling technique is applied to flatten the surface. After the CV vectors of the selected are calculated, they are transformed back to the 3D volume. The methodology can be seen in Figure 4 accuracy is assessed with a model generated with an MRI scan, for the 3D chamber geometry, fiber atlas, and monodomain equations. The maps are created simulating an endocardial recording with the Lasso catheter, which has a 4 mm electrode spacing between electrodes. Forty percent of the measurements were estimated with an error under 20º, yet, the absolute mean error was 24.78º±2.37º.

An additional method to derive the fiber direction is developed by the same group that makes use of three activation maps from the same region but obtained after pacing in three different sites [13]. First, the local CV vectors (0.5 cm x 0.5 cm subgrid) are derived in each map assuming a planar wavefront with their original method. Second, an ellipse is geometrically fitted using non-linear LS, similar to Houben *et al.*, to the three local CV vectors. The long axis of the ellipse is the fiber direction. This second method performs better, as 70% of the fibers were estimated with less than 20° error and the mean absolute error was 11.53º±0.73º.

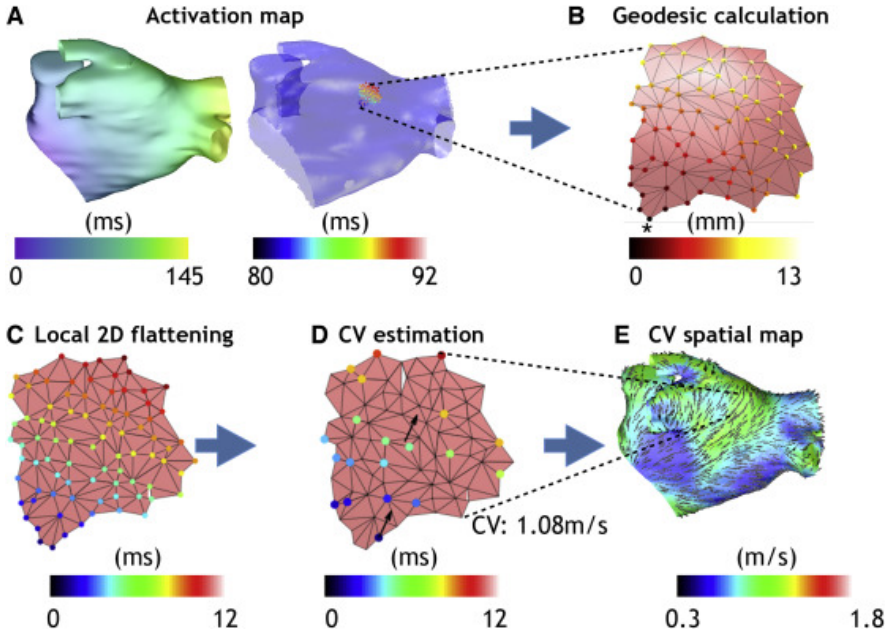

Figure 4: Steps to derive the CV vectors from a 3D atrial geometry. Select the region of interest (A). Calculate the geodesic distances (B). Apply a multi-dimensional scaling technique to flatten the surface (C). Calculate the CV vectors through the original method developed by Roney *et al.* [21] (D). Repeat the same for different 1cm x 1cm areas in the tissue and transform back to 3D geometry (E). [13]

3.1.3 Other methods

Instead of using velocity vectors, Grandits *et al.* and Lubrecht *et al.* identify the fiber direction with the Personalized Inverse Eikonal Model from cardiac Electro-Anatomical Maps (PIEMAP) method [22], [18]. PIEMAP consists in solving the inverse problem and deriving the conductivity tensor by minimizing the difference between clinical data and the output of the Eikonal Model through a regularized LS technique. The conductivity tensor undergoes eigenvalue decomposition, as shown in Equation **??**, to retrieve the eigenvector with the largest eigenvalue as it indicates the fiber direction. An atrial model was generated by combining information from an MRI scan, histological atlases and the eikonal equations. The method had poor performance (absolute mean error of 38.88º±0.84º), especially in areas with heterogeneous architecture such as the mitral ring and pulmonary veins where the error was greater than 50º. Fiber orientation in smoother areas was estimated with an error lower than 20º. Rather than employing LS, the same authors propose the combination of a Physics Informed Neural Network with the Inverse Eikonal Model to find the conductivity tensor [23]. However, no reports have been found analyzing its accuracy.

Finally, De Vries *et al.* have come up with a way of deriving the fiber direction using the reciprocal of the CV vector, known as the conduction slowness vector [14]. The conduction slowness vector is calculated at each electrode (or node) computing the gradient of the activation map, and the set of values is projected into the conduction slowness space. The coordinates of the conduction slowness

vector in the slowness space (s_x and s_y) are fitted to an ellipse rectangular coordinate equation, seen in Equation 6, where p_1, p_2 and p_3 are unknown coefficients defining the ellipse geometry.

$$p_1 s_x^2 + p_2 s_x s_y + p_3 s_y^2 = 1 \tag{6}$$

The fitting is achieved by minimizing Equation 7, in which the slowness coordinates ($s_x, s_x s_y, s_y$) for each electrode are grouped into a matrix (S) and the ellipse coefficients are grouped into a vector (p).

$$\min_p \|Sp - 1\|_2^2 \tag{7}$$

From p, the longitudinal conduction direction (θ) and anisotropy ratio (α_σ) are obtained using Equation 8 and 9.

$$\theta = \arctan\left(\frac{p_3 - p_1 - \sqrt{(p_2 - p_1)^2 + p_2^2}}{p_2}\right) + \frac{\pi}{2} \tag{8}$$

$$\alpha_\sigma = \frac{p_1 + p_3 - \sqrt{(p_3 - p_1)^2 + p_2^2}}{p_1 + p_3 + \sqrt{(p_3 - p_1)^2 + p_2^2}} \tag{9}$$

This method presented a lower estimation error than ellipse fitting to CV vectors, when carrying out a 2D monodomain model simulation with a 40 x 40 node array, and considering the LAT the time point at which V_m was greater than -40 mV. Generally, the errors were found within a small range, 0° and 2.5°, and were dependent on the distance of the measurement and stimulus site, as well as the homogeneity of the tissue.

3.2 Factors affecting the fiber direction estimation

While the methods mentioned above may aid in detecting the fiber direction, the propagation of electrical signals through the heart is complex. This complexity is manifested in the EGMs and must be taken into account when deriving the fiber orientation, particularly when utilizing indicators such as the CV vectors. Although there are various external factors that may affect EGM measurements, such as motion artifacts or the presence of blood, this review will concentrate on those related to the structural and electrical characteristics of the cardiac tissue itself.

3.2.1 3D structure of the heart

The atria wall thickness ranges from 0.6 to 4.5 mm, and the fiber architecture changes across the depth of this wall and region. In areas where no major bundles dominate, Pashakhanloo *et al.* showed that there are two distinct layers, corresponding to the epicardium and endocardium with nearly perpendicular fiber directions [10]. This will be reflected in the voltage and activation maps.

Extensive research has been conducted on the effect of ventricular wall thickness on electrical recordings, as opposed to atria, due to their thicker wall and known smooth intramural fiber rotation. Ghazanfari *et al.* identified a distortion of the observed epicardial wave propagation in EGMs caused by the electrical coupling of the epicardium with the underlying layers [24]. When combining a 3D block and the monodomain model to simulate the ventricular wall, the major axes of the elliptical epicardial isochrones obtained were found to be misaligned with the fiber direction at the superficial layer. Additionally, this misalignment was more significant with thinner tissue slabs, and the ellipse axes rotated over time following the rotation of the fibers throughout the wall. The explanation given for the first phenomenon is that in thinner tissues the orientation difference between adjacent layers is much more pronounced. The variation with time was explained by the fact that it takes some time for deeper layers to become excited after epicardial stimulation, but once activated they have an electrotonic effect on the surface. Similarly, the intramural fiber rotation also affects the voltage distributions, specifically, the isopotentials and the orientation of the voltage maxima [15], [25], [26]. Contrarily, Calvo *et al.* reported a dissociation between the atrial epicardium and endocardium during sinus rhythm in regions with large bundles. For instance, at the Bachmann's bundle and septopulmonary bundle location, since the former runs subepicardial whereas the latter runs endocardial [27].

Keener *et al.* and Taccardi *et al.* also reported the appearance of breakthroughs [28]. An electrical impulse originating in the epicardial tissue can enter the mid-wall region, where it propagates at high speed along the fibers, to then reemerge in the epicardial surface earlier than the wave propagating across the epicardial layer. If the fibers underneath have a different orientation, the estimated fiber direction from activation maps will not be accurate.

Furthermore, Taccardi *et al.* and Muzikant *et al.* point out that simply considering a stack of sheets to reproduce the cardiac wall is insufficient for a reliable model, as fibers are not necessarily all in the same plane [15], [29]. Results from a simulation showed that after 5ms of intramural stimulation, the epicardial potential maps displayed an asymmetric behavior with a larger potential maximum at one side of the pacing site than the other. The aforementioned finding was ascribed to the oblique nature of the fibers, in other words, the plane of the electrode array (or epicardial wall) and the fibers under study create an angle, referred to as the imbrication angle.

3.2.2 Spatial resolution

The spatial resolution of the measurements is another crucial aspect to consider when using CV-based methods. It has been previously reported that at a macroscopic level, the atrial tissue is not anisotropic resulting in the same values of CV along and across the fibers [30]. Electrodes are not capable of detecting the signals coming from a single cell, but rather from a group of fibers due to their limited miniaturization capabilities. Hence, the CVs of fibers running in different directions cancel each other out. Furthermore, as indicated by Mazeh *et al.*, fiber curvature causes adjacent areas in the tissue to be depolarized and hyperpolarized resulting in complex activation maps and erroneous fiber orientation estimation [31].

3.2.3 Source and sink mismatch

EGMs will also suffer from the effect of current source and sink mismatch, also known as a source-load mismatch. If the amount of current is insufficient to stimulate the adjacent tissue a conduction delay or block can appear. Bakker *et al.* describe two of the several causes of such mismatch; a sudden change in the bundle diameter or a sharp turn in the fiber direction [32]. Locations where these changes are found are the transition from the crista terminalis to the limbus or the pulmonary veins. A relation between slow conduction and anatomical boundaries has also been reported by many other researchers [2], [33], [34]. For instance, Badie *et al.* showed that at the location where the RV-free wall is inserted into the septum, there is a local conduction slowing. They also found that conduction blocks were generated in highly heterogeneous structures. Hence, patients with hypertrophic cardiomyopathy that present cardiac disarray or spatially disorganized cardiomyocytes will have more blocks and delays. These changes in the fiber architecture are reflected as delays in the LAT which will make the fiber direction estimation challenging.

The mismatch does not necessarily need to be caused by structural changes but can also be provoked by the presence of non-conducting tissue patches, such as the appearance of longitudinal strands or patches of connective tissue in diseased tissue. The presence of conduction blocks will make the signal find alternative conduction pathways not necessarily following the longitudinal axis of the fibers, increasing the path length and altering the observed CV [35]. A block can also result in the breakage of a wave into multiple wavelets, and distorted maps [36].

3.2.4 Wavefront propagation direction

It has been observed that the direction of the wavefront propagation has an impact on the CV values, and hence, the estimations derived from CV values from a single map are not reliable [7]. The direction of the wavefront varies from one heartbeat to another, thereby resulting in variability even during sinus rhythm. Furthermore, Franzone *et al.* demonstrated that the shape of the unipolar EGM is heavily influenced by the direction in which the wavefront reaches the recording site, indicating whether it traveled along or across the fibers [37]. These variations are apparent as monophasic or biphasic EGMs in cases of across-fiber and along-fiber propagation, respectively. Moreover, Jacquemet *et al.* noted a modification in the amplitude and symmetry (the difference between positive and negative deflections) due to changes in anisotropy or propagation direction [38].

3.2.5 Atrial Fibrillation

During AF the direction of the activation waves changes constantly, creating a chaotic activation pattern and hampering fiber direction detection [16]. As described by Papageorgiou *et al.*, this condition generates multiple reentrant wavelets that can collide, break into more wavelets, or disappear [39]. Therefore, recordings made during AF will reveal the complex electrical behavior.

Structural remodeling of the tissue, which results in a morphological alteration of the atrial substrate, has been found to be a cause of reentry paths and generate AF [31]. However, AF can also be the cause of this structural remodeling. Interestingly, Maesen *et al.* observed that in atria with a normal structure, epicardial fibrillation waves propagated faster along the direction of the endocardial bundles, yet in structurally remodeled atria by AF the fast propagation waves followed the direction of the epicardial fibers [30]. This was attributed to an endo-epicardial dissociation of electrical activity caused by the remodeling of the atria induced by persistent AF. Thus, patients suffering from AF will have an intricate fiber architecture, which will complicate the fiber direction estimation.

4 Discussion and future work

4.1 Performance

Over the years, several methods have been proposed to determine the fiber orientation from EGMs with varying degrees of accuracy (Table 2). However, selecting the most accurate approach is not possible as they have been evaluated under very different conditions. The conditions vary according to the origin (monodomain model, eikonal model, or clinical), the type of recording (endocardial or epicardial), the dimensions of the sample (2D or 3D tissue), the exact anatomical location in which the electrodes are placed (fiber heterogeneity), and the electrode array used (number of electrodes and spacing between the electrodes). Each of these parameters will determine the complexity of the model and independently influence the outcomes of the validation studies.

Among the tested methods, using conduction slowness vectors appears to be one of the most accurate with errors always below 3º. However, this approach was validated using a 2D monodomain model, which is a very simple setup. On the other hand, the techniques of Taccardi *et al.* and Muzikant *et al.* (potential maxima, ellipse fitting to stimulus equipotential, and ellipse fitting to isochrone) demonstrated good performance with mean error 3.22±1.08º using a 3D monodomain planar model of the ventricles. This model comes closer to the reality, but it considers a smooth fiber orientation rotation and variation, which is very different from what is found in human hearts.

In contrast, Roney *et al.* and Grandits *et al.* used simulated endocardial EAM from a monodomain or eikonal model, respectively. Both use atrial MRI scans and a fiber atlas to construct a transmurally homogeneous atrial model. Within this more realistic setup, the error found was not lower than 11º and 35º with ellipse fitting to local CV vectors from three maps or with the PIEMAP method, respectively. Furthermore, errors were very high at tissue boundaries (e.g. mitral ring and pulmonary vein). Additionally, their methods are validated with electrical recordings that are far away from the pacing site and have been developed not to require any specialized pacing protocols, which is not the case with all the other methods.

Finally, ellipse fitting to local CV vectors derived with PSF was the only one tested with clinical EGM recordings, showing a mean error below 2º. Hence, one could conclude that this is the best method. Nonetheless, it was only assessed in EGM taken from the pectinate muscles, where the propagation has a clear preferential conduction direction.

To select the best approach and further develop it, it is necessary to compare the methods under the same conditions. De Vries *et al.* already demonstrated that using conduction slowness parameters instead of CV vectors followed by ellipse fitting results in superior accuracy under the same simulations. The PIEMAP and ellipse fitting to local CV vectors from three activation maps methods could also be compared with each other since they use similar data. The latter shows much higher performance. Considering all this, using conduction slowness vectors, described by De Vries *et al.*, and local CV conduction vectors obtained through a geometric approximation, described by Roney *et al.* seem to be the most promising methods, and would need to be evaluated in more realistic models.

4.2 Limitations and future improvements

As mentioned in Section 3.2, many anatomical and electrophysiological characteristics of the heart are responsible for the variability in the electrical recordings and should be kept in mind when developing methods to derive the local fiber orientation. However, non of the current methods do so.

One of the most important and influencing characteristics is the wall thickness, this is, the intramural fiber rotation, breakthroughs, or the obliqueness of the fibers. Activation maps will also contain information related to the electrical signals propagating at deeper layers. Consequently, the parameters derived from these maps, such as the CV or slowness measurements, will not be exclusively related to the wave traveling in the epicardial surface, but rather the result of the interaction of different waves at different layers. Although most research is focused on the ventricles, some of the results can be transferred to the atria. Even more, the effect of transmural fiber rotation might be more pronounced in the upper chambers than in the lower ones, due to its less thick wall, as suggested by Ghazanfari *et al.* [24]. Nonetheless, given the complex network of fibers in the atria, compensating for this misalignment would be difficult.

Therefore, many of the techniques use a pace-mapping approach and employ the maps obtained directly after pacing as they show an ellipse-shaped propagation that vanishes when the signal propagates to other layers. It might be favorable not to use the maps obtained during stimulation as they would reflect a passive depolarization and not the propagation of the action potential [24]. Roney *et al.* and Grandits *et al.* have been the only authors to develop a method (ellipse fitting to local CV vectors from three maps and PIEMAP) which has as input the EGMs from locations far from the pacing site, without needing any pacing protocol. This might be the cause for the presented lower accuracy, however, it is much more realistic when wanting to visualize the fiber architecture in the whole atrial chamber, as signals originating from the SA are sufficient.

Another determinant is spatial resolution, which can be varied with the design of the electrode array. None of these studies evaluate the effect of changing the number of electrodes, spacing between electrodes, or size of the electrodes on the methods' accuracy. It might be so that by miniaturizing the electrodes and reducing the spacing between electrodes, information from single fibers could be detected. Abdi *et al.* reports that the optimal electrode diameter is 0.5 mm and the optimal inter-electrode distance is 1.9 mm, for capturing tissue heterogeneities in a 2D monodomain model [40]. Further testing in a more realistic environment would be needed in order to find the best electrode design capable of detecting microscopic conduction variations and locations of source-load mismatch.

Additionally, potential and activation maps are heavily influenced by the wavefront direction, hence, data will vary according to the location of the point stimulation and across beats, as the wavefront direction changes across beats [37], [41]. To remove any artifacts caused by this variability, data from different pacing sites or beats could be averaged. Furthermore, the wavefront curvature will also be a determinant of the conduction velocity, as, at a certain curvature radius, the wave will not propagate and a conduction block will be detected [42]. Interestingly, all the methods take advantage of the ellipse geometry of the wavefront reflected in the isochrones, potential map, CV vector distribution, and conduction slowness distribution. Thus, other wavefront morphologies (e.g. planar or circular) are not taken into account. Adding a wavefront classification step before computing the fiber direction could increase the techniques' accuracy.

Furthermore, using available fiber atlases as priors to the estimation of the local fiber orientation can improve the accuracy of the methods. The ellipse fitting could be constrained with the regularization of least squares from prior knowledge [22].

Finally, to overcome the shortcomings of the different approaches, they could be combined. For instance, using ellipse fitting to CV vectors to derive the fiber orientation might be improved if accurate local CV vectors were computed. Employing the DVV method, instead of PSF, might aid in detecting heterogeneous fiber morphology as it has already been proven to perform better than PSF or FiD [6]. This also applies to the 'Average vector' method. Additionally, the technique used by Roney *et al.* to flatten a 3D surface could be incorporated into the other methods before deriving the CV vectors. This would be possible if anatomical information is available either from the same measurement, through EAM, or from anatomical atlases. Furthermore, LAT maps are normally constructed by taking the time point at which the maximum derivative of the EGM is found, however, Muzikant *et al.* proposes using a V_m threshold instead. Their results do not show any decrease in accuracy, but avoiding the derivative calculation is less computationally demanding and more suitable for real-life applications.

4.3 Applications

Given the anisotropy of the tissue, fiber orientation will determine the direction of the fastest conduction and how the electrical signal propagates throughout the heart. Hence, its incorporation in electrophysiological models is essential for reliable predictions and interpretation of recorded EGMs.

The heart undergoes a fiber rearrangement under different diseases, such as AF or myocardial fibrosis. In a recent study, Kamali *et al.* observed a significant difference in fiber angles between the LA of AF-inducible and non-inducible caprine hearts [3]. They suggested that fiber architecture is a key determinant of the number and location of AF drivers, highlighting the importance of incorporating functional fiber atlases of AF patients in cardiac models to better understand the relationship between architecture and AF, as well as the underlying mechanisms of the arrhythmia. Whereas currently used techniques for fiber visualization are limited to ex vivo studies or unsuitable for atrial tissue due to its thin wall and complex geometry (e.g. histological data and DT-MRI), epicardial EGMs would allow for in vivo atrial fiber visualization. Patient-specific models with fiber architecture are crucial to improve our understanding of AF and interpreting clinical measurements. Specifically, solving the inverse problem, and reliably estimating the direction-dependent tissue conductivity properties is only possible if the fiber orientation is known. Currently, experts either manually select the orientation or use ruled-based methods or available healthy tissue atlases. However, with the patient-specific fiber geometry conductivity estimators would be much more accurate. Additionally, AF-specific electrophysiological models could deepen our knowledge of the mechanisms underlying AF.

However, such methods should not be limited only to epicardial EGMs, as they can only be obtained from patients undergoing open surgery, discouraging their use for treatment planning. The fiber direction could also be derived from endocardial EGMs, recorded in less invasive procedures through intracardiac electrode catheters. These catheters have fewer electrodes with a larger inter-electrode distance than the ones used for epicardial mapping, leading to a poorer fiber orientation estimation, as shown by Roney *et al.* and Grandits *et al.*. Nonetheless, they are employed for guiding ablation therapy, and knowledge of the fiber architecture might help in identifying ablation sites and improving clinical outcomes.

5 Conclusion

This paper presents an overview of the methods that have been developed for estimating the fiber orientation from EGMs and the factors influencing their performance. Several methods, using isochrones, CV vectors or conduction slowness vectors, among others, have been proposed over the years and have demonstrated high accuracy. However, these approaches have been evaluated in overly simplistic setups that do not account for the intricate interactions between the layers of the cardiac wall or sudden changes in fiber orientation. In order to find the best method, validation with clinical data from human hearts should be carried out. Furthermore, by combining the most promising techniques and implementing additional improvements, it may be possible to improve the accuracy of fiber direction estimation and enhance its applicability for developing detailed cardiac models. Patient-specific models have become increasingly relevant for assessing the electrical properties of the heart under various pathologies, including the most prevalent arrhythmia, AF. Despite its widespread occurrence, the underlying mechanisms of AF are not yet fully understood. With models that incorporate the patient fiber geometry and accurately predict the behavior of the atria, it will be possible to understand AF mechanisms and identify opportunities for therapeutic intervention

References

[1] P. Colli Franzone, L. F. Pavarino, and S. Scacchi, *Mathematical Cardiac Electrophysiology*, vol. 13 of *MS&A*. Cham: Springer International Publishing, 2014.

[2] O. V. Aslanidi, M. R. Boyett, H. Dobrzynski, J. Li, and H. Zhang, "Mechanisms of Transition from Normal to Reentrant Electrical Activity in a Model of Rabbit Atrial Tissue: Interaction of Tissue Heterogeneity and Anisotropy," *Biophysical Journal*, vol. 96, pp. 798–817, 2 2009.

[3] R. Kamali, E. Kwan, M. Regouski, T. J. Bunch, D. J. Dosdall, E. Hsu, R. S. Macleod, I. Polejaeva, and R. Ranjan, "Contribution of atrial myofiber architecture to atrial fibrillation," *PloS one*, vol. 18, p. e0279974, 1 2023.

[4] J. Kornej, C. S. Börschel, E. J. Benjamin, and R. B. Schnabel, "Epidemiology of Atrial Fibrillation in the 21st Century," *Circulation Research*, vol. 127, pp. 4–20, 6 2020.

[5] J. M. de Bakker, "Electrogram recording and analyzing techniques to optimize selection of target sites for ablation of cardiac arrhythmias," 12 2019. This work is licensed under the Creative Commons Attribution 4.0 International License (CC BY 4.0). To view a copy of this license, visit `http://creativecommons.org/licenses/by/4.0/`.

[6] M. S. van Schie, A. Heida, Y. J. H. J. Taverne, A. J. J. C. Bogers, and N. M. S. de Groot, "Identification of local atrial conduction heterogeneities using high-density conduction velocity estimation," *EP Europace*, vol. 23, pp. 1815–1825, 11 2021.

[7] M. Sun, N. M. de Groot, and R. C. Hendriks, "Joint cardiac tissue conductivity and activation time estimation using confirmatory factor analysis," *Computers in Biology and Medicine*, vol. 144, p. 105393, 5 2022.

[8] E. Gilboa, P. S. La Rosa, and A. Nehorai, "Estimating electrical conductivity tensors of biological tissues using microelectrode arrays," *Annals of biomedical engineering*, vol. 40, pp. 2140–2155, 10 2012.

[9] B. Abdi, R. C. Hendriks, A. J. van der Veen, and N. M. de Groot, "A compact matrix model for atrial electrograms for tissue conductivity estimation," *Computers in biology and medicine*, vol. 107, pp. 284–291, 4 2019.

[10] F. Pashakhanloo, D. A. Herzka, H. Ashikaga, S. Mori, N. Gai, D. A. Bluemke, N. A. Trayanova, and E. R. McVeigh, "Myofiber Architecture of the Human Atria as Revealed by Sub-Millimeter Diffusion Tensor Imaging," *Circulation. Arrhythmia and electrophysiology*, vol. 9, p. e004133, 4 2016.

[11] P. Pathmanathan and R. A. Gray, "Validation and trustworthiness of multiscale models of cardiac electrophysiology," *Frontiers in Physiology*, vol. 9, 2 2018.

[12] A. L. Muzikant and C. S. Henriquez, "Paced Activation Mapping Reveals Organization of Myocardial Fibers: A Simulation Study," *J Cardiovasc Eleclrophysiol*, vol. 8, pp. 2–294, 1997.

[13] C. H. Roney, J. Whitaker, I. Sim, L. O'Neill, R. K. Mukherjee, O. Razeghi, E. J. Vigmond, M. Wright, M. D. O'Neill, S. E. Williams, and S. A. Niederer, "A technique for measuring anisotropy in atrial conduction to estimate conduction velocity and atrial fibre direction," *Computers in Biology and Medicine*, vol. 104, pp. 278–290, 1 2019. This work is licensed under the Creative Commons Attribution 4.0 International License (CC BY 4.0). To view a copy of this license, visit `http://creativecommons.org/licenses/by/4.0/`.

[14] J. Willem De Vries, "Estimation of atrial fibre directions based on epicardial electrograms," 2022.

[15] B. Taccardi, E. Macchi, R. L. Lux, P. R. Ershler, S. Spaggiari, S. Barufdi, and Y. Vyhmeister, "Effect of myocardial fiber direction on epicardial potentials," *Circulation*, vol. 90, no. 6, pp. 3076–3090, 1994.

[16] R. P. Houben, N. M. de Groot, J. L. Smeets, A. E. Becker, F. W. Lindemans, and M. A. Allessie, "S-wave predominance of epicardial electrograms during atrial fibrillation in humans: Indirect evidence for a role of the thin subepicardial layer," *Heart Rhythm*, vol. 1, pp. 639–647, 12 2004.

[17] A. C. Linnenbank, J. M. de Bakker, and R. Coronel, "How to measure propagation velocity in cardiac tissue: A simulation study," *Frontiers in Physiology*, vol. 5 JUL, p. 267, 7 2014.

[18] T. Grandits, S. Pezzuto, J. M. Lubrecht, T. Pock, G. Plank, and R. Krause, "PIEMAP: Personalized Inverse Eikonal Model from Cardiac Electro-Anatomical Maps," *Lecture Notes in Computer Science (including subseries Lecture Notes in Artificial Intelligence and Lecture Notes in Bioinformatics)*, vol. 12592 LNCS, pp. 76–86, 2021.

[19] E. Macchi, M. Cavalieri, D. Stilli, E. Musso, S. Baruffi, G. Olivetti, P. R. Ershler, R. L. Lux, and B. Taccardi, "High-density epicardial mapping during current injection and ventricular activation in rat hearts," *American Journal of Physiology - Heart and Circulatory Physiology*, vol. 275, no. 5 44-5, 1998.

[20] A. L. Muzikant, E. K. Weitzel, and C. S. Henriquez, "Estimating fiber directions from local activation mapping: a model study," *Annual International Conference of the IEEE Engineering in Medicine and Biology - Proceedings*, vol. 17, no. 1, pp. 81–82, 1995.

[21] C. H. Roney, C. D. Cantwell, N. A. Qureshi, R. L. Ali, E. T. Chang, P. B. Lim, S. J. Sherwin, N. S. Peters, J. H. Siggers, and F. S. Ng, "An automated algorithm for determining conduction velocity, wavefront direction and origin of focal cardiac arrhythmias using a multipolar catheter," in *2014 36th Annual International Conference of the IEEE Engineering in Medicine and Biology Society, EMBC 2014*, pp. 1583–1586, Institute of Electrical and Electronics Engineers Inc., 11 2014.

[22] J. M. Lubrecht, T. Grandits, A. Gharaviri, U. Schotten, T. Pock, G. Plank, R. Krause, A. Auricchio, G. Conte, and S. Pezzuto, "Automatic reconstruction of the left atrium activation from sparse intracardiac contact recordings by inverse estimate of fibre structure and anisotropic conduction in a patient-specific model," *Europace*, vol. 23, pp. I63–I70, 3 2021.

[23] T. Grandits, S. Pezzuto, F. Sahli Costabal, P. Perdikaris, T. Pock, G. Plank, and R. Krause, "Learning Atrial Fiber Orientations and Conductivity Tensors from Intracardiac Maps Using Physics-Informed Neural Networks," *LNCS*, vol. 12738, pp. 650–658, 2021.

[24] A. Ghazanfari, M. P. Rodriguez, E. Vigmond, and A. Nygren, "Computer simulation of cardiac propagation: Effects of fiber rotation, intramural conductivity, and optical mapping," *IEEE Transactions on Biomedical Engineering*, vol. 61, no. 7, pp. 2041–2048, 2014.

[25] H. S. Oster, B. Taccardi, R. L. Lux, P. R. Ershler, and Y. Rudy, "Electrocardiographic imaging: Noninvasive characterization of intramural myocardial activation from inverse-reconstructed epicardial potentials and electrograms," *Circulation*, vol. 97, pp. 1496–1507, 4 1998.

[26] D. E. Roberts, L. T. Hersh, and A. M. Scher, "Influence of cardiac fiber orientation on wavefront voltage, conduction velocity, and tissue resistivity in the dog," *Circulation Research*, vol. 44, no. 5, pp. 701–712, 1979.

[27] D. Calvo, D. Filgueiras-Rama, and J. Jalife, "Propagation of Sinus Waves in the Atrial Architecture When Laminar Electrical Fluxes Turn Turbulent," *Circ Arrhythm Electrophysiol*, vol. 10, p. 5699, 2017.

[28] J. P. Keener, "An eikonal-curvature equation for action potential propagation in myocardium," *Journal of Mathematical Biology*, vol. 29, no. 7, pp. 629–651, 1991.

[29] A. L. Muzikant, E. W. Hsu, P. D. Wolf, and C. S. Henriquez, "Region specific modeling of cardiac muscle: Comparison of simulated and experimental potentials," *Annals of Biomedical Engineering*, vol. 30, no. 7, pp. 867–883, 2002.

[30] B. Maesen, S. Zeemering, C. Afonso, J. Eckstein, R. A. Burton, A. Van Hunnik, D. J. Stuckey, D. Tyler, J. Maessen, V. Grau, S. Verheule, P. Kohl, and U. Schotten, "Rearrangement of atrial bundle architecture and consequent changes in anisotropy of conduction constitute the 3-dimensional substrate for atrial fibrillation," *Circulation: Arrhythmia and Electrophysiology*, vol. 6, pp. 967–975, 10 2013.

[31] N. Mazeh, D. E. Haines, M. W. Kay, and B. J. Roth, "A Simplified Approach for Simultaneous Measurements of Wavefront Velocity and Curvature in the Heart Using Activation Times," *Cardiovascular Engineering and Technology*, vol. 4, pp. 520–534, 12 2013.

[32] J. M. De Bakker and H. M. Van Rijen, "Continuous and Discontinuous Propagation in Heart Muscle," *Journal of Cardiovascular Electrophysiology*, vol. 17, pp. 567–573, 5 2006.

[33] A. Hassankhani, B. Yao, and G. K. Feld, "Conduction velocity around the tricuspid valve annulus during type 1 atrial flutter: Defining the location of areas of slow conduction by three-dimensional electroanatomical mapping," *Journal of Interventional Cardiac Electrophysiology*, vol. 8, pp. 121–127, 4 2003.

[34] N. Badie, J. A. Scull, R. Y. Klinger, A. Krol, and N. Bursac, "Conduction block in micropatterned cardiomyocyte cultures replicating the structure of ventricular cross-sections," *Cardiovascular research*, vol. 93, pp. 263–271, 2 2012.

[35] M. S. Spach, P. C. Dolber, and J. F. Heidlage, "Influence of the passive anisotropic properties on directional differences in propagation following modification of the sodium conductance in human atrial muscle. A model of reentry based on anisotropic discontinuous propagation," *Circulation research*, vol. 62, no. 4, pp. 811–832, 1988.

[36] E. J. Ciaccio, A. B. Biviano, E. Y. Wan, N. S. Peters, and H. Garan, "Development of an automaton model of rotational activity driving atrial fibrillation," *Computers in Biology and Medicine*, vol. 83, pp. 166–181, 4 2017.

[37] P. C. Franzone, L. Guerri, M. Pennacchio, and B. Taccardi, "Anisotropic mechanisms for multiphasic unipolar electrograms: Simulation studies and experimental recordings," *Annals of Biomedical Engineering*, vol. 28, no. 11, pp. 1326–1342, 2000.

[38] V. Jacquemet, N. Virag, Z. Ihara, L. Dang, O. Blanc, S. Zozor, J. M. Vesin, L. Kappenberger, and C. Henriquez, "Study of Unipolar Electrogram Morphology in a Computer Model of Atrial Fibrillation," *Journal of Cardiovascular Electrophysiology*, vol. 14, pp. S172–S179, 10 2003.

[39] P. Papageorgiou, K. Monahan, N. G. Boyle, M. J. Seifert, P. Beswick, J. Zebede, L. M. Epstein, and M. E. Josephson, "Site-Dependent Intra-Atrial Conduction Delay," *Circulation*, vol. 94, pp. 384–389, 8 1996.

[40] B. Abdi, M. S. van Schie, N. M. Groot, and R. C. Hendriks, "Analyzing the effect of electrode size on electrogram and activation map properties," *Computers in Biology and Medicine*, vol. 134, p. 104467, 7 2021.

[41] O. Berenfeld, A. V. Zaitsev, S. F. Mironov, A. M. Pertsov, and J. Jalife, "Frequency-dependent breakdown of wave propagation into fibrillatory conduction across the pectinate muscle network in the isolated sheep right atrium," *Circulation Research*, vol. 90, no. 11, pp. 1173–1180, 2002.

[42] R. H. Clayton, O. Bernus, E. M. Cherry, H. Dierckx, F. H. Fenton, L. Mirabella, A. V. Panfilov, F. B. Sachse, G. Seemann, and H. Zhang, "Models of cardiac tissue electrophysiology: Progress, challenges and open questions," *Progress in Biophysics and Molecular Biology*, vol. 104, pp. 22–48, 1 2011.

Appendix

B

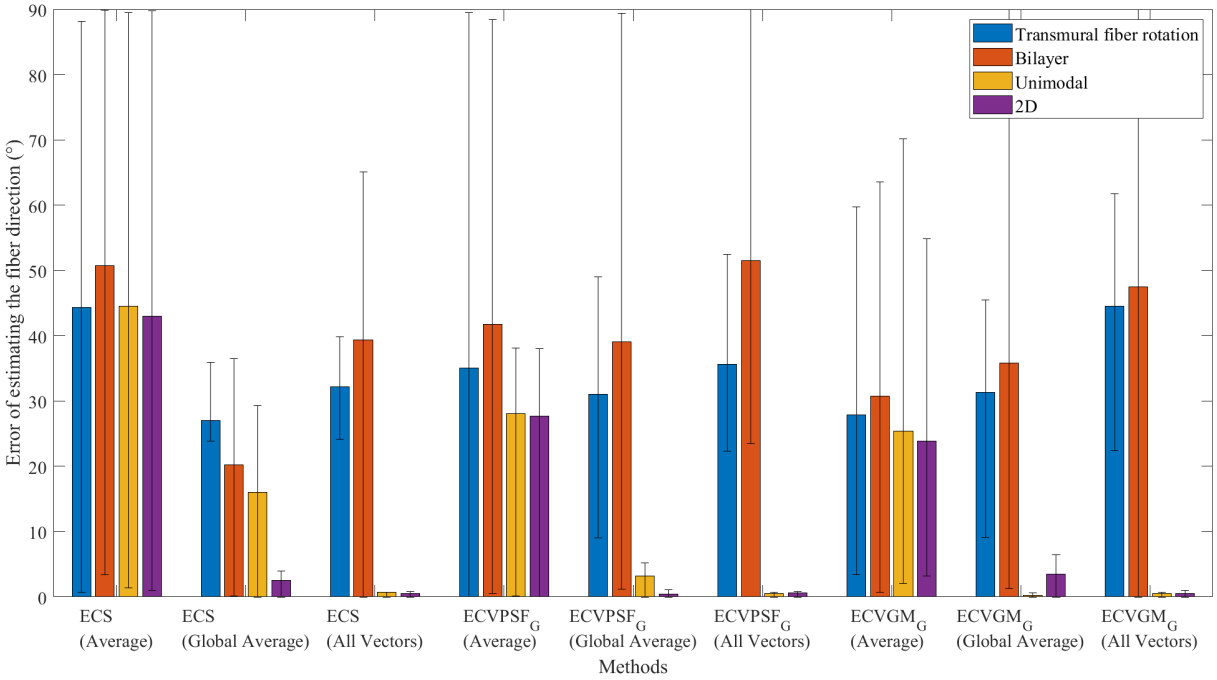

Figure B.1: Comparison of mean absolute error, along with the maximum and minimum non-outlier error, in global fiber direction estimation methods modified to use three epicardial LAT maps with three different approaches: *Average*, *Global Average* and *All Vectors*. In the first approach, an ellipse is fitted to three local CS or CV vectors from three separate LAT maps but from the same electrode location, after which all the local angle values are averaged out to find a global fiber direction. In the second approach, three global fiber direction estimates are averaged. In the third approach, an ellipse is fitted to all local CS or CV vectors from the three maps, with the orientation of the elongated axis of this single ellipse representing the fiber direction. The LAT maps used are generated by stimulating at different locations within the epicardial layer of four different tissue model configurations: 2D, unimodal, bilayer and transmural fiber rotation.

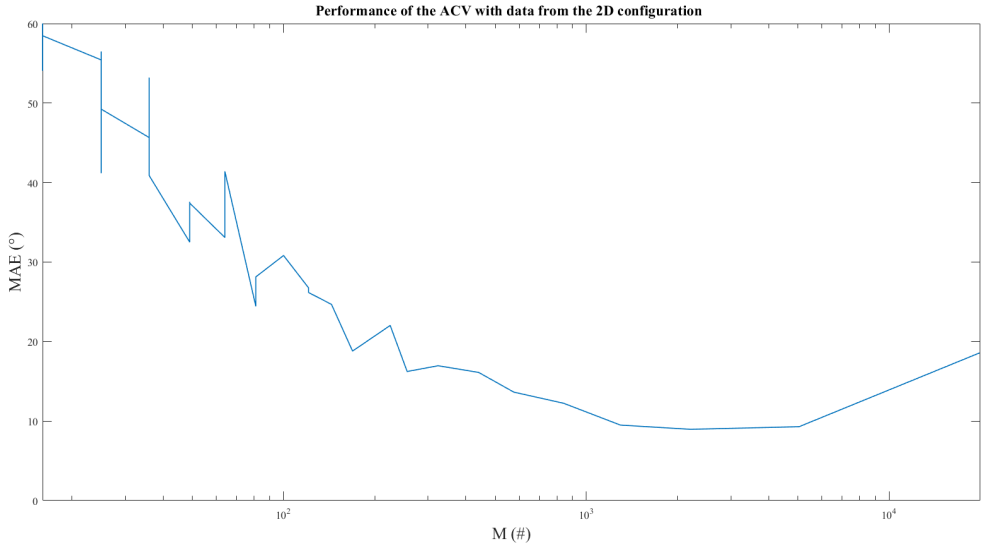

Figure B.2: Mean absolute error (MAE) in estimating the fiber direction when using ACV as a function of the size of the LAT maps (M).

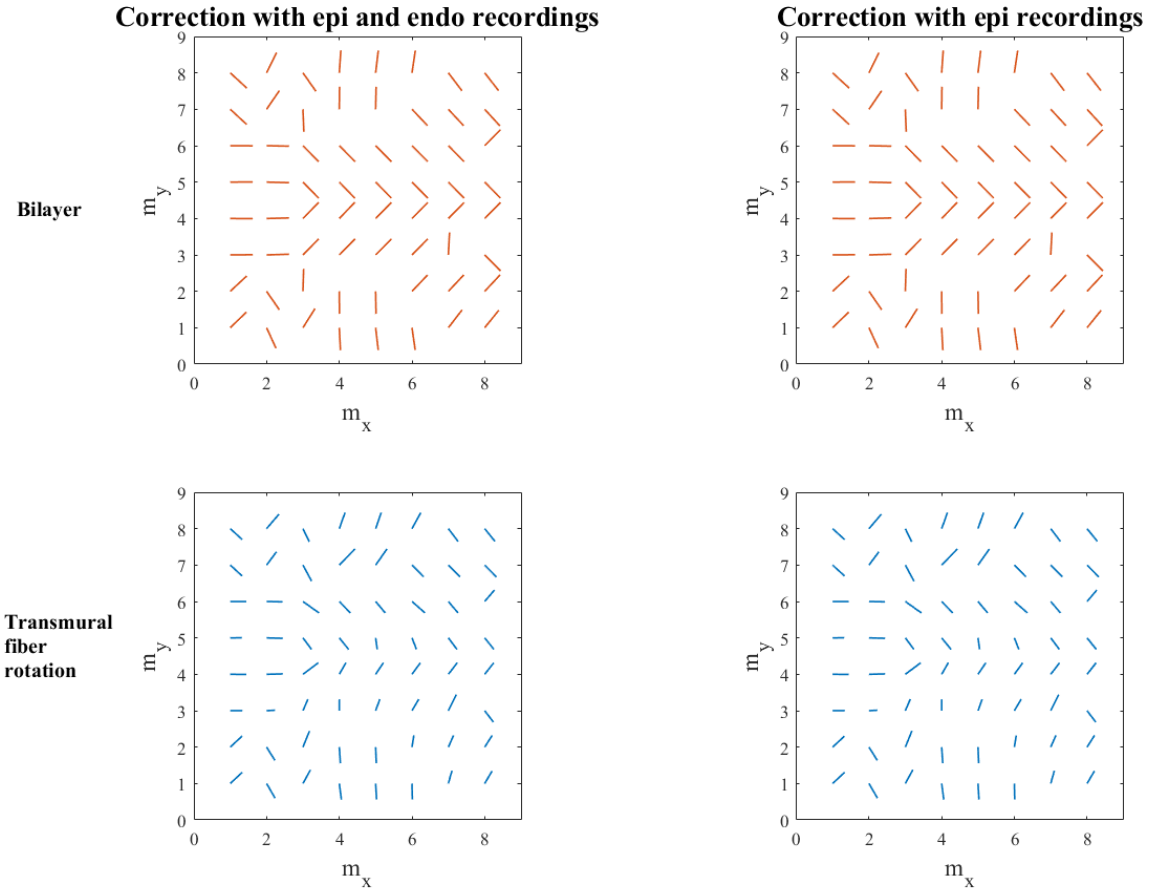

Figure B.3: Local fiber direction estimates computed using the ECS_L method, and corrected to include endocardial information obtained by stimulating the endocardium and recording at the endocardium or stimulating the endocardium and recording at the epicardium. The LAT maps used are obtained when stimulating the side of the epicardium in the 2D, unimodal, bilayer and transmural fiber rotation tissue models. The true local fiber direction is 0º for all maps and all electrodes.

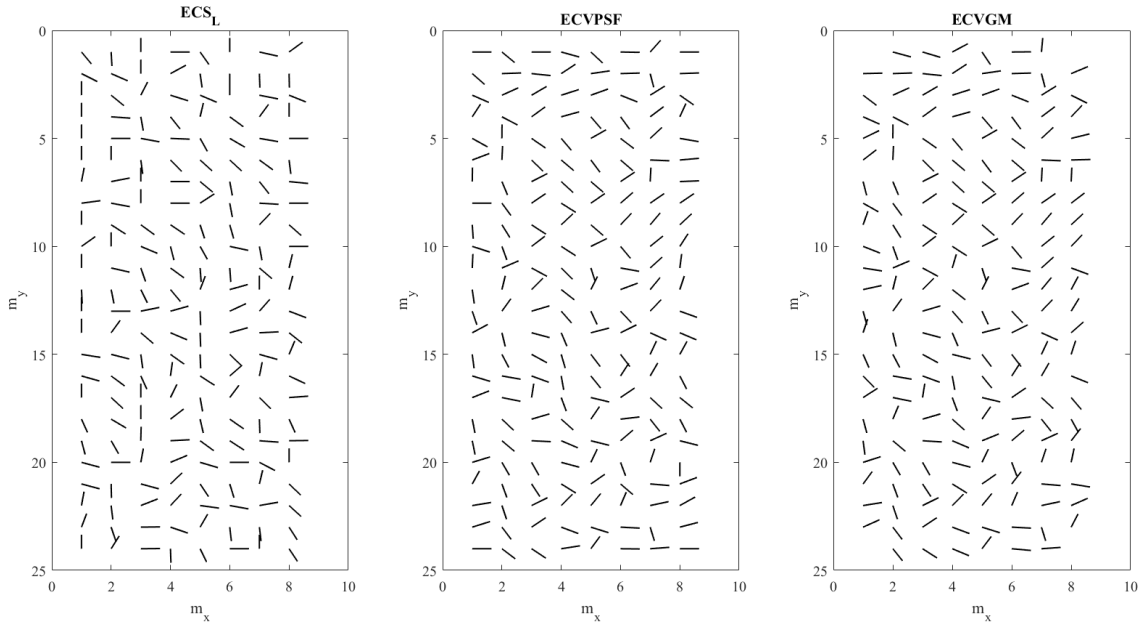

Figure B.4: Local fiber direction estimates computed using three methods, ECS_L, ECVPSF and ECVGM. The three LAT maps employed to estimate the fiber direction are obtained from the BB during three different heartbeats in SR. The true local fiber direction is assumed to be 0° for all the electrodes.

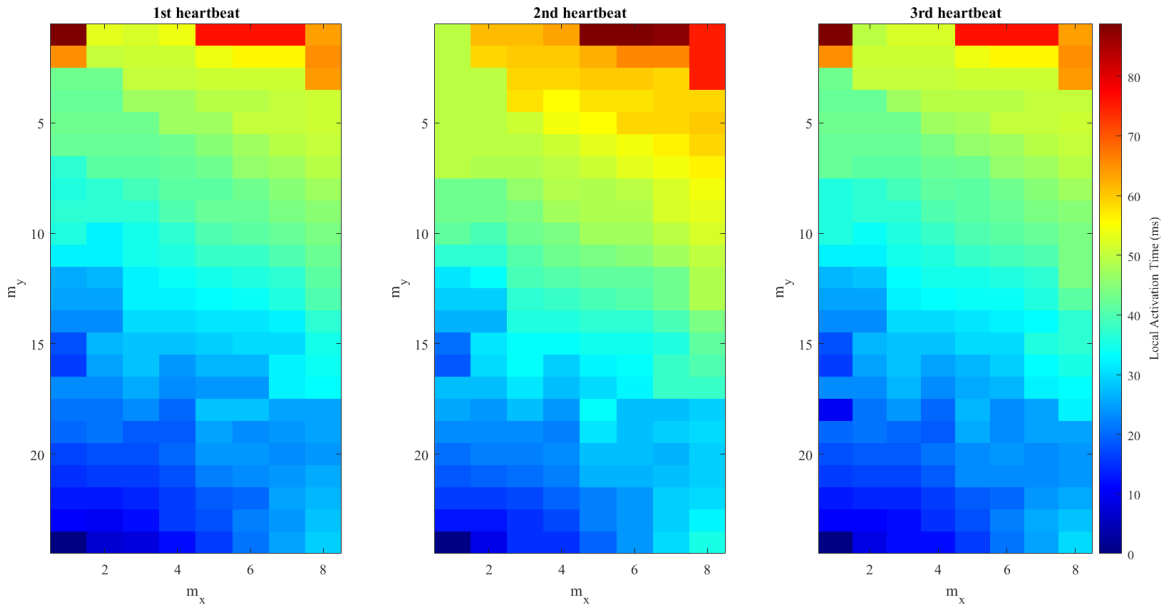

Figure B.5: LAT maps, corresponding to consecutive heartbeats, obtained from the BB during SR.

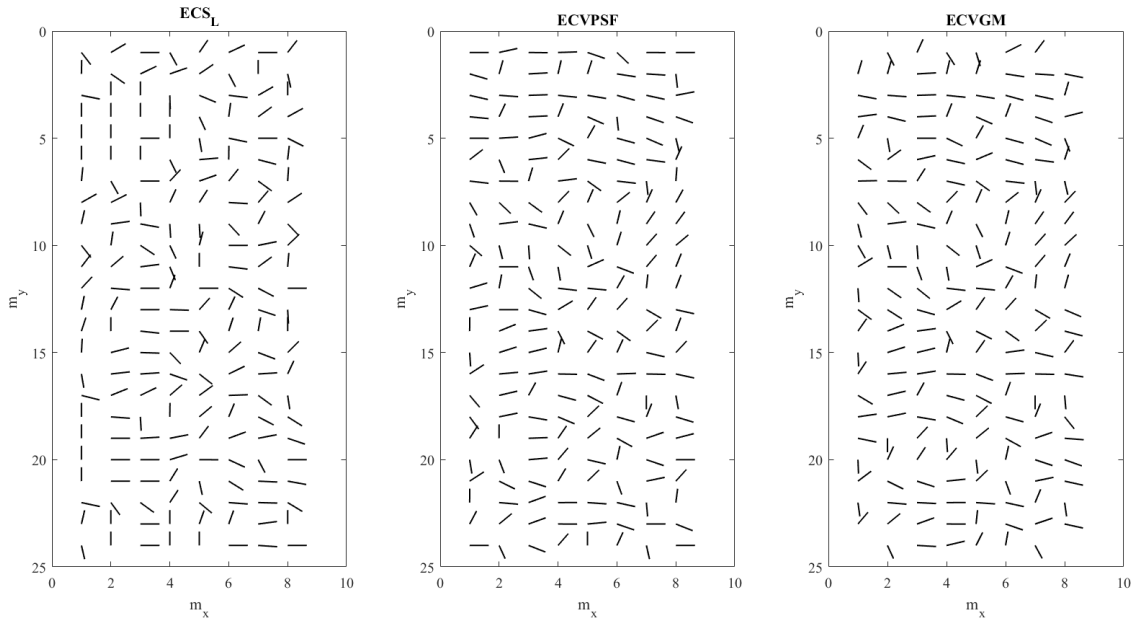

Figure B.6: Local fiber direction estimates computed using three methods, ECS_L, ECVPSF and ECVGM. The LAT maps used are obtained from the BB after pacing in three different locations, the LA appendage (LAA), the RA appendage (RAA), and the inferior RA (RAinf). The true local fiber direction is assumed to be 0° for all the electrodes.

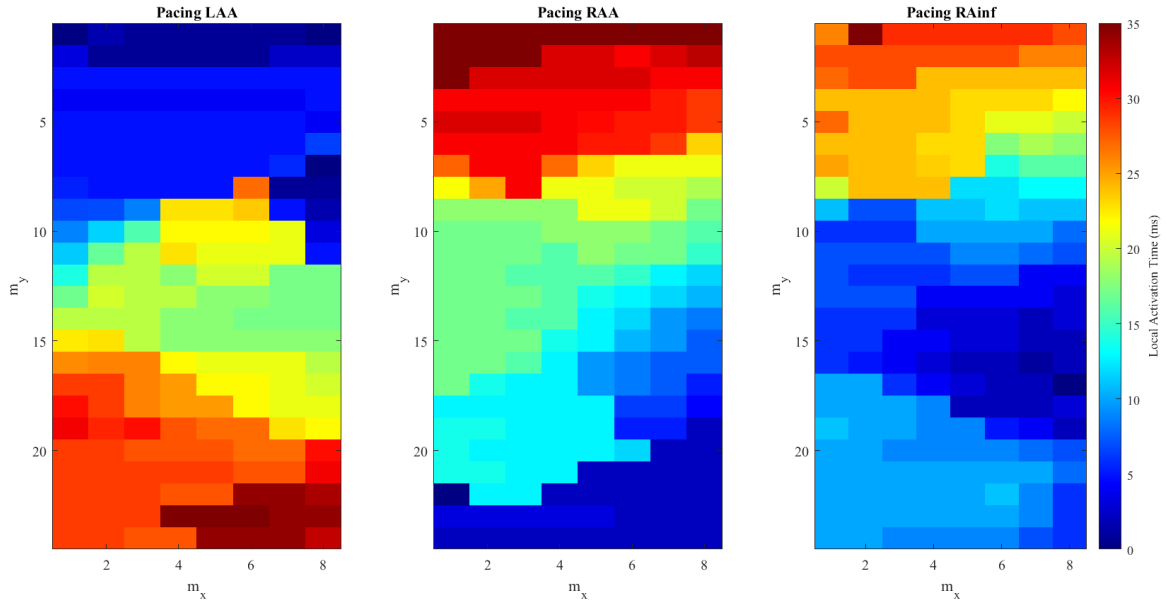

Figure B.7: LAT maps obtained from the BB after pacing in three different locations, the LA appendage (LAA), the RA appendage (RAA), and the inferior RA (RAinf).

Bibliography

[1] M. Shenasa, G. Hindricks, D. J. Callans, J. M. Miller, and M. E. Josephson, *Cardiac Mapping, Fifth Edition*. Wiley-Blackwell, 5 ed., 2019.

[2] S. Y. Ho, "Anatomy and myoarchitecture of the left ventricular wall in normal and in disease," *European Journal of Echocardiography*, vol. 10, pp. 3–7, 12 2009.

[3] S. Y. Ho and P. Nihoyannopoulos, "Anatomy, echocardiography, and normal right ventricular dimensions," *Heart*, vol. 92, pp. 2–13, 4 2006.

[4] A. L. Muzikant, E. W. Hsu, P. D. Wolf, and C. S. Henriquez, "Region specific modeling of cardiac muscle: Comparison of simulated and experimental potentials," *Annals of Biomedical Engineering*, vol. 30, no. 7, pp. 867–883, 2002.

[5] M. Varela, R. Morgan, A. Theron, D. DIllon-Murphy, H. Chubb, J. Whitaker, M. Henningsson, P. Aljabar, T. Schaeffter, C. Kolbitsch, and O. V. Aslanidi, "Novel MRI Technique Enables Non-Invasive Measurement of Atrial Wall Thickness," *IEEE Transactions on Medical Imaging*, vol. 36, pp. 1607–1614, 8 2017.

[6] F. Pashakhanloo, D. A. Herzka, H. Ashikaga, S. Mori, N. Gai, D. A. Bluemke, N. A. Trayanova, and E. R. McVeigh, "Myofiber Architecture of the Human Atria as Revealed by Sub-Millimeter Diffusion Tensor Imaging," *Circulation. Arrhythmia and electrophysiology*, vol. 9, 4 2016.

[7] J. Betts, K. Young, and W. James, *Anatomy and Physiology*. No. 184, OpenStax, 2013. This work is licensed under the Creative Commons Attribution 4.0 International License (CC BY 4.0). To view a copy of this license, visit http://creativecommons.org/licenses/by/4.0/.

[8] S. C. Salvage, C. L. Huang, and A. P. Jackson, "Cell-adhesion properties of β-subunits in the regulation of cardiomyocyte sodium channels," *Biomolecules*, vol. 10, pp. 1–22, 7 2020.

[9] P. Franzone, L. F. Pavarino, and S. Scacchi, *Mathematical Cardiac Electrophysiology*, vol. 13 of *MS&A*. Cham: Springer International Publishing, 2014.

[10] "File:Action potential ventr myocyte.gif - Wikimedia Commons." This work is licensed under the Creative Commons Attribution-ShareAlike 3.0 Unported License (CC BY-SA 3.0). To view a copy of this license, visit https://creativecommons.org/licenses/by-sa/3.0/deed.en.

[11] M. Valderrábano, "Influence of anisotropic conduction properties in the propagation of the cardiac action potential," *Progress in biophysics and molecular biology*, vol. 94, p. 144, 5 2007.

[12] I. Kotadia, J. Whitaker, C. Roney, S. Niederer, M. O'Neill, M. Bishop, and M. Wright, "Anisotropic cardiac conduction," *Arrhythmia and Electrophysiology Review*, vol. 9, no. 4, pp. 202–210, 2021.

[13] R. Kamali, E. Kwan, M. Regouski, T. J. Bunch, D. J. Dosdall, E. Hsu, R. S. Macleod, I. Polejaeva, and R. Ranjan, "Contribution of atrial myofiber architecture to atrial fibrillation," *PloS one*, vol. 18, p. e0279974, 1 2023.

[14] O. V. Aslanidi, M. A. Colman, J. Stott, H. Dobrzynski, M. R. Boyett, A. V. Holden, and H. Zhang, "3D virtual human atria: A computational platform for studying clinical atrial fibrillation," *Progress in Biophysics and Molecular Biology*, vol. 107, pp. 156–168, 10 2011.

[15] A. G. Brooks, M. K. Stiles, J. Laborderie, D. H. Lau, P. Kuklik, N. J. Shipp, L. F. Hsu, and P. Sanders, "Outcomes of long-standing persistent atrial fibrillation ablation: A systematic review," *Heart Rhythm*, vol. 7, pp. 835–846, 6 2010.

[16] C. H. Roney, J. D. Bayer, H. Cochet, M. Meo, R. M. Dubois, P. Jaïs, and E. J. Vigmond, "Variability in pulmonary vein electrophysiology and fibrosis determines arrhythmia susceptibility and dynamics," *Plos Computatinal Biology*, vol. 14, no. 5, 2018.

[17] M. Sermesant, R. Chabiniok, P. Chinchapatnam, T. Mansi, F. Billet, P. Moireau, J. M. Peyrat, K. Wong, J. Relan, K. Rhode, M. Ginks, P. Lambiase, H. Delingette, M. Sorine, C. A. Rinaldi, D. Chapelle, R. Razavi, and N. Ayache, "Patient-specific electromechanical models of the heart for the prediction of pacing acute effects in CRT: a preliminary clinical validation," *Medical image analysis*, vol. 16, pp. 201–215, 1 2012.

[18] W. G. Stevenson and K. Soejima, "Recording techniques for clinical electrophysiology," *Journal of cardiovascular electrophysiology*, vol. 16, pp. 1017–1022, 9 2005.

[19] J. M. de Bakker, "Electrogram recording and analyzing techniques to optimize selection of target sites for ablation of cardiac arrhythmias," 12 2019. This work is licensed under the Creative Commons Attribution 4.0 International License (CC BY 4.0). To view a copy of this license, visit http://creativecommons.org/licenses/by/4.0/.

[20] C. H. Roney, J. Whitaker, I. Sim, L. O'Neill, R. K. Mukherjee, O. Razeghi, E. J. Vigmond, M. Wright, M. D. O'Neill, S. E. Williams, and S. A. Niederer, "A technique for measuring anisotropy in atrial conduction to estimate conduction velocity and atrial fibre direction," *Computers in Biology and Medicine*, vol. 104, pp. 278–290, 1 2019.

[21] B. Nowak, J. Sperzel, F. Rauscha, L. Mont, J. Alzueta, P. J. Senden, and J. Meyer, "Diagnostic value of onset-recordings and marker annotations in dual chamber pacemaker stored electrograms," *EP Europace*, vol. 5, pp. 103–109, 1 2003.

[22] A. L. Muzikant and C. S. Henriquez, "Paced Activation Mapping Reveals Organization of Myocardial Fibers: A Simulation Study," *J Cardiovasc Eleclrophysiol*, vol. 8, pp. 2–294, 1997.

[23] R. H. Clayton, O. Bernus, E. M. Cherry, H. Dierckx, F. H. Fenton, L. Mirabella, A. V. Panfilov, F. B. Sachse, G. Seemann, and H. Zhang, "Models of cardiac tissue electrophysiology: Progress, challenges and open questions," *Progress in Biophysics and Molecular Biology*, vol. 104, pp. 22–48, 1 2011.

[24] P. Pathmanathan and R. A. Gray, "Validation and trustworthiness of multiscale models of cardiac electrophysiology," *Frontiers in Physiology*, vol. 9, 2 2018.

[25] C. Henriquez, "Simulating the electrical behavior of cardiac tissue using the bidomain model.," *Critical reviews in biomedical engineering*, vol. 21, no. 1, pp. 1–77, 1993.

[26] M. Sun, N. M. de Groot, and R. C. Hendriks, "Joint cardiac tissue conductivity and activation time estimation using confirmatory factor analysis," *Computers in Biology and Medicine*, vol. 144, p. 105393, 5 2022.

[27] B. Abdi, R. C. Hendriks, A. J. van der Veen, and N. M. de Groot, "A compact matrix model for atrial electrograms for tissue conductivity estimation," *Computers in biology and medicine*, vol. 107, pp. 284–291, 4 2019.

[28] E. Gilboa, P. S. La Rosa, and A. Nehorai, "Estimating electrical conductivity tensors of biological tissues using microelectrode arrays," *Annals of biomedical engineering*, vol. 40, pp. 2140–2155, 10 2012.

[29] T. Grandits, S. Pezzuto, J. M. Lubrecht, T. Pock, G. Plank, and R. Krause, "PIEMAP: Personalized Inverse Eikonal Model from Cardiac Electro-Anatomical Maps," *Lecture Notes in Computer Science*, vol. 12592, pp. 76–86, 2021.

[30] H. Dejea, A. Bonnin, A. C. Cook, and P. Garcia-Canadilla, "Cardiac multi-scale investigation of the right and left ventricle ex vivo: a review," *Cardiovascular Diagnosis and Therapy*, vol. 10, p. 1701, 10 2020.

[31] B. Taccardi, E. Macchi, R. L. Lux, P. R. Ershler, S. Spaggiari, S. Barufdi, and Y. Vyhmeister, "Effect of myocardial fiber direction on epicardial potentials," *Circulation*, vol. 90, no. 6, pp. 3076–3090, 1994.

[32] R. P. Houben, N. M. de Groot, J. L. Smeets, A. E. Becker, F. W. Lindemans, and M. A. Allessie, "S-wave predominance of epicardial electrograms during atrial fibrillation in humans: Indirect evidence for a role of the thin subepicardial layer," *Heart Rhythm*, vol. 1, pp. 639–647, 12 2004.

[33] A. C. Linnenbank, J. M. de Bakker, and R. Coronel, "How to measure propagation velocity in cardiac tissue: A simulation study," *Frontiers in Physiology*, vol. 5, p. 267, 7 2014.

[34] J. W. de Vries, M. Sun, N. M. de Groot, and R. C. Hendriks, "Estimation of Cardiac Fibre Direction Based on Activation Maps," *ICASSP 2023 - 2023 IEEE International Conference on Acoustics, Speech and Signal Processing (ICASSP)*, pp. 1–5, 5 2023.

[35] D. Hart, A. J. Rudman, D. Hart, and A. J. Rudman, "Least-squares fit of an ellipse to anisotropic polar data: Application to azimuthal resistivity surveys in karst regions," *Computer & Geosciences*, vol. 23, no. 2, pp. 189–194, 1997.

[36] A. L. Muzikant, E. K. Weitzel, and C. S. Henriquez, "Estimating fiber directions from local activation mapping: a model study," *Annual International Conference of the IEEE Engineering in Medicine and Biology - Proceedings*, vol. 17, no. 1, pp. 81–82, 1995.

[37] B. PV, K. BH, R. JM, H. RE, I. RE, and S. WM, "Estimation of conduction velocity vector fields from epicardial mapping data," *IEEE transactions on bio-medical engineering*, vol. 45, no. 5, pp. 563–571, 1998.

[38] A. Chambolle and T. Pock, "A first-order primal-dual algorithm for convex problems with applications to imaging," *Journal of Mathematical Imaging and Vision volume*, vol. 40, pp. 120–145, 2010.

[39] M. Courtemanche, R. J. Ramirez, and S. Nattel, "Ionic mechanisms underlying human atrial action potential properties: insights from a mathematical model," *The American journal of physiology*, vol. 275, no. 1, 1998.

[40] V. Jacquemet, N. Virag, Z. Ihara, L. Dang, O. Blanc, S. Zozor, J.-M. Vesing, L. Kappenberger, and C. Henriquez, "Study of Unipolar Electrogram Morphology in a Computer Model of Atrial Fibrillation," *Journal of Cardiovascular Electrophysiology*, vol. 14, pp. S172–S179, 10 2003.

[41] B. Taccardi, R. L. Lux, P. R. Ershler, R. MacLeod, C. Zabawa, and Y. Vyhmeister, "Potential Distributions and Excitation Time Maps Recorded with High Spatial Resolution from the Entire Ventricular Surface of Exposed Dog Hearts," *Proceedings Computers in Cardiology*, pp. 1–4, 1992.

[42] B. Taccardi, B. B. Punske, E. Macchi, R. S. MacLeod, and P. R. Ershler, "Epicardial and intramural excitation during ventricular pacing: effect of myocardial structure," *American journal of physiology. Heart and circulatory physiology*, vol. 294, p. H1753, 4 2008.

[43] S. Coveney, C. Cantwell, and C. Roney, "Atrial conduction velocity mapping: clinical tools, algorithms and approaches for understanding the arrhythmogenic substrate," *Medical & Biological Engineering & Computing*, vol. 60, p. 2463, 9 2022.

[44] M. A. Reiger, J. W. Dyer, D. B. Geselowitz, and E. J. Berbari, "Interpolation of local activation times versus potentials to derive an activation map in infarcted myocardium," *Computers in Cardiology*, vol. 0, no. 0, pp. 137–140, 1996.

[45] M. Sanromán-Junquera, R. Díaz-Valencia, A. García-Alberola, J. L. Rojo-´ Alvarez, and I. Mora-Jiménez, "Effect of Interpolation on Electroanatomical Mapping," *Computing in Cardiology*, vol. 42, pp. 361–364, 2015.

[46] Z. Huang, H. Wang, and R. Zhang, "An Improved Kriging Interpolation Technique Based on SVM and Its Recovery Experiment in Oceanic Missing Data," *American Journal of Computational Mathematics*, vol. 2012, pp. 56–60, 3 2012.

[47] C. H. Roney, R. Bendikas, F. Pashakhanloo, C. Corrado, E. J. Vigmond, E. R. McVeigh, N. A. Trayanova, and S. A. Niederer, "Constructing a Human Atrial Fibre Atlas," *Annals of biomedical engineering*, vol. 49, pp. 233–250, 1 2021.

[48] A. Thiagalingam, C. R. Campbell, A. C. Boyd, V. E. Eipper, D. L. Ross, and P. Kovoor, "Cooled Intramural Needle Catheter Ablation Creates Deeper Lesions than Irrigated Tip Catheter Ablation," *Pacing and Clinical Electrophysiology*, vol. 27, pp. 965–970, 7 2004.

[49] S. R. Dukkipati, T. Nakamura, I. Nakajima, C. Oates, R. Narui, S. Tanigawa, T. Sljapic, W. Whang, J. S. Koruth, S. Choudry, B. Schaeffer, A. Fujii, U. B. Tedrow, J. L. Sapp, W. G. Stevenson, and V. Y. Reddy, "Intramural Needle Ablation for Refractory Premature Ventricular Contractions," *Circulation. Arrhythmia and electrophysiology*, vol. 15, p. e010020, 5 2022.

[50] P. S. Azevedo, B. F. Polegato, M. F. Minicucci, S. A. Paiva, and L. A. Zornoff, "Cardiac Remodeling: Concepts, Clinical Impact, Pathophysiological }Mechanisms and Pharmacologic Treatment," *Arquivos Brasileiros de Cardiologia*, vol. 106, p. 62, 1 2016.

[51] T. Hoshino, H. Fujiwara, and C. Y. Kawai Hamashima, "Myocardial fiber diameter and regional distribution in the ventricular wall of normal adult hearts, hypertensive hearts and hearts with hypertrophic cardiomyopathy," *Circulation*, vol. 67, no. 5, pp. 1109–1116, 1983.

[52] M. S. van Schie, A. Heida, Y. J. H. J. Taverne, A. J. J. C. Bogers, and N. M. S. de Groot, "Identification of local atrial conduction heterogeneities using high-density conduction velocity estimation," *EP Europace*, vol. 23, pp. 1815–1825, 11 2021.

[53] J. R. Padilla, R. D. Anderson, C. Joens, S. Masse, A. Bhaskaran, A. Niri, P. Lai, M. A. Azam, G. Lee, E. Vigmond, and K. Nanthakumar, "Orientation of conduction velocity vectors on cardiac mapping surfaces," *EP Europace*, vol. 25, pp. 1172–1182, 3 2023.

[54] K. T. Konings, J. L. Smeets, O. C. Penn, H. J. Wellens, and M. A. Allessie, "Configuration of Unipolar Atrial Electrograms During Electrically Induced Atrial Fibrillation in Humans," *Circulation*, vol. 95, pp. 1231–1241, 3 1997.

[55] M. S. van Schie, N. L. Ramdat Misier, P. Knops, A. Heida, Y. J. Taverne, and N. M. de Groot, "Mapping-guided atrial lead placement determines optimal conduction across Bachmann's bundle: a rationale for patient-tailored pacing therapy," *Europace*, vol. 25, p. 1432, 4 2023.

[56] C. Papadacci, V. Finel, J. Provost, O. Villemain, P. Bruneval, J. L. Gennisson, M. Tanter, M. Fink, and M. Pernot, "Imaging the dynamics of cardiac fiber orientation in vivo using 3D Ultrasound Backscatter Tensor Imaging," *Scientific Reports 2017 7:1*, vol. 7, pp. 1–9, 4 2017.

[57] D. B. Ennis, T. C. Nguyen, J. C. Riboh, L. Wigström, K. B. Harrington, G. T. Daughters, N. B. Ingels, and D. C. Miller, "Myofiber angle distributions in the ovine left ventricle do not conform to computationally optimized predictions," *Journal of biomechanics*, vol. 41, p. 3219, 11 2008.

[58] Y. Wang, K. Zhang, N. B. Wasala, X. Yao, D. Duan, G. Yao, D. D. Streeter, H. M. Spotnitz, D. P. Patel, J. Ross, and E. H. Sonnenblick, "Histology validation of mapping depth-resolved cardiac fiber orientation in fresh mouse heart using optical polarization tractography," *Biomedical Optics Express, Vol. 5, Issue 8, pp. 2843-2855*, vol. 5, pp. 2843–2855, 8 2014.